SUMMARY REPORT

APOLLO INFRARED ACQUISITION AND TRACKING SYSTEM

BY

HERBERT L. RICHARD
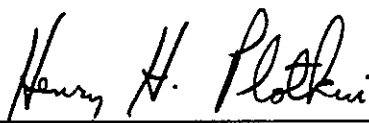
SEPTEMBER 1965

GODDARD SPACE FI I'GHT CENTER

GREENBELT, MA
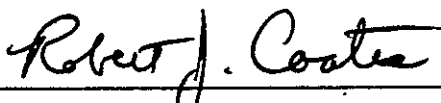
SUMMARY REPORT

APOLLO INFRARED ACQUISITION

AND

TRACKING SYSTEM

September 1965

Approved: _____

Henry H. Plotkin
Head, Optical Systems Branch

_____

Robert J. Coates
Chief, Advanced Development Division

GODDARD SPACE FLIGHT CENTER
Greenbelt, Maryland

CONTENTS

<div align="center">LIST OF FIGURES</div>

SUMMARY REPORT

APOLLO INFRARED ACQUISITION

AND

TRACKING SYSTEM

by

Herbert L. Richard

SYNOPSIS

The re-entering Apollo Command Module on return from a lunar mission will generate sufficient energy in the infrared band to permit daylight detection, acquisiton, and tracking from an aircraft at a range of 500 nautical miles. The tracking information derived can be used ·to predict the impact point within a small area, thereby aiding the quick and safe recovery of the astronauts and the spacecraft equipment.

This function can be performed, irregardless of the expected extensive communication blackout, by a completely passive infrared system. By being passive, no weight, power, space of reliability allowance is required of the spacecraft. The infrared system requires no large ship or real estate and associated large antenna investment and it is highly mobile so that for any unforeseen event it can quickly span continents and oceans to be on site during a spacecraft re-entry.

The surface temperatures of the spacecraft will lie between the char-ablation temperature of 1000°K and 2500°K. The 500 nautical mile range capability is calculated for the minimum temperature condition which is expected to be reached ten seconds after re-entry starts at 400,000 feet.

Atmospheric effects, scattered sunlight and atmospheric thermal emission, present a background radiation with a minimum radiance across a 3 to 5 micron infrared band. This also conveniently falls at a "window" in the atmosphere where infrared transmission is high, namely the 3 to 4.5 micron band. The atmospheric transmission is especially high at the aircraft altitude of 35,000 feet. Also at this altitude, over the Apollo re-entry area, a cloud cover analysis has shown a minimal condition to

exist. Radiation from celestial objects falls off appreciably at infrared wavelengths so that very few celestial objects are expected to be detected.

An examination of the state-of-the-art shows that systems exist today with the acquisition, range and tracking capability to perform the mission. What has to be done is to utilize the state-of-the-art of existing systems and to mechanize these components into a system configured to perform the desired functions. Two conceptual designs are presented.

With re-entry events of such large magnitude occurring during Gemini and Apollo re-entries, every effort should be made to take advantage of these events for scientific purposes of verifying the theoretical and laboratory experimental work. No better proving ground could be obtained for gathering scientific information and determining the operational capability of prototype infrared acquisition systems for lunar and planetary missions.

Recommendations for further work are presented and specifications for a system design are given in Appendix A.

APOLLO INFRARED ACQUISITION AND
TRACKING SYSTEM

INTRODUCTION

When a spacecraft re-enters the earth's atmosphere, it must dissipate a considerable amount of kinetic energy to land safely. Most of this energy is transformed into heat as the air about the spacecraft is decelerated and compressed. Dissociation and thermal ionization of the air occurs and as a result radiant energy is released.

Temperatures on the surface of the spacecraft reach high values predominately as a result of the convective heat transfer. An additional heat input is the radiative heat transfer from the air radiation.

It is not only the aerodynamic heating problem which is of interest, but the fact that at very high air temperatures, the air about the spacecraft becomes electrically conductive and introduces new problems in radio wave transmission and reception. In the most critical case, radio communication is completely blacked out. This "blackout" condition has already been experienced during the re-entry of the Mercury and Gemini spacecraft. A much more serious condition of tracking and communication blackout is expected for spacecraft re-entering the earth's atmosphere at hypervelocity speeds, which is the case for the Apollo vehicle on return from a lunar mission. It is particularly critical since its occurrence will coincide with the maneuver phase of the spacecraft (see Figure 1). This loss in communications may severely limit the ground support during a vital portion of this phase or even during the entire regime of re-entry flight depending upon the type of re-entry trajectory. Figure 2 depicts a nominal trajectory of 2000 nautical mile range. Indicated are the expected communication blackout boundaries. In this case, "blackout" could occur for 85% of the re-entry distance travelled.

It is to this problem that we have directed our attention. With this consideration (the loss in communications and tracking signals), we have investigated the capability of an infrared search and track system, which would acquire the Apollo spacecraft from the self-generated, thermal heating — the same phenomenon which caused the communication blackout.
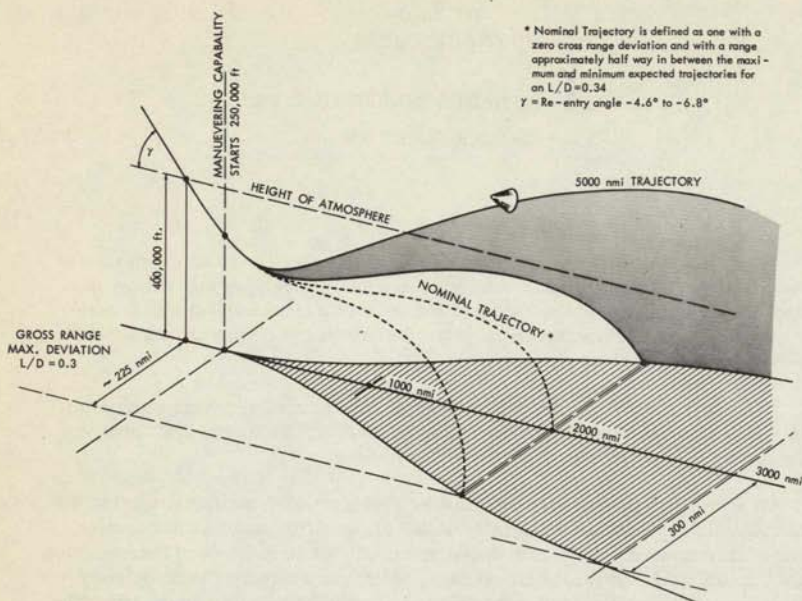
Figure 1—Down Range and Cross Range Foot Print for Maneuvering Apollo Spacecraft
(Adapted from GSFC Document X-513-65-4[16].)

The convective and radiative heating effects to the spacecraft during re-entry will cause the exterior to reach such temperatures that the spacecraft is essentially and literally a "blackbody" radiating energy predominately in the infrared part of the spectrum.

It is this radiant energy which would be utilized by a passive infrared system, a system requiring no weight, power, or space on board the Apollo spacecraft.

Fundamentally, the infrared acquisition and tracking system (IRATS) would serve to:

   a. Point and slave the unified S-band communication antenna on board the Apollo range instrumented aircraft.

2
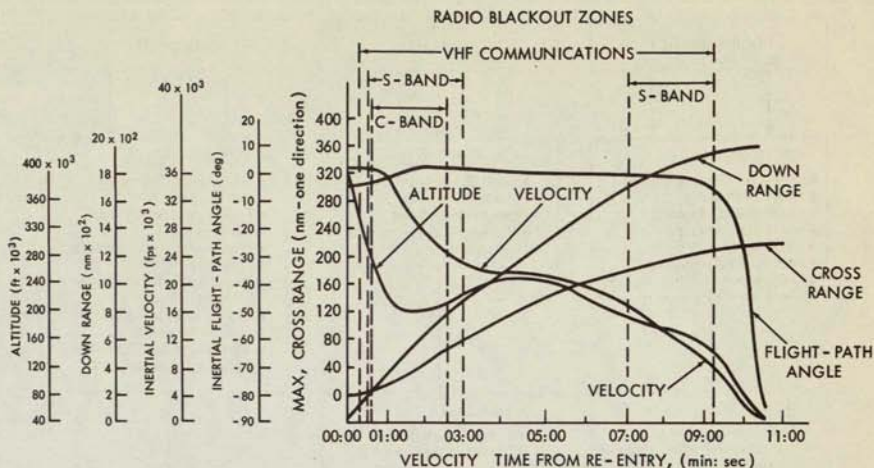
Figure 2–Typical trajectory parameters as a function of time for an initial flight-path angle of – 6.4° and a re-entry range of 2000 n.m., L/D = 0.4. Indicated are the Radio Blackout Zones, Reference 16 and 29.

 b. Provide angle track data for trajectory calculations in real time.

 c. Provide data for postflight analysis.

A more complete description of the IRATS requirements and operation is given in the GSFC Specification, "Infrared Acquisition and Tracking System." This specification was written for the development of a system to perform the above functions from aircraft cruising at approximately 35,000 feet. A copy of this specification is included as Appendix A of this report.

In examining the infrared radiance characteristics of the re-entering Apollo spacecraft, it is well to examine the total spectral radiance characteristics (source signal characteristics) of a body re-entering the earth's atmosphere at super-orbital velocities. On this basis, one can then proceed to develop the sensor equipment to optimally work with the energy available considering atmospheric and background effects, detector sensor characteristics, range and resolution requirements, and mission and operational requirements. These considerations can be set forth in the form of a functional block diagram, Figure 3. This diagram depicts the processes and series of events, in the order in which they occur, which must be taken into account.

| SYSTEM FUNCTION | λ LIMITS | SENSITIVITY |

CONSIDERATION OF:
- What is system required to do?
- Field of view required - instantaneous and total
- Search scan required?
- Focal length?
- Monochromatic or waveband?
- Meteorological Conditions - Clouds

CONSIDERATION OF:
- Signal Characteristics
- Source temperature
- Background Radiation
- Atmospheric or environment obsorption

CONSIDERATION OF:
- Source intensity temperature, area, range, aspect
- Background intensity and temperature
- Atmospheric or environmental transmission
- Transmission characteristics of optics, chopper
- Spectral sensitivity of detector
- Amplifier bandwidth
- Noise level of detection system
- Signal conversion efficiency

INDICATES:
- Type of optical system - reflective, refractive, simple, or complex
- Optical quality required
- Accuracy required
- Operational Requirements

INDICATES:
- Suitable detectors
- Suitable IR dome, window, filter, optical materials

INDICATES:
- Size of optics
- Signal - to - noise ratio required for reliable detection
- Detector Detectivity

PRELIMINARY
DESIGN OF
IR SYSTEM

Figure 3—Preliminary design considerations. (Adapted from H. L. Hackforth, "Infrared Radiation." McGraw-Hill Book Company, Inc., New York, 1960.)

A PERT diagram was developed for the Apollo IRATS project giving a conceptual picture of the events in chronological order and tasks which had to be accomplished for the effective procurement, design, construction, test and operational usage of the infrared re-entry acquisition and tracking equipment. A copy of the PERT diagram is included as Appendix B of this report. Of course this reflects the dates considered at the time the project was started. The time to accomplish a particular task is however still relevant.

SOURCE RADIATION CHARACTERISTICS

No direct spectral measurements have been made of a vehicle re-entering the earth's atmosphere at super-orbital velocities, except for the recent project Fire re-entry. However, the results are somewhat inconclusive insofar as defining the spectral profile of the vehicle.

Nevertheless, considerable experimental data has been obtained and sufficient theory generated so that a fairly good prediction of the re-entry radiation can be made.

A notable example of the theoretical and supporting experimental work is that carried on at NASA-Ames Research Center, by Craig, Davey and Page and Arnold (references 1 and 2). To simulate the high re-entry velocities, the Ames hypersonic free-flight facilities were used.

A typical plot of the spectral radiant emission characteristics versus wavelength of Lexan at high re-entry velocities is shown in Figure 4. Lexan is a polycarbonate type of heat shield material with characteristics similar to the Apollo heat shield ablative material.

The test results on other materials such as Aluminum, Polyethylene, and GE124 are reported and shown in Figure 5 (reference 2 and 6). In every case the
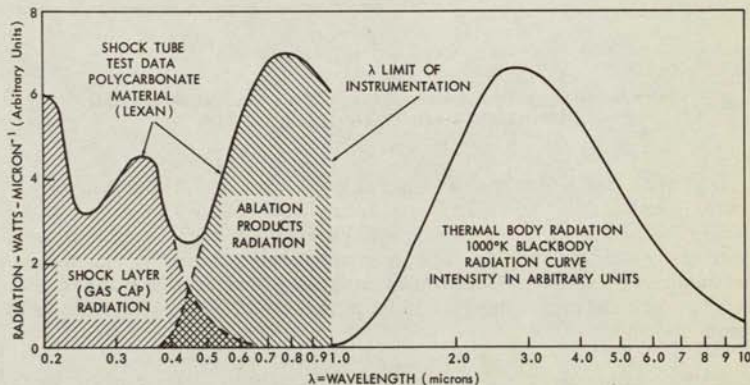
Figure 4—Typical radiant emission characteristics for a spacecraft re-entering the earth's atmosphere at hypervelocity speeds
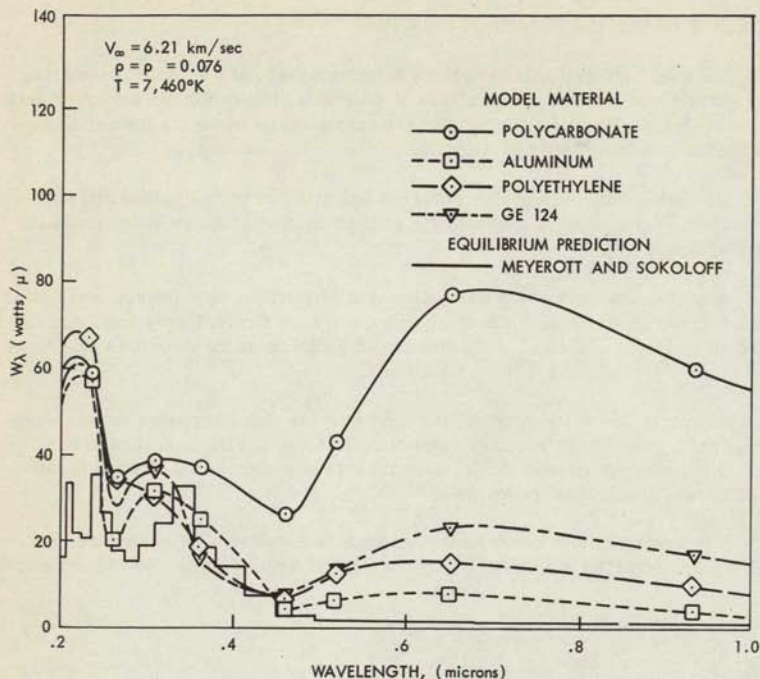
Figure 5—Radiant emission characteristics of different heat shield materials.
(From NASA Report TR R-193, April 1964[2].)

polycarbonate material exhibited a higher ablation product radiation than the other three materials. The experimental results at Ames have shown that radiant energy below 0.5 micron is predominately from the shock layer, the region in front of the blunt face vehicle. Energy at wavelengths longer than 0.5 micron is predominately ablation products radiation in the region starting at the edges of the blunt face and proceeding back to form the wake of the re-entry vehicle as shown in Figure 6.

Instrumentation used did not measure radiation above 1.0 microns. It therefore remains to predict the ablation products radiation above 1.0 micron and also the thermal blackbody radiation (infrared) resulting from vehicular heating. This

6
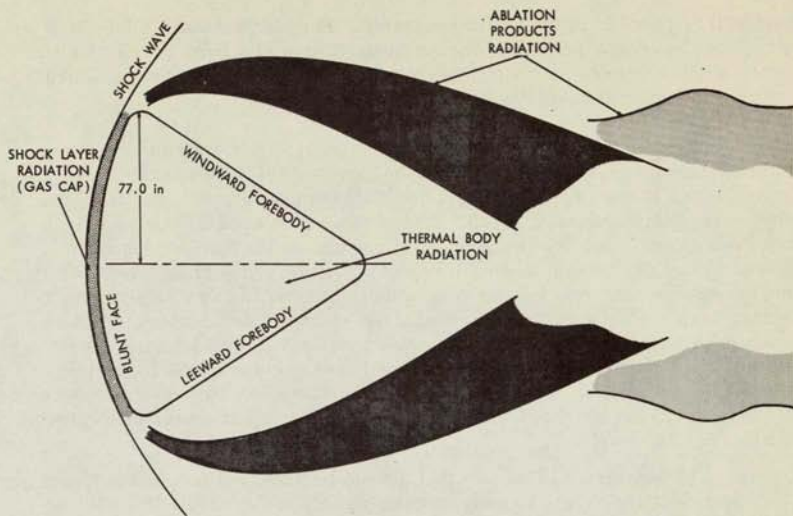
Figure 6—Apollo Command Module Radiation Regions

effect can be drawn in as was done in Figure 4, thereby providing essentially the total spectral profile of a re-entry vehicle.

Detection Wavelength Considerations

There are several good reasons for considering only the thermal body radiation and not the shock layer or ablation products radiation as the means for acquiring and tracking the Apollo vehicle during re-entry.

The shock layer (ultraviolet) radiation is seriously attenuated by the atmosphere and since the Apollo mission is planned for a daylight re-entry, the ultraviolet as well as the visible and near infrared would be difficult to detect in the presence of sunlit sky background.

By being responsive to the thermal body radiation (middle infrared), this would permit detection early in the re-entry cycle. Also, during any skip period where there is less ultraviolet or visible radiation, acquisition and tracking

7

would still be possible on the heated spacecraft. For clarification the following approximate waveband definitions are set forth: Ultraviolet from 1×10^{-4} to 0.4 micron; Visible from 0.4 to 0.7 micron; Near IR from 0.7 to 2.7 microns; Middle IR from 3 to 5 microns; and Far IR from 8 to 13 microns.

The radiation from the spacecraft (thermal body) is fairly predictable knowing the surface material composition and the expected heat rate inputs. An extensive amount of theoretical and experimental work has been done on the thermodynamic effects to the spacecraft. In fact, this is one area that had to be extensively investigated before design could proceed on the Apollo Command Module. Not so predictable is the ultraviolet or visible and near infrared radiation (shock layer and ablation products) which of course varies with altitude, re-entry angle, velocity, trajectory, range, etc. Also, experimental data indicates more scattering of radiation at shorter wavelengths. In addition, the day light sky background radiation which one would have to contend with by working in the ultraviolet, visible or near infrared is unpredictable. Data on atmospheric sky background however shows a noticeable dip in intensity at approximately four microns (see Figure 7).

Also to be considered is the fact that the sun impingement problem is a factor of approximately 20 less by being responsive only to the middle IR. The end result is of having less of a "dead zone" as the system scans across the sun.

There would also be less false target signals resulting from stars or other extraterrestrial sources.

Infrared Radiation

Although experimental and theoretical work has proceeded quite far in defining the radiation characteristics of a super orbital re-entry vehicle, it still remains a problem to predict the full scale infrared radiation from the heated surface of the Apollo spacecraft during re-entry. A study was therefore undertaken to define the boundary values for the maximum and minimum infrared radiation that the Apollo vehicle could generate (reference 3).

Although the final design will consider such factors as area of the source and aspect angles, in the following analysis, only maximum and minimum temperatures will be estimated. It will be shown that the temperature of the object lies between two values: a minimum temperature approximately equal to the ablation temperature of the material of the heat shield (assumed to be 1000°K) and a maximum temperature of approximately equal to the equilibrium temperature of the spacecraft at the stagnation point (2500°K).
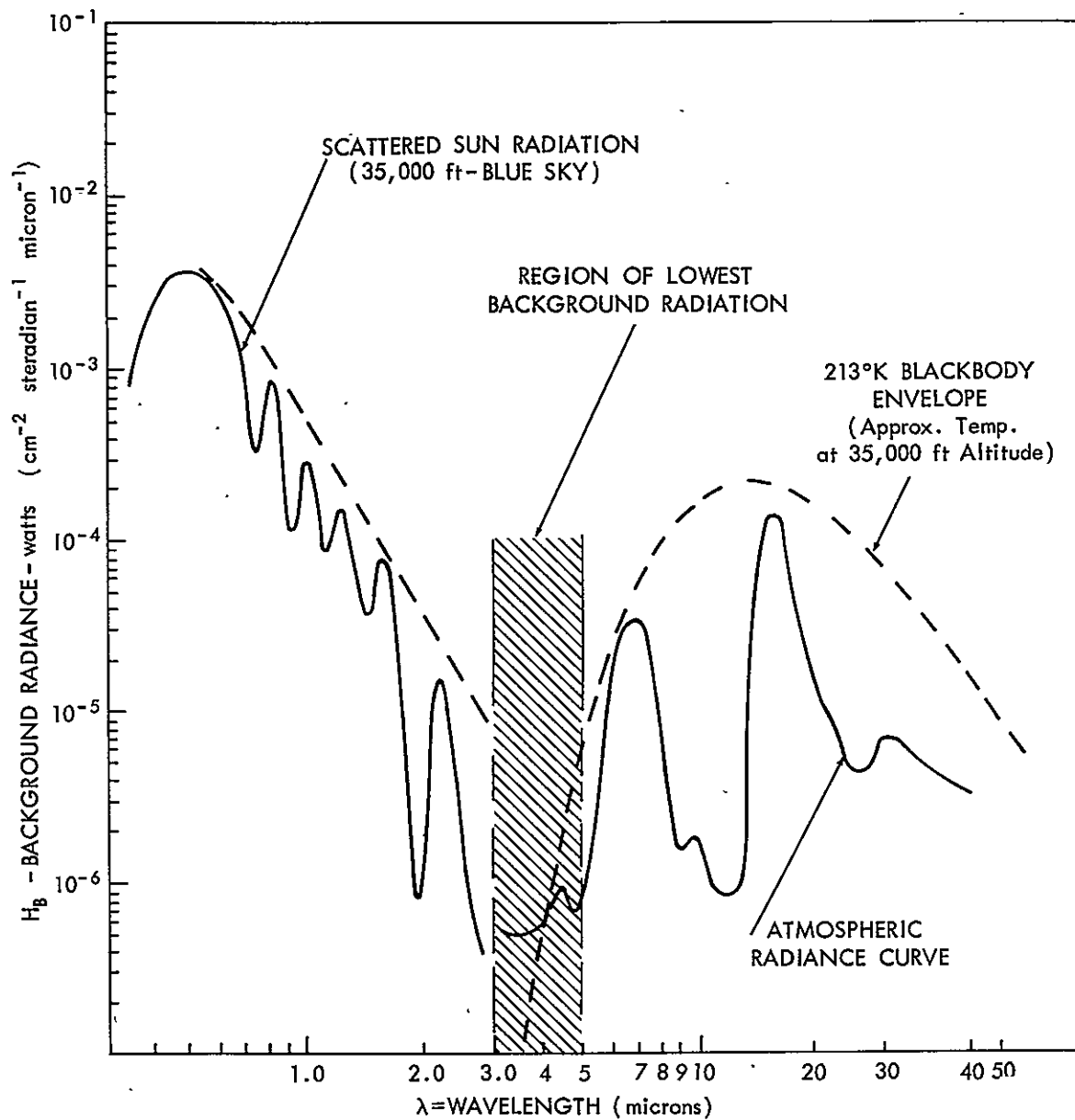
8

Figure 7—Typical atmospheric background radiance

The boundary values are established by making certain idealistic assumptions about the Apollo vehicle surface material. The maximum value is obtained by assuming a perfect radiative heat shield wherein all heat inputs are completely absorbed and radiated out. It is assumed that no heat is conducted into the vehicle and that the shield has no thermal capacity. These conditions result in an equilibrium temperature which is quite high and constitutes the "hottest" target possible.

The temperature at which the spacecraft reaches equilibrium is determined by calculating the rate of heat transfer to the spacecraft in the stagnation region which results from both friction with air molecules and from radiation of heated air within the shock wave. The total of these values results in an equivalent temperature of the spacecraft which is assumed to radiate as a blackbody at the equivalent temperature.

The minimum value is obtained by assuming a perfect ablative heat shield wherein all heat inputs are absorbed until the surface reaches 1000°K at which time the material ablates trading mass for thermal energy with no further increase in surface temperature and no re-radiation by the ablative products. Thus, the temperature of the minimum target would not exceed 1000°K.

Of course, neither of these idealistic heat shields exists in theory or practice but they do represent limiting characteristics of the ablative process.

Figure 6 illustrates the conditions existing during ablative re-entry. A shock layer of definite thickness is formed in front of the leading surface of the spacecraft as the material of the heat shield ablating product is transferred into a wake around the spacecraft.

As the Apollo vehicle enters the atmosphere, the heating process commences and the surface-temperature rises. When it reaches ablation temperature, further heat inputs are absorbed in changing the state of the ablation matter, say from solid to gas, which in turn is ejected into the boundary layer and carried away. If this process was ideal, the surface would remain at the ablation temperature. However, it is not ideal as the ablation temperature varies with reentry conditions and the ablation products injected into the boundary layer re-radiate at temperatures ranging from the ablation temperature to the stagnation temperature. Consequently, the infrared radiation can be expected to exceed that based on the ablation temperature alone once the ablation temperature is reached. As the ablation process proceeds, the ablative material recedes from the surface leaving behind a char. This char acts like a radiative heat shield in that it has low thermal capacity and poor thermal conductivity. Consequently, the char surface becomes hotter than the ablation temperature and radiates away some of the

heat input. It is obvious that the equilibrium temperature of the char will not reach that of the ideal radiative heat shield because some of the heat input is absorbed in the ablation process. Consequently, the infrared radiation can be expected to be less than that based on the equilibrium temperature of an ideal radiative heat shield.

The following analysis therefore endeavors to calculate the total heat input due to convective and radiative processes and from this determine the equilibrium temperature. The equilibrium and ablation temperature are then used to compute the boundary infrared radiation limits. The ablation radiation is calculated from extrapolated shock tube test data and represents the probable infrared radiation value. The shock wave is evaluated for its contribution to the infrared radiation and is merely added on to the above values. All calculations are based on stagnation point conditions for the Apollo size vehicle.

Convective Heating

Convective heating is due to direct contact of the vehicle with air molecules. Little (reference 4) cites a number of methods for calculating laminar stagnation point convective heating, and points out that most are too unwieldy for approximate heating analyses. He gives as a noteworthy exception the approximation of Lees (reference 5) which has been found to produce results close to the numerical mean of all methods considered for dissociating gases.

$$\dot{q}_c = 23.6 \sqrt{\frac{P_\infty}{R_o}} \, u_\infty^3 \times 10^{-9} \ \text{w/cm}^2 \tag{1}$$

where $\dot{q}_c$ = laminar stagnation point convective heating rate in w/cm²

P_∞ = free-stream density in slugs/ft³. This is based on the 1959 ARDC standard atmosphere and is plotted in Figure 9

R_o = axial radius (≈ 6.5 ft) of the spacecraft at the heat shield (see Figure 6)

u_∞ = velocity in ft/sec

This equation was used for calculating the laminar stagnation point convective heating rates for the Apollo size re-entry vehicle, and the results are plotted in Figure 8 as a function of altitude and velocity so that the heating rates for any re-entry trajectory may be obtained directly.

11
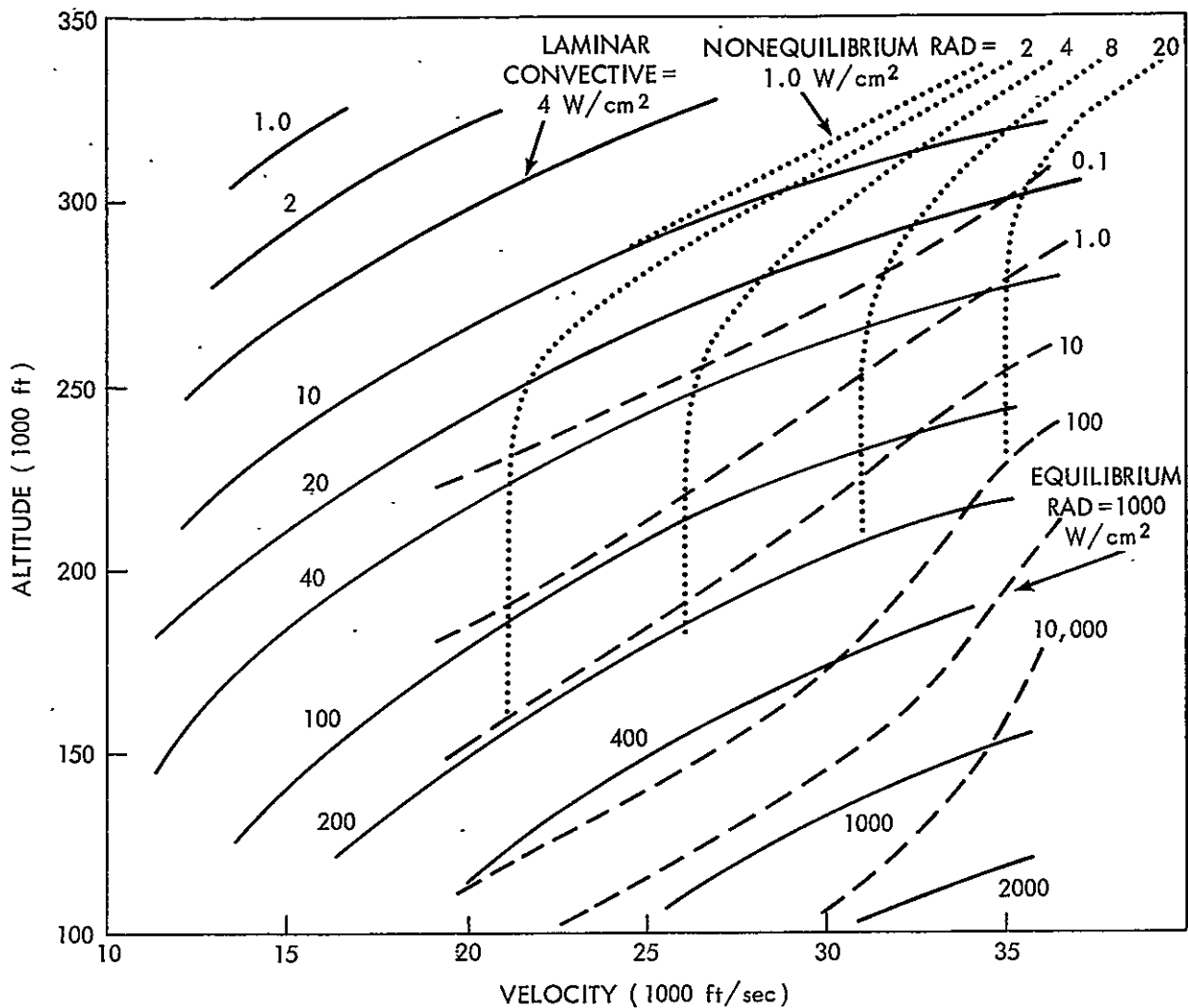
Figure 8—Apollo type re-entry stagnation point heating rates

A sample calculation is given below.

Given: Altitude = 200,000 ft

Velocity = 30,000 ft/sec.

R_o = 6.5 ft

P_∞ = 5.95×10^{-7} slug/ft^3. This is derived by reading from the curve of Figure 9 as follows:

$P_\infty = P_\infty/P_o \times P_o$, where P_o is the sea level density

= $2.5 \times 10^{-4} \times 2.38 \times 10^{-3}$

= 5.95×10^{-7} slug/ft^3

$$P_0 = 2.38 \times 10^{-3} \text{ SLUGS/ft}^3$$
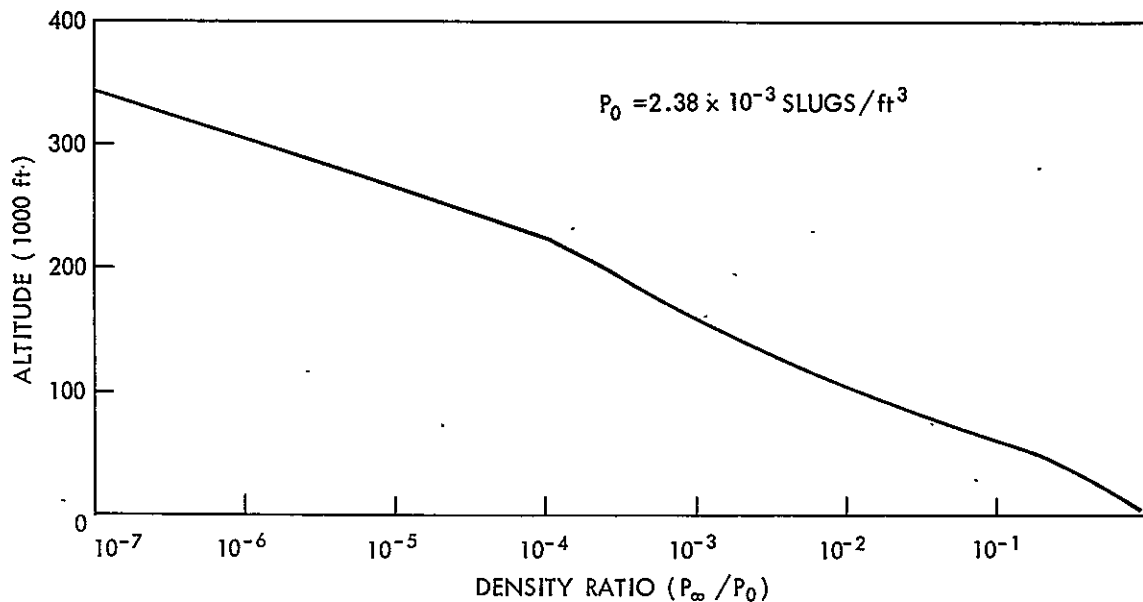
Figure 9—1959 ARDC standard atmospheric density

Substituting these values in Equation (1),

$$\dot{q} = 23.6 \sqrt{\frac{5.95 \times 10^{-7}}{6.5}} \times (3 \times 10^4)^3 \times 10^{-9} = 193 \text{ w/cm}^2$$

Radiative Heating

Figure 10 shows that the re-entering Apollo vehicle will encounter high shock layer temperatures. Thus, the emissivity of heated air becomes significant so that radiative heating from the shock layer becomes an important contributor.

There is a finite time for gas to react chemically to changes in temperature and, although small, is sometimes significant when compared to the time required for gas particles to move through the shock layer of a hypervelocity vehicle. This reaction\zone is referred to as a region of nonequilibrium. It constitutes a transition period between air at atmospheric temperature and density to air at shock layer temperature and density equilibrium, and thus exists at the forefront of all hypersonic shock waves.

Page (reference 6) refers to two distances into the forefront of the shock layer (δ_e, the excitation distance, and δ_r, the relaxation distance) which describe the depth of the nonequilibrium state. Page describes a model of the nonequilibrium state wherein there exists a temperature overshoot at δ_e resulting in the integral of radiation taken over the distance δ_r being larger than the radiation from an equivalent depth of equilibrium shock layer. Further, his model indicates that the integral of radiation taken over the distance δ_r is a constant independent of density.
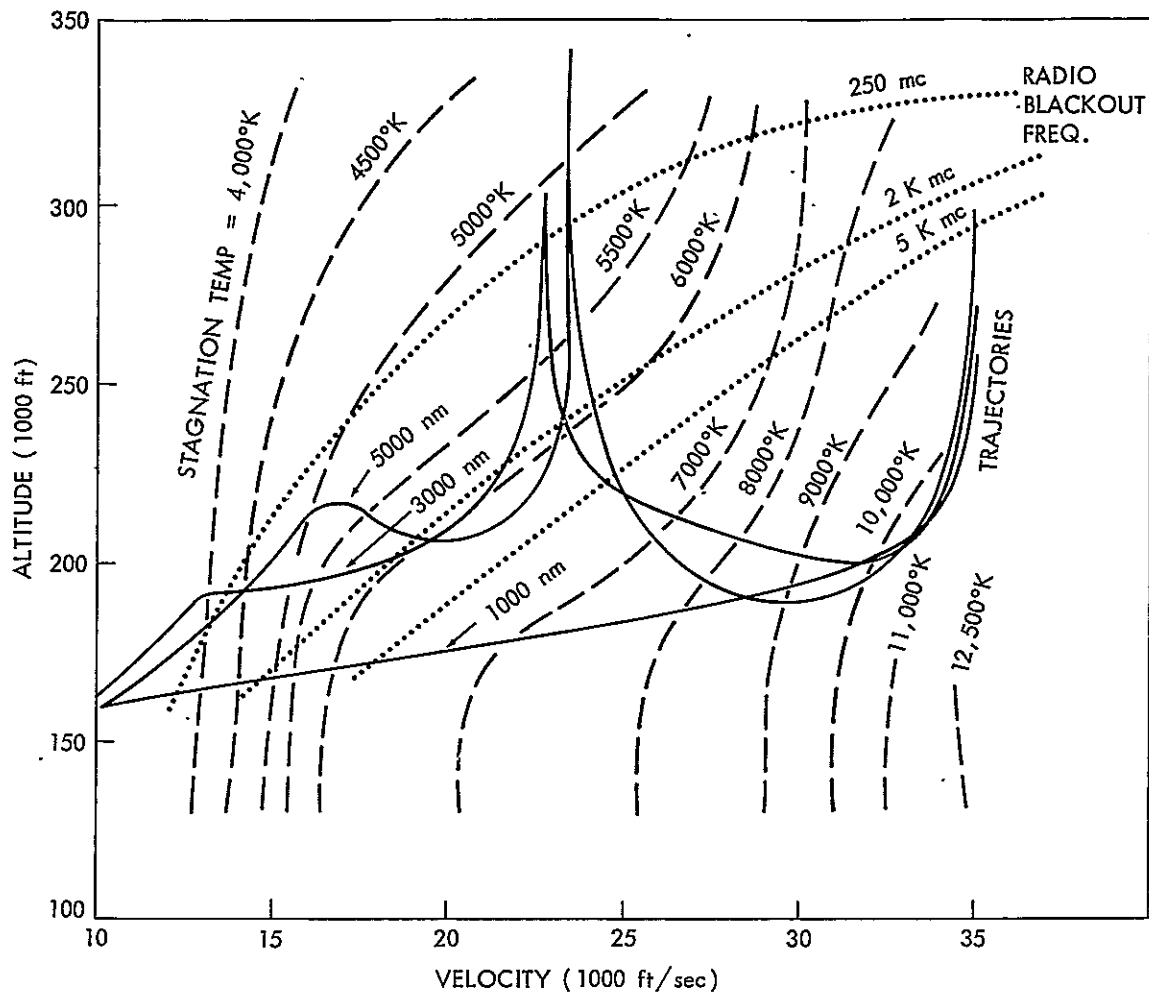
Figure 10—Apollo re-entry vehicle profiles. (Adapted from
NASA TN D-2732, March 1965[29].)

Both results are pertinent to any radiative heating analysis as may be better
understood from the following relations. Figure 11 illustrates the temperature
transition phenomenon as described above. The depth of the shock layer is de-
signated by δ_s and approximated by Page as

$$\delta_s = \frac{3R_o}{4\,P/P_\infty} \tag{2}$$

It can be seen that δ_s increases with density and size of the vehicle. Inasmuch
as the equilibrium radiation is proportional to this depth, it will likewise increase
with density and vehicle size. The nonequilibrium radiation in Page's model, how-
ever, is fixed and independent of both these factors so long as $\delta_s > \delta_r$. Conse-
quently, if the density and size are such that $\delta_s > \delta_r$, then the equilibrium

14
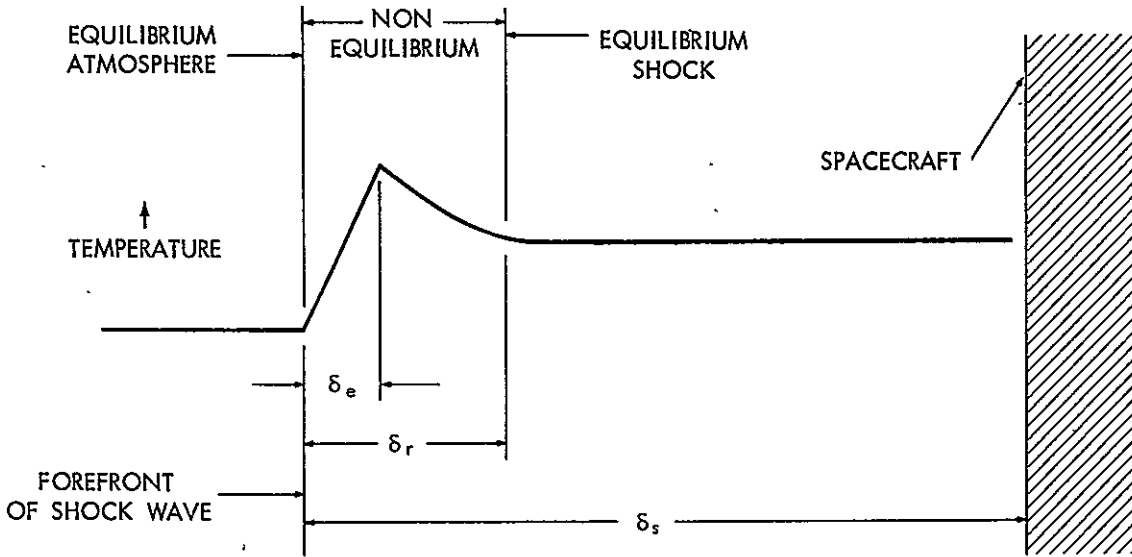
Figure 11—Shock layer temperature transition

radiation will constitute the principal source of radiation heating. If, on the other hand, these factors are such that δ_s approaches δ_r, then the nonequilibrium radiation will constitute the principal radiative heating source.

Any excited air which passes completely through the shock layer is expected to be quickly quenched. Therefore, if the flow time from the shock to the stagnation point is less than the relaxation time, the nonequilibrium radiation will be significantly reduced. This effect is called truncation.

In general, as a hypersonic velocity vehicle enters the atmosphere one can expect a nonequilibrium component of radiation to develop which will be an increasing function of density until such a density is reached that the shock layer thickness, δ_s, exceeds the relaxation distance, δ_r. This nonequilibrium component of radiation will then remain constant for all further density increases. However, as the density continues to increase with continual descent in altitude, the shock wave thickness, δ_s will approach a value where the equilibrium radiation equals the nonequilibrium value. Up to the time that this density was approached, the nonequilibrium component of radiation comprised the major source of radiative heating. From this corresponding density on to increasing values (or, conversely, altitude, on to decreasing values), the equilibrium radiation will continue to increase swamping out the fixed nonequilibrium component and thus prevail as the dominant radiative heating source. The magnitude of equilibrium radiation will be an increasing function of vehicle velocity and size. The magnitude of the nonequilibrium component will also be an increasing function of velocity

15

but independent of vehicle size. However, the altitude or density at which the nonequilibrium component reaches full maturity will be a function of vehicle size, since the shock standoff distance is proportioned to vehicle size.

Equilibrium Radiation. – Kivel (reference 7) presents data on the equilibrium radiation of hot air. Figure 12 taken from reference 8 gives the amount of radiation toward a body per cubic centimeter of air as a function of velocity and altitude. Also given is the stagnation point density ratio.

The equilibrium radiation heat rate is computed by selecting the radiation value per cubic centimeter from Figure 12 and multiplying this by the shock wave depth as determined from Equation 2. These results are also plotted in Figure 8.

A sample calculation is given below.

Given: altitude = 200,000 ft

velocity = 30,000 ft/sec

R_o = 6.5 ft.

The free-stream density ratio corresponding to the given altitude is obtained from Figure 9.

$$P_\infty/P = 2.5 \times 10^{-4}$$

The stagnation point density ratio corresponding to this free-stream density ratio and the given velocity is obtained from Figure 12.

$$P/P_o = 4 \times 10^{-3}$$

The ratio of stagnation point density to free-stream density is then

$$P/P_\infty = \frac{P}{P_o} \times \frac{P_o}{P_\infty} = \frac{4 \times 10^{-3}}{2.5 \times 10^{-4}} = 16$$

Inserting this ratio and R_o (6.5 ft = 198 cm) into Equation 2 yields the shock thickness.

$$\delta_s = \frac{0.75 \times 198}{16} = 9.3 \text{ cm}$$

16
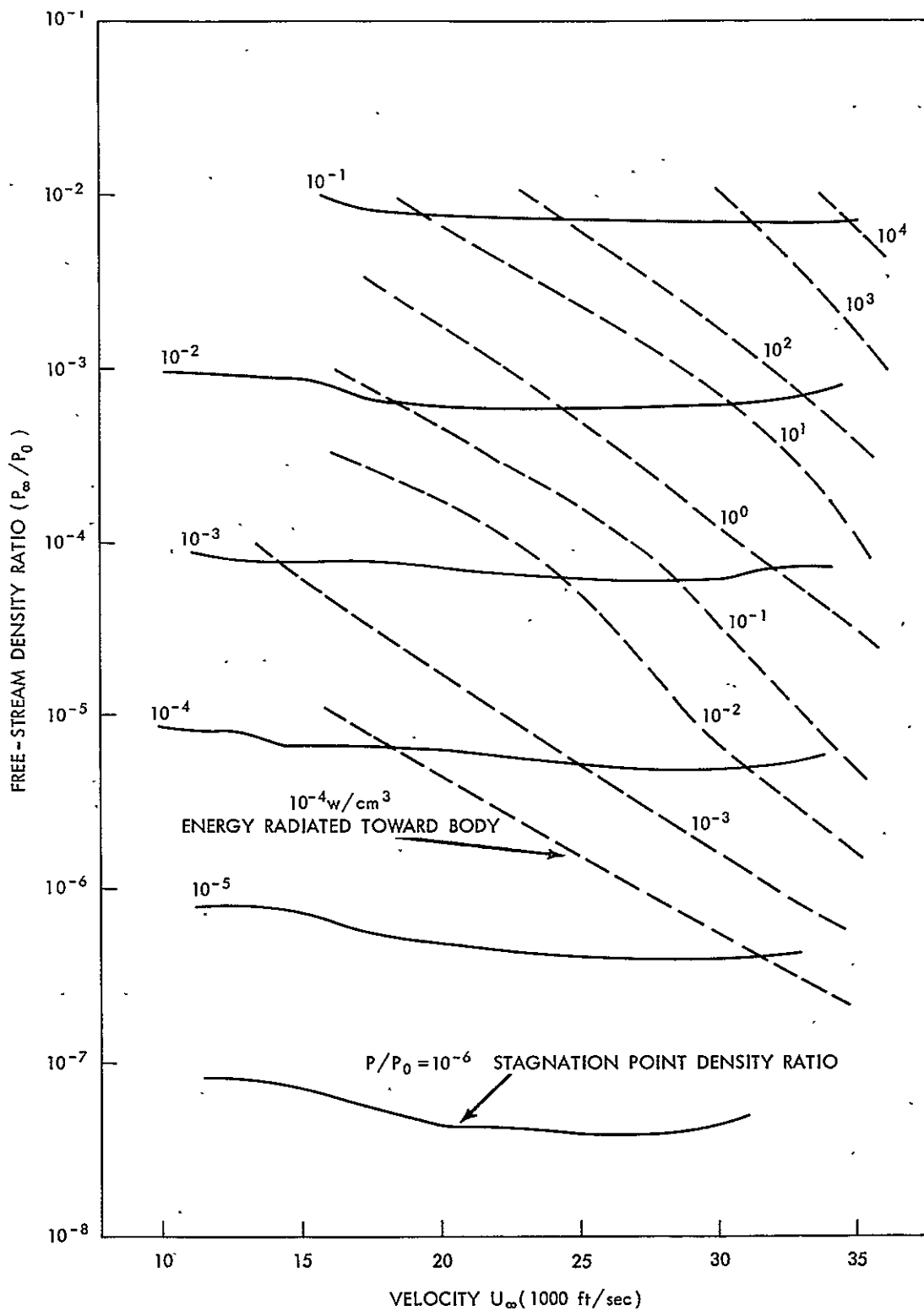
Figure 12—Equilibrium radiation

The energy radiated toward the body for the given altitude and velocity is obtained from Figure 12 and is seen to be approximately 3 watt/cm^3. Multiplying this value by the shock layer thickness yields the stagnation point equilibrium radiation heating rate, $\dot{q}_r$

$$\dot{q}_r = 3 \times 9.3 = 28 \text{w/cm}^2$$

Nonequilibrium Radiation.— Page (reference 6) has obtained measurements of total radiation for several velocities as a function of free-stream density. As a result, he was able to determine the free-stream density associated with each velocity at which the shock standoff distance just equaled the nonequilibrium relaxation distance, and consequently, the magnitude of the nonequilibrium radiation.

His measured data are shown by the solid curves in Figure 13. The dashed lines in Figure 13 are the predicted equilibrium radiation values. The difference between the measured total radiation and the predicted equilibrium radiation gives the nonequilibrium component.
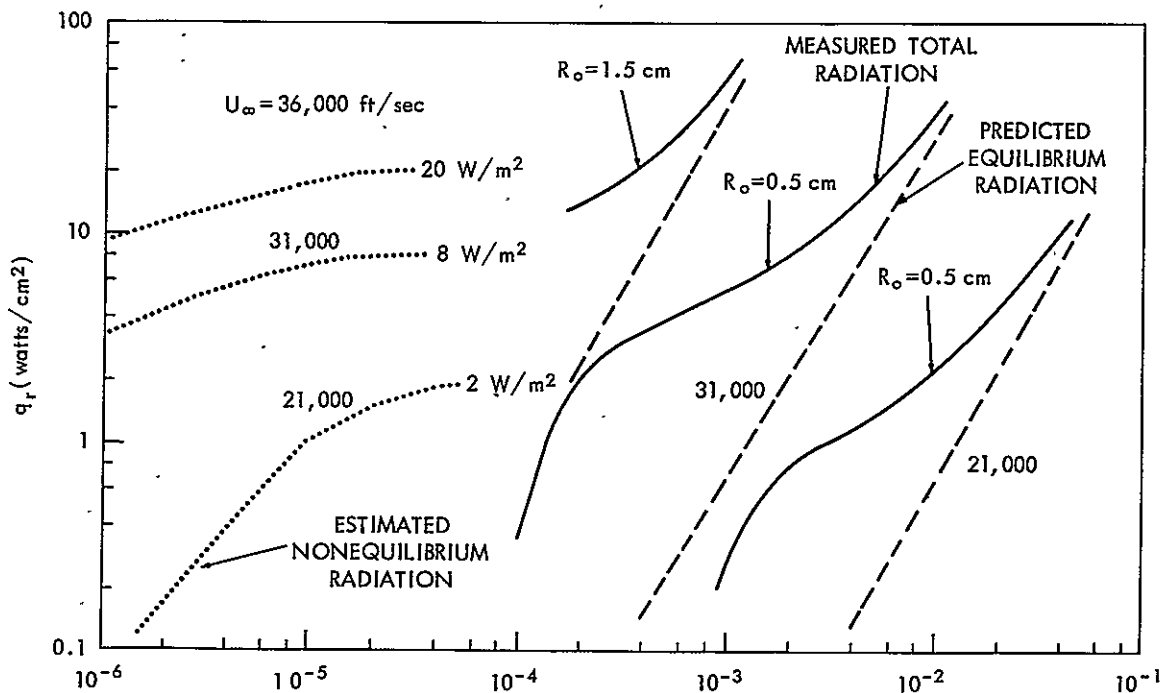
Figure 13—Nonequilibrium radiation

In accordance with Page's theory discussed earlier, this nonequilibrium component remains constant at any given velocity and is not a function of body size except for truncation effects. The width of the nonequilibrium zone is proportional to density, and the shock width is proportional to nose radius. Therefore, to determine the density at which the nonequilibrium component develops in the Apollo case, it is necessary to translate Page's nonequilibrium measurements by the ratio of the model nose radius to the Apollo vehicle nose radius. These results are shown as the dotted curves in Figure 13.

Using these curves as a basis, extrapolations of nonequilibrium radiation as a function of velocity and altitude are obtained and plotted in Figure 9. A sample calculation for the model is given below.

Given: R_o = 0.5 cm

U_∞ = 31,000 ft/sec

P_∞/P_o = 2 × 10^{-3}

The total radiation measured by Page shown in the Solid curve of Figure 13 for these conditions is

$$I_T = 8 \text{ w/cm}^2$$

The predicted component of equilibrium radiation from the dashed curve of Figure 13 is

$$I_e = 2 \text{ w/cm}^2$$

Therefore, the nonequilibrium component (I_n) is:

$$I_n = I_T - I_e = 6 \text{ w/cm}^2$$

Now the Apollo vehicle nose radius is approximately 200 cm while the model radius is only 0.5 cm. Therefore, the density at which this 6 w/cm^2 value of nonequilibrium radiation would be obtained in the Apollo case is 400 times lower than the given density or

$$P_\infty/P_{o(Apollo)} = 2 \times 10^{-3} \times \frac{0.5}{200} = 5 \times 10^{-6}$$

Hence, 6 w/cm^2 is plotted at this density in the dotted curve.

Conclusions

Surface Radiation Limits. – The boundary values of surface emission may now be obtained. The re-entry trajectory is first superimposed on Figure 8 and the total heat inputs are summed up for every point on the trajectory. The equilibrium temperature is then determined by solving Plank's blackbody equation.

$$T_{eq} = \sqrt[4]{\frac{\dot{q} \text{ total}}{\sigma_{\epsilon}}} \; °K$$

A sample calculation is given below.

Given: Altitude = 200,000 ft

Velocity = 30,000 ft/sec

From Figure 8 the input heat rates are:

convective $\dot{q}_c$ = 193 w/cm²

radiative { equilibrium $\dot{q}_e$ = 28 w/cm²

nonequilibrium $\dot{q}_n$ = 7.5 w/cm²

Total $\dot{q}_T$ 228.5 w/cm²

The equilibrium temperature from equation 3 is then

$$T_{eq} = \sqrt[4]{\frac{228.5}{5.7 \times 10^{-12}}} = 2500°K$$

The temperature of the re-entering spacecraft during ablative re-entry will lie between 1000°K and 2500°K.

ATMOSPHERIC TRANSMISSION AND BACKGROUND RADIATION

Atmospheric Transmission

A number of different atmospheric constituents act to attenuate an infrared signal as it passes through the atmosphere from the source to the receiving apparatus.

The effect of the earth's atmosphere must therefore be seriously considered in the analyses of the capability of infrared sensing equipment.

The atmosphere is composed of a mixture of gases in which are suspended a wide variety of particles distributed over a great range in size and which also differ in chemical composition. These gases cause radiation to be absorbed, and the suspended particles scatter the radiation.

The gases present in greatest abundance in the earth's atmosphere (reference 9) are nitrogen, oxygen, water vapor, carbon dioxide, methane, nitrous oxide, carbon monoxide, and ozone. Fortunately, the two gases present at the highest concentrations, N_2 and O_2, are homonuclear. They, therefore, possess neither a permanent nor an induced electric moment and hence do not exhibit molecular absorption bands.

Over the range of altitudes extending from sea level to approximately 40,000 feet, water vapor and carbon dioxide are by far the most important absorbing molecules. The concentration of H_2O varies between $10^{-3}\%$ and 1% (by volume), depending upon geographical location, altitude, time of year, and local meteorological conditions. Carbon dioxide, CO_2, is much more uniformly distributed; it varies between 0.03 and 0.04% and is greater in an air mass which has been over heavy vegetation than in the atmosphere over the ocean. The distribution is more uniform at higher altitudes where the mixing is more complete. Methane, CH_4, is present at a concentration between 1×10^{-4} and 2×10^{-4}, and is very uniformly distributed in altitude. Nitrous oxide, N_2O, at concentrations of 3×10^{-5} to $4 \times 10^{-5}\%$ and carbon monoxide, CO, with a typical concentration of $2 \times 10^{-5}\%$ have bands which show up if long paths are utilized. Ozone, O_3, is present at concentrations as large as $10^{-3}\%$ at altitudes near 100,000 feet, but it is present at much lower concentrations at other altitudes.

The atmospheric transmission was calculated by using the procedures established by Altshuler (reference 10). He considers a model consisting of infrared absorbing atmospheric constituents CO_2, O_3, N_2O, CH_4, CO, and water vapor and their variation in accordance with temperature and pressure changes with altitude based upon the 1959 ARDC model atmosphere. He also takes into account the earth's curvature and refraction of infrared in the earth's atmosphere.

Consideration of the relative distribution with altitude above 40,000 feet of the CO_2 and water vapor absorbers as derived from Altshuler indicates that the bulk of the absorber exists below 100,000 feet. Therefore, the absorbing atmosphere was considered to exist only to an altitude of 100,000 feet. It is then sufficient to calculate the atmospheric transmission between the altitudes of 40,000 and 100,000 feet as a function of look angle from 0 to 90 degrees and apply the results directly to the Apollo case regardless of the Apollo vehicle altitude.

Based on the above considerations, Altshuler's procedures were used to calculate the spectral transmission of the atmosphere out to a wavelength of 3.5 microns as a function of look angle from 0 to 90 degrees from a 40,000 foot platform. These results are plotted in Figure 14.
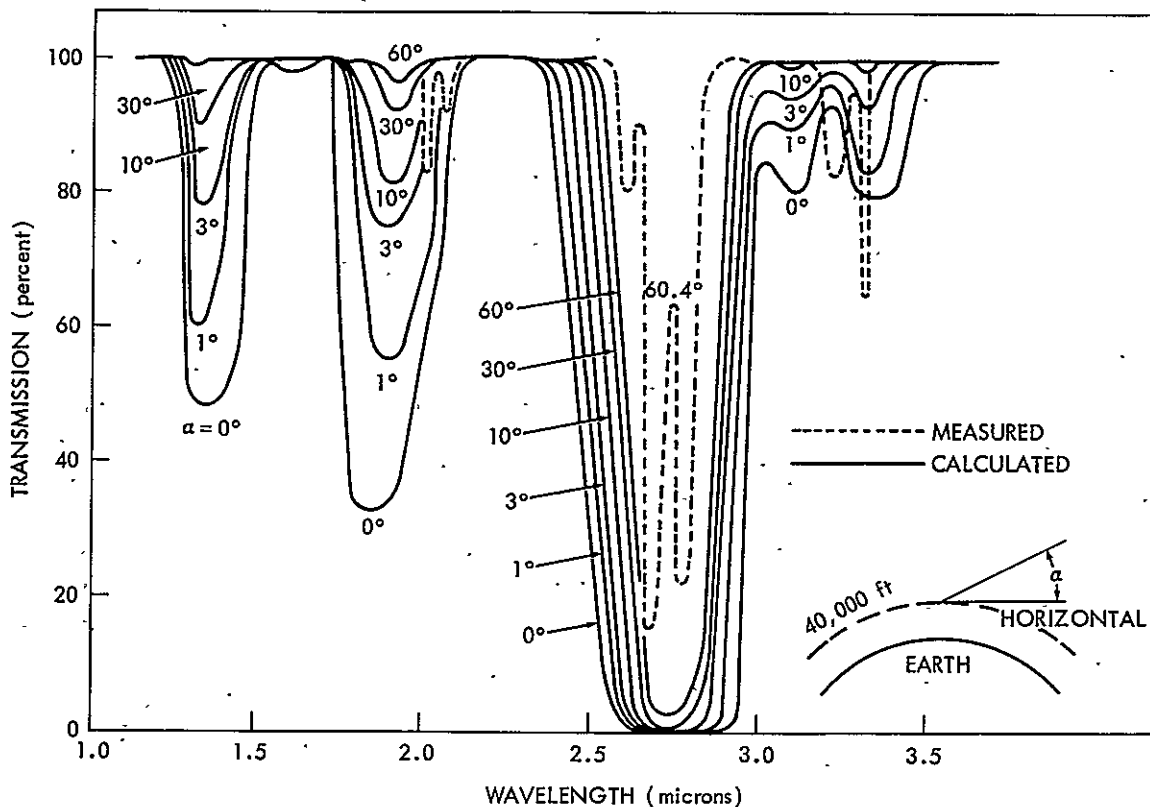

Figure 14—Atmospheric transmission

To check the validity of these results to the actual case, the calculated results were compared with experimental measurements. Murcray (reference 11) has made measurements with a balloon of the atmospheric transmission as a

22

function of altitude. . A set of his data obtained at 40,000 feet with a look angle of 60.5 degrees is also shown in Figure 14. Although his data shows a higher resolution, it is in good agreement with the calculated curves. of Figure 14 and one can therefore conclude that these curves are both realistic and applicable.

It remains then to calculate the atmospheric transmission out to a wavelength of 5 microns to cover the 3 to 5 micron transmission band; however, there is no reason to believe that with the above considerations and using Altshuler's procedures that the calculations would not be in good agreement with actual measured conditions.

Background Radiation

The infrared system must acquire the target source radiation while discriminating against other sources of radiation within the field of view of the infrared system. Since all objects at temperatures above absolute zero emit energy in the infrared, the background radiation is always present and thus it competes with the target source radiation. It is therefore necessary to consider the characteristics of the background radiation in the effective analysis of any infrared system.

Competing background radiation can exist in many forms.

Background radiation from the sky is caused by scattered sunlight from water droplets, molecules, and other particles, suspended in the atmosphere and from the thermal emission of the atmospheric constituents themselves:

Extraterrestrial sources such as the sun, moon, stars and planets contribute to the overall sky background radiation. However, the larger effect, except for the sun, is one of appearing as false targets, or as in the case of the sun of limiting the usefulness of the scanner as the infrared system scans across the sun.

Radiation associated with the instrumentation platform and the instrument itself has to be considered. In this case, the platform is a high altitude multi-engine jet aircraft and the radiation of the jet engine exhausts would have to be considered for their effect, if any. Also, any aircraft appendages such as the vertical stabilizer could reflect and radiate energy into the infrared receiver. The heating of the optics from the friction of the high speed air moving over the optics has to be considered.

Another "false target" worth mentioning is the Apollo Service Module which could also be re-entering the earth's atmosphere at about the same time and in near proximity to the real target — the Apollo Command Module.

23

Sky Background

The radiation from a clear sky results mainly from two sources:

1. The scattering of the radiation from the sun.

2. The thermal emission from the constituents of the atmosphere.

The sun radiates nearly as a 6000°K blackbody and is radiating approximately 3×10^3 watts cm^{-2} μ^{-1} steradian $^{-1}$. Measured on the earth's surface the clear sky radiance is approximately 3×10^{-3} watt cm$^{-2}\mu^{-1}$steradian^{-1} at .5 micron. An exact measurement of the scattered sunlight in the wave band of interest and at the desired altitude would necessarily have to take into account the meteoro- logical conditions and the position of the sun in reference to the infrared equip- ment. Sky maps showing lines of constant radiance in the .6-2μ region taken at Pikes Peak (elevation 14,000) (reference 12) are shown in Figure 15. Additional material in the referenced article also shows sky radiance maps taken at 1000 and 6000 feet as a comparison. The variance of sky radiance is apparent and is to be expected as the infrared system scans the hemisphere. This variation in intensity would give rise to a low frequency signal which if large enough could cause limiting in the infrared system preamplifier circuitry. Less variation in intensity is to be expected at the higher aircraft altitude of 35,000 feet.
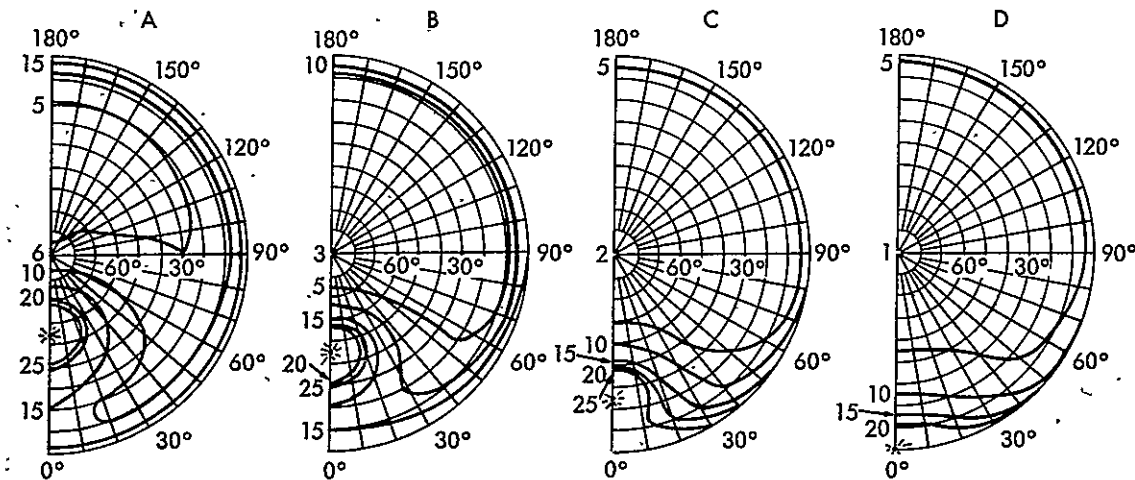
Figure 15—Sky maps showing lines of constant radiance in w/m^2-sterad in the 0.6-2μ wave- length region at Pikes Peak, September 15. The data were taken at: A, 12:05 P.M., sun elev. 54.°; B, 2:06 P.M., sun elev. 43°: C, 3:47 P.M., sun elev. 27°; and D, 6:05 P.M., sun elev. 0.°. (From the Journal of the Optical Society of America[12].)

As to be expected at the longer wavelengths, the scattered sunlight is less because of the reduced intensity of the sun's radiation at the longer wavelengths. At above 4 microns, the atmospheric thermal emission is predominate and the scattered sunlight can be neglected for most practical purposes at these wavelengths. In fact, it has been found experimentally that under nearly all conditions, the atmospheric emission and scattered sunlight are equal in the 3 to 4 micron range. Measurements taken at high altitude (30,000 to 40,000 feet) show this to be true but over a broader range extending to 5 microns. Two curves are presented from the measurements made by Bell et al, reference 13, in Figures 16 and 17. These curves are a measure of the clear sky thermal emission at Pikes Peak and Colorado Springs and of the clear sky sun scattered radiation and thermal emission measured at Colorado Springs, Colorado.

Figure 16—Clear zenith sky thermal emission measured at Pikes Peak, Colo.; elevation 14,110 ft.; ambient temperature 2.5°C and Colorado Springs, Colo.; elevation 6000 ft.; ambient temperature 27.5°C. (By permission McGraw-Hill Book Company, Inc., New York[20].)
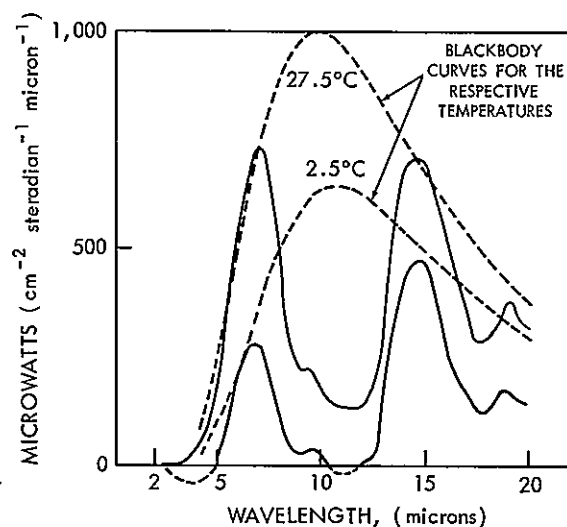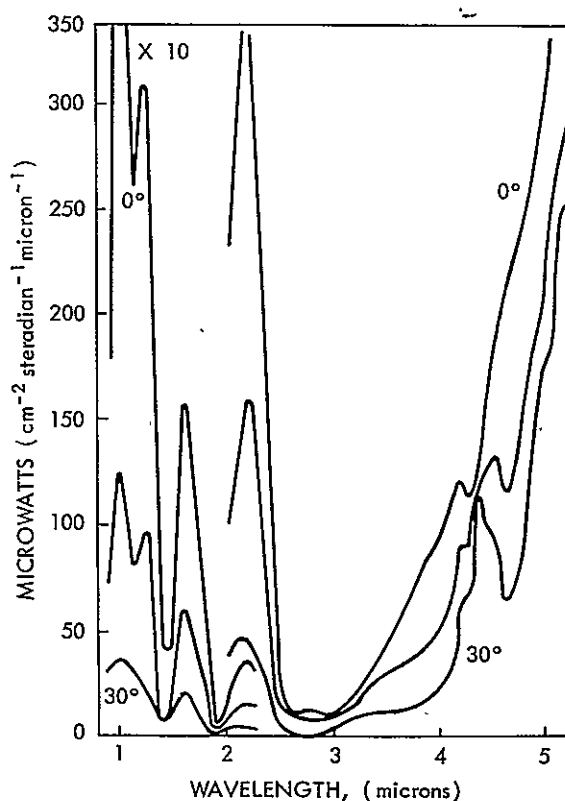
Figure 17—The spectral radiance of the clear noon sky as measured from Colorado Springs, Colo. The elevation angles starting with the upper curve are 0°, 7.2°, and 30°. Note that the radiance values, below about 2μ, are ten times larger than the ordinate scale shown. (By permission McGraw-Hill Book Company, Inc., New York[20].)

25

Celestial Background

Celestial background is not considered to be a problem in the middle and far infrared except for the sun and the moon. It is interesting, nevertheless to look at the stellar irradiance in the infrared of several stars and compare this with the irradiance in the visible the basis upon which the above conclusion can be drawn.

A notable piece of work done in this area is that by Walker and D'Agati, Reference 14, who have compiled data on seventy-one stars. The data is in the form of a table in absolute energy units and is for discrete wavelength in the infrared region from 1.0 to 10.0. Also given is the response at .566 for comparison.

It is not unreasonable to consider an infrared system with a sensitivity of 10^{-12} watts-cm^{-2}. An examination of the table in the referenced material will reveal that at wavelengths longer than 2.5 there are very few stars with irradiance values greater than 10^{-12} watts-cm^2.

However, at wavelengths shorter than 2.5 microns and especially in the visible, there are many stars with energy levels greater than 10^{-12} watts-cm^2. These would be detected and would show up as false targets on the operators screen. In fact the ability to see stars in the daylight with small field-of-view star tracker systems is used by aircraft to obtain guidance information for navigation purposes.

Other infrared stellar measurement programs indicate the same result — the absence of sources of detectable intensity at the longer infrared wavelengths. For instance, the study by Hall (Reference 15) presents the results of an infrared stellar mapping program where measurements were made of the clear night sky in three spectral regions of the infrared.

Significant results were obtained only for the shorter wavelength region (1.3-3.0). Figure 18 is included to show the relationship of the blackbody radiation curves for some celestial objects.

Platform and Optics Radiation

The location of the scanner exterior to the aircraft is such that the scanner would be subject to air friction heating and the vertical stabilizer would partially obscure the field-of-view of the infrared system and it would also act to reflect background radiation into the system. See Figure 19.
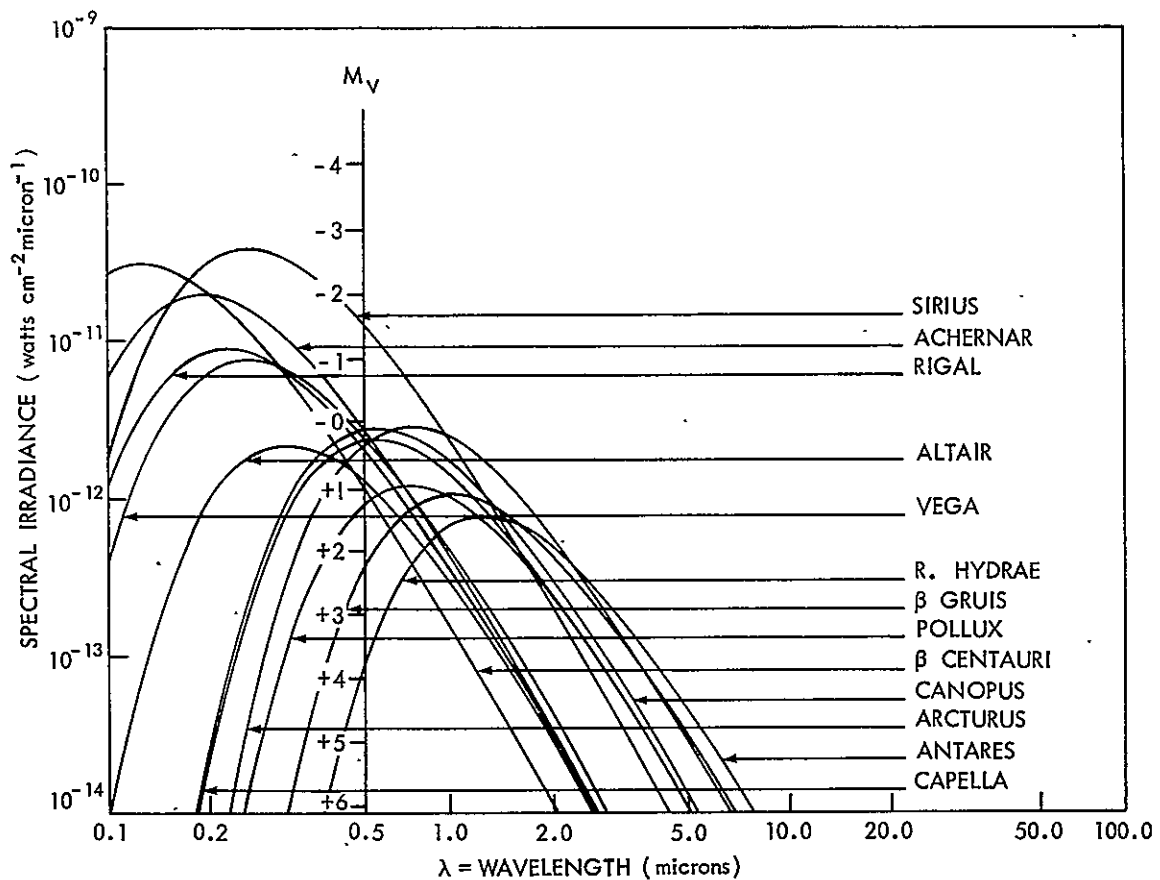
Figure 18—Spectral irradiance of bright stars

Radiation from the jet engines or exhaust is not considered a serious problem because of the location of the scanner on top of the aircraft fuselage and the limited downward scan angle.

Figure 20 is a plot of the stagnation temperature on an irdome or optics versus aircraft mach number. It may be seen that at the expected aircraft altitude (30k to 40k feet) and at a speed less than mach 1 that the temperature of the irdome or optics is actually less than standard room temperature conditions. Therefore, no degradation in performance would be expected; in fact, a slight improvement should be experienced.

Cloud-Cover Analysis

Of direct concern, obviously is the occurrence of clouds over the expected Apollo re-entry area. Clouds above the aircraft altitude of 35,000 feet, if between
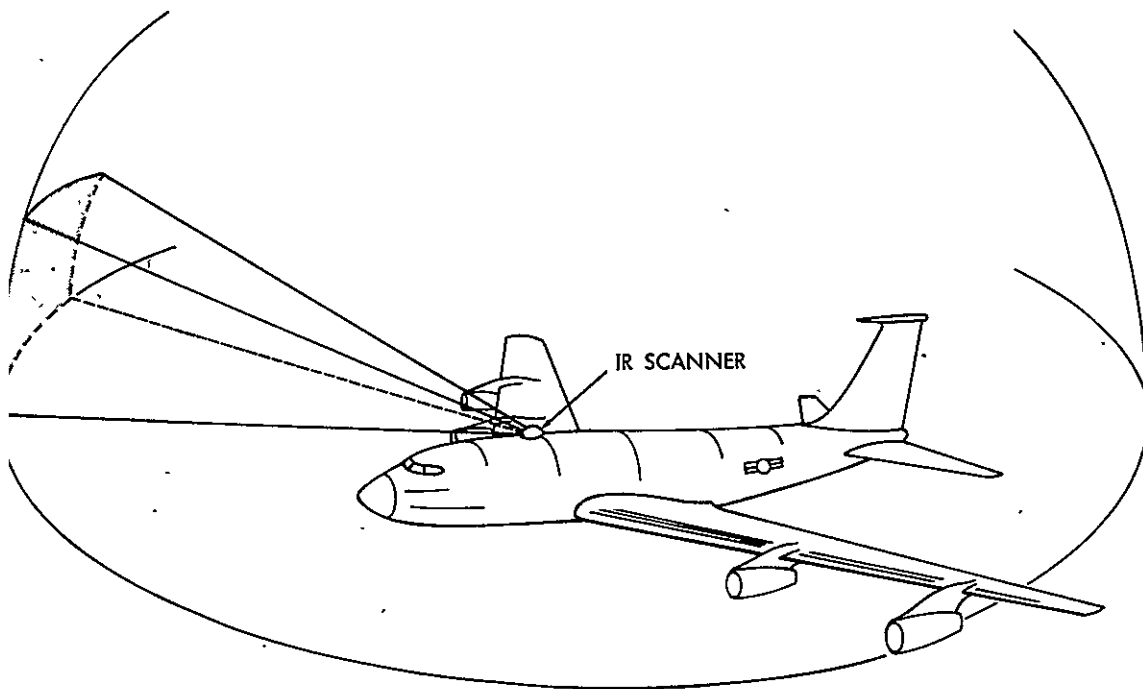
Figure 19—Location of infrared scanner on aircraft

the target and the sensor, would seriously attenuate the signal received by any optical device. If the clouds were not in the line of sight but still within the search field of the infrared equipment, then the cloud could reflect sufficient sunlight to appear as a target on the operators screen. This is not considered a serious problem since discrimination·circuitry is available to cancel cloud background signals and also the operator can exercise a good deal of judgement in choosing the real target — the Apollo command module from the relative velocity of the target in respect to the background and from the trace on the operator's screen.

The more serious of the two problems is the one of having clouds above the aircraft altitude which would block the radiation reaching the sensor and thereby reducing its operational capability. This problem was considered early in the conceptual stages for the development of the infrared system and accordingly the U. S. Weather Bureau, Space Flight Meteorological Group, was asked for assistance in defining the cloud problem over the Apollo re-entry area. The area encompasses approximately 18 million square miles in the Western Pacific. A study was undertaken by this group compiling data taken over several years to arrive at a climatology analysis. The results of this study are presented in Appendix C.

$$T = T_\infty + u_\infty^2 / 2\,g\,j\,C_P$$
u = VELOCITY (ft/sec)
g = 32.2 ft/sec^2
j = 778.2 ft lb/btu
C_P = .25 btu/lbs °R
T_∞ = FREE STREAM TEMP.
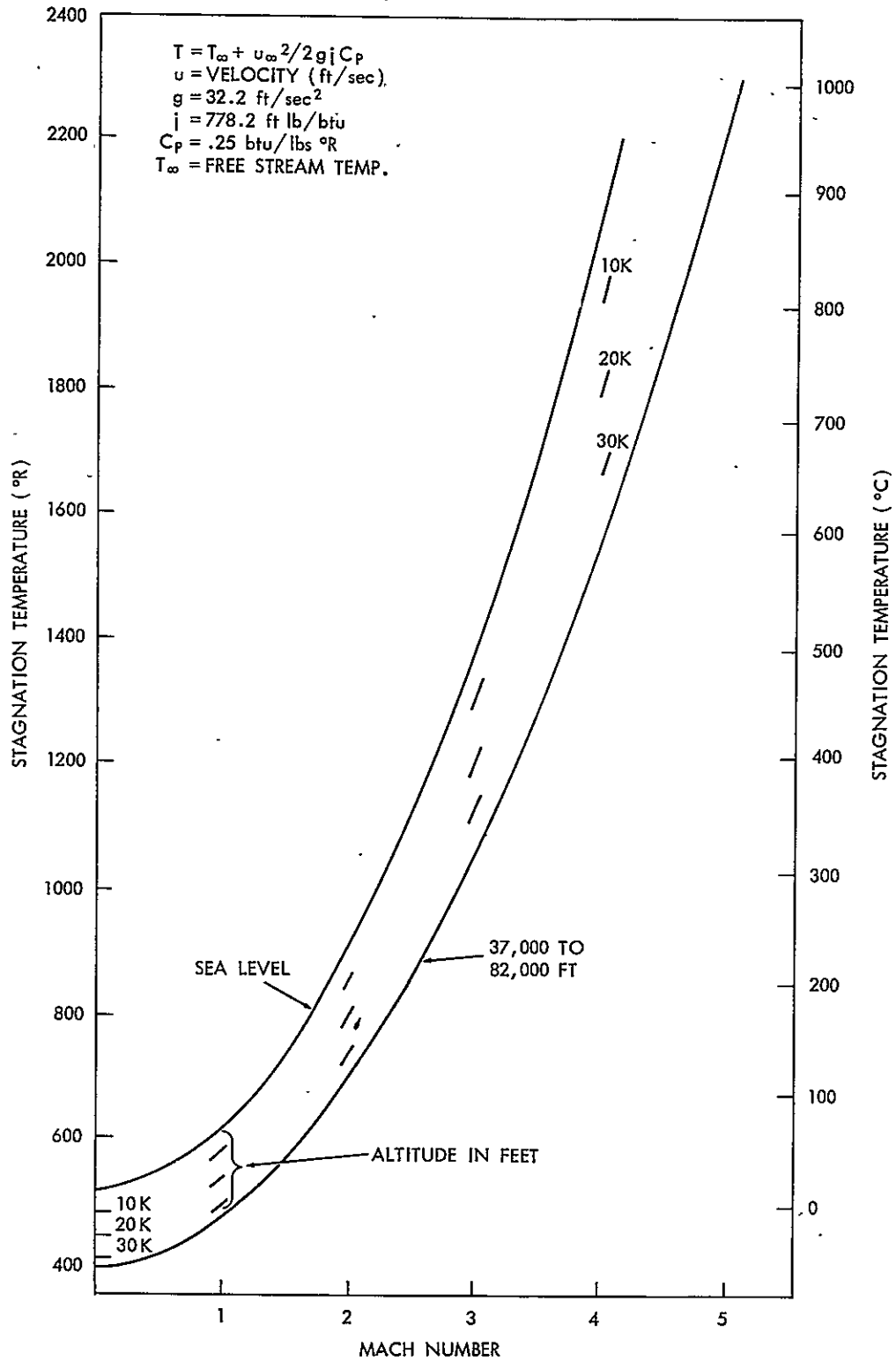
Figure 20—Irdome stagnation temperature vs. mach number

Briefly, the average results show that for 45 percent of the re-entry area there would be clear skies greater than 90 percent of the time above the aircraft. For 50 percent of the area there would be clear skies from 50 to 90 percent of the time, and for 5 percent of the area, less than 50 percent of the time would there be clear skies.

It is interesting to note that the area of high cloudiness is a result of the inter-tropical convergence zone which is a rather well defined area. In fact if one would station an aircraft fifty miles from a cloud top which reached 50,000 feet, viewing would still be possible down to less than three degrees above the horizon. It should also be stressed that eight aircraft would be deployed to cover the re-entry trajectory so that if the field of view of one infrared system was obscured by clouds it would be highly unlikely that the other systems would be which are situated hundreds of miles apart, Reference 16.

Also, if the field of view of any one of the infrared systems was partially obscured by clouds so that there were clear spaces between the clouds, continuous spacecraft tracking would still be possible across the sky because of the memory track capability built into the system.

It was therefore concluded from the report that the Apollo operational requirements could be met by the infrared systems operating on highly mobile aircraft flying at high altitudes.

SYSTEM DESIGN CONSIDERATIONS

The mission support requirements for the infrared system are such, Reference 16, that it should have the capability of searching out the total hemisphere, acquiring the target, and locking onto and tracking the target thereby generating angle coordinate information for pointing other communication antennas, derivation and recording of the Apollo re-entry trajectory, and generation of impact point prediction.

The angular rate of the Apollo vehicle in reference to the infrared system, see Figure 21, requires that constraints be placed upon the time allowed to search out the hemisphere and associated "lock on" time once the target has been identified. Since these constraints directly enter into the design of an infrared system in terms of dwell time, bandwidth, resolution, etc., an analysis of the problem is herein presented.

Hemispherical Search

The geometry of the problem is as shown in Figure 22. Here it is seen that. the hemispheric search volume is truncated on the top at the altitude above which the Apollo vehicle can neither be detected because it has not re-entered the atmosphere to generate sufficient radiation for detection and because the skip trajectory is not expected to exceed this altitude. The effect of limiting the required range above this altitude is to limit the required dynamic range of the infrared system. For the analysis however, a hemisphere is considered and the equations are derived on this basis.

Design Analysis

The design analysis proceeds by first deriving a general equation for calculating the sensitivity of an infrared search system considering the geometry of the problem and other parameters involved. The equation is presented for calculating the irradiance at the receiver and appropriate range, atmospheric transmission. Optical and detector parameters are inserted in the equations and a comparison is made between the irradiance at the receiver and the system sensitivity.

The geometry of the problem is presented in Figure 23, where

A = Total azimuth search field - radians
B = Total elevation search field - radians
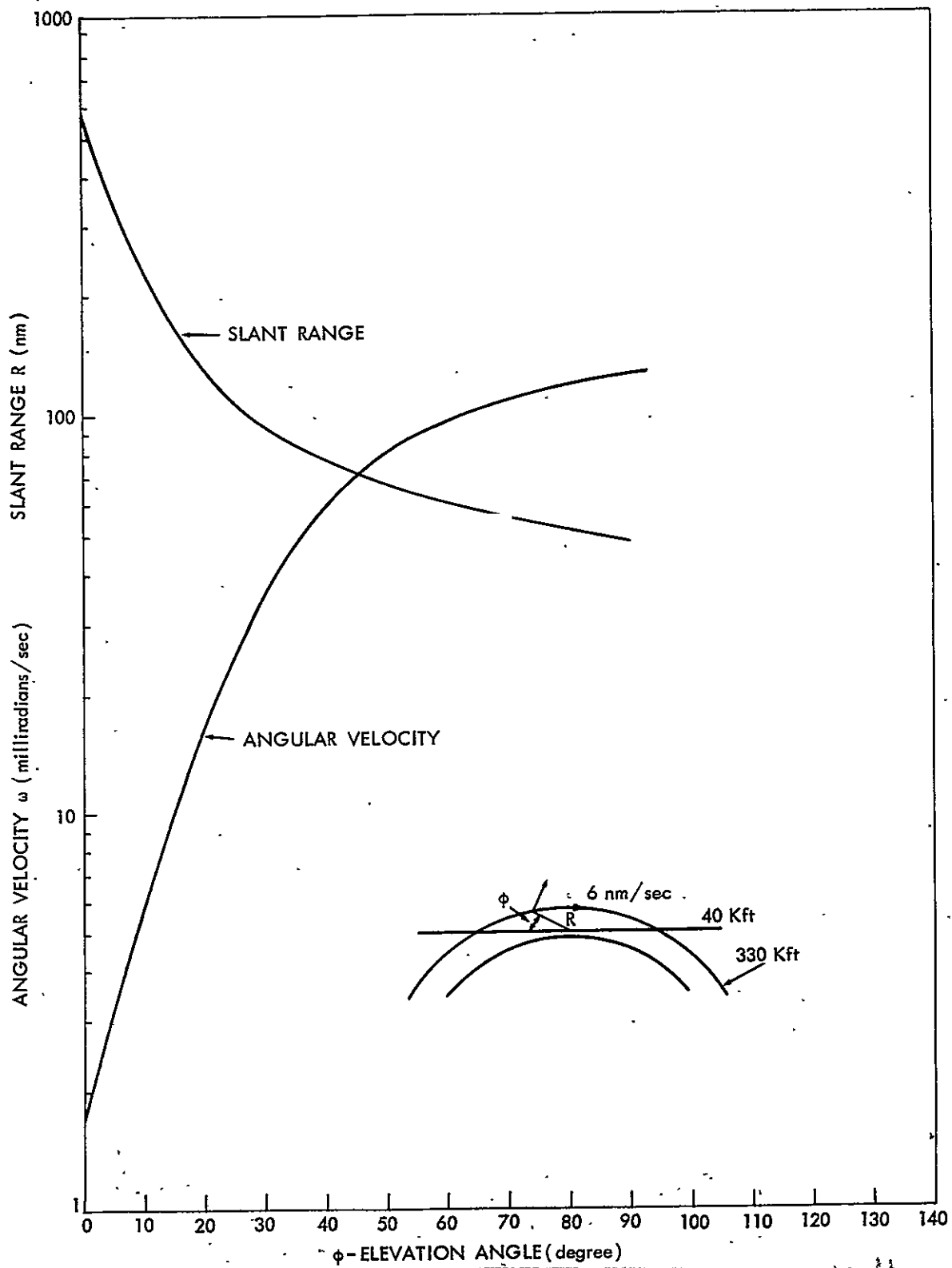
Figure 21—Angular velocity and slant range versus elevation angle
of the IR tracker during Apollo re-entry.
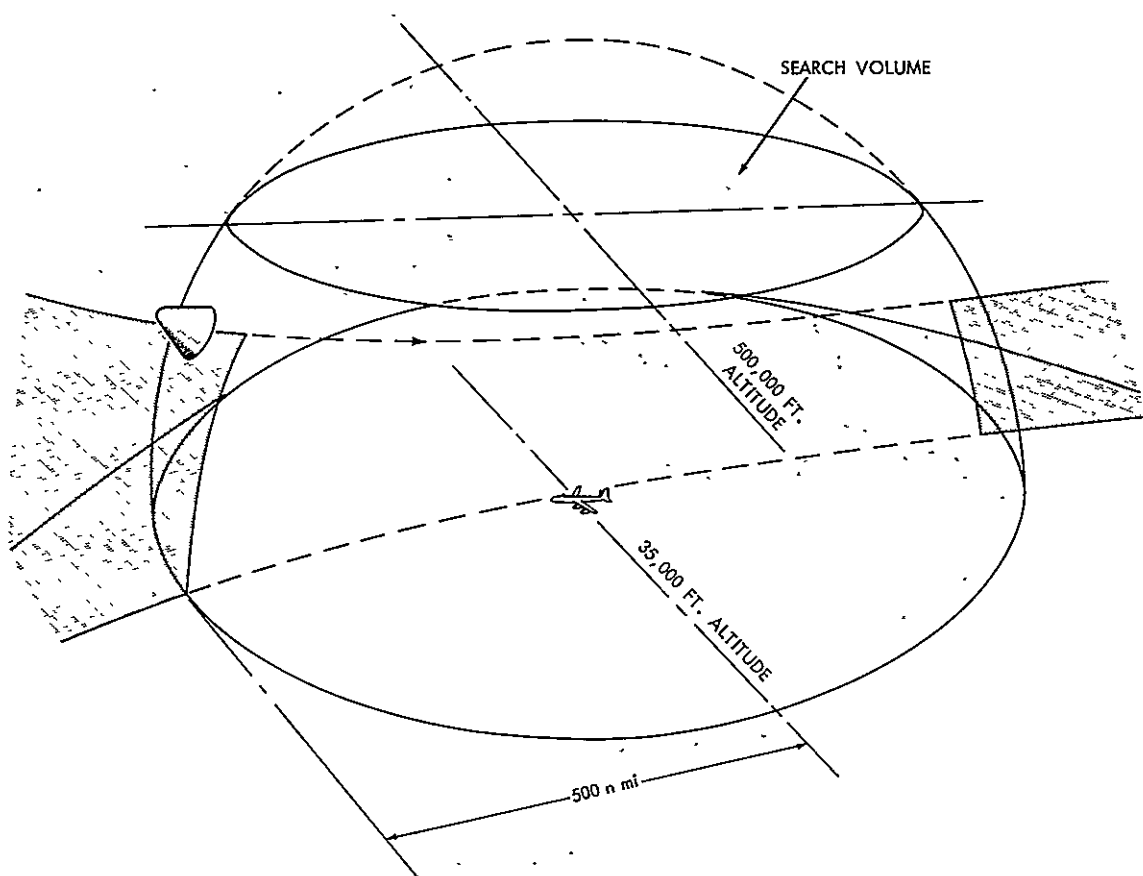
Figure 22—Apollo re-entry — IR search volume

a = Instantaneous azimuth field of view – radians

b = Instantaneous elevation field of view – radians

D_o = Entrance aperture diameter of collecting optics – cm

θ = Angle of projected instantaneous field of view – radians

f_L = Focal length of optics – cm

d_w = Width dimension of detector – cm

d_ℓ = Length dimension of detector – cm.
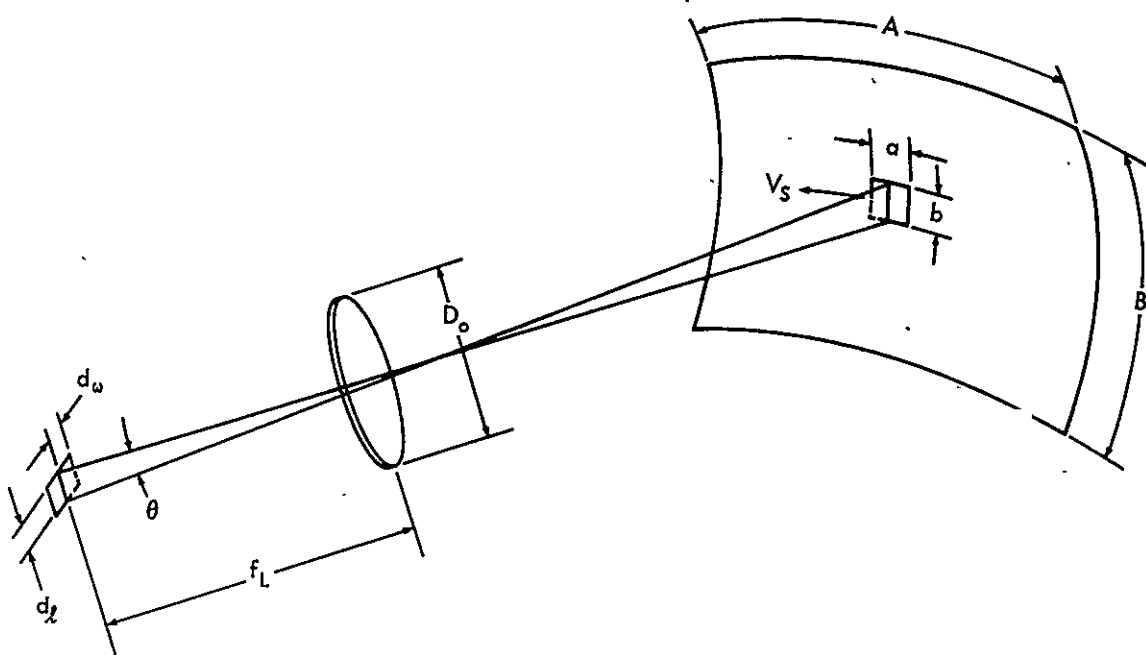
Figure 23—Search geometry

Assuming simple geometric optics, the detector area A_d can be equated in terms of the optical parameters and instantaneous field of view.

$$\tan \theta = \frac{d_\ell}{f_L} = \theta \text{ (in radians)} \tag{1}$$

A point detector is considered and the instantaneous field of view is small. For small angles, the tangent of the angle is equal to the angle in radians. Also, $f_L \gg d_\ell$.

The optics f/ratio is defined as

$$\text{f/ratio} = F = \frac{f_L}{D_o} \tag{2}$$

therefore equation (1) can be rewritten as

$$d_\ell = FD_o \theta_\ell \tag{3}$$

34

similarly

$$d_w = FD_o\theta_w \tag{4}$$

consequently, the detector Area A_d may be expressed as

$$A_d = d_\ell d_w = (FD_o)^2 \, ab \tag{5}$$

Where from the geometry of the problem

$$ab = \theta^2 \text{ steradians} \tag{6}$$

If the search field is to be scanned in a frame time T_f, then the search rate S_r, scan velocity V_s and dwell time T_d may be derived from the geometry of Figure 23.

$$\text{Search rate, } S_r = \frac{AB}{T_f} \text{ steradians/second} \tag{7}$$

To determine the scan velocity V_s, a line scan in the azimuth direction is considered. The width of the "line" is the instantaneous field of view in the elevation direction.

$$\text{Scan Velocity, } V_s = \frac{\text{number of lines} \times \text{length per line}}{\text{frame time}}$$

$$V_s = \frac{BA}{bT_f} = \frac{S_r}{b} \text{ radians/second} \tag{8}$$

$$\text{Dwell time, } T_d = \frac{a}{V_s} = \frac{ab}{S_r} = \frac{\theta^2}{S_r} \text{ seconds} \tag{9}$$

35

System Sensitivity

The system sensitivity is defined in terms of the noise equivalent flux density (NEFD) - watts/cm^2. This is the irradiance at the receiver aperture which will produce a signal from the detector which is just equal to the inherent noise of the detector.

The detector noise is often given in terms of noise equivalent power (NEP) - watts. This is the amount of radiation falling on the detector which will produce a signal equal to the detector inherent noise level. This expression for the different detector noise processes always contains the factor $\sqrt{A\Delta f}$. Therefore, one can say that

$$NEP \propto \sqrt{A\Delta f} \tag{10}$$

Jones suggested that a quantity D^* be defined as:

$$D^* = \frac{\sqrt{A_d \Delta f}}{NEP} \tag{11}$$

which serves to characterize the detector in terms of the intrinsic properties of the material of which it is made, Reference 17.

The noise equivalent flux density can now be defined in terms of the detector noise equivalent power, optical and electronic parameters.

$$NEFD = \frac{NEP}{A_o \tau_o K} \tag{12}$$

where A_o = total clear aperture area of optics

τ_o = optical efficiency

K = conversion efficiency which includes the effects of the electronic filter, optical transfer characteristics (i.e.), blur circle size, reticle function, etc.

The collecting area of the optics may be defined as

$$A_o = \frac{\pi D_o^2}{4} \, cm^2 \tag{13}$$

36

Substituting equations (5) and (6) into (11) yields an expression of NEP in terms of the optical parameters.

$$NEP = \frac{FD_o \sqrt{\theta^2 \Delta f}}{D^*} \text{ watts} \tag{14}$$

now equation (13) and (14) may be substituted into (12) to express NEFD in terms of the optical parameters.

$$NEFD = \frac{4F \sqrt{\theta^2 \Delta f}}{\pi D_o \tau_o K D^*} \text{ watts-cm}^{-2} \tag{15}$$

Substituting equation (9) in (15) yields NEFD in terms of dwell time and search rate

$$NEFD = \frac{4F \sqrt{T_D S_r \Delta f}}{\pi D_o \tau_o K D^*} \text{watts-cm}^{-2} \tag{16}$$

The above equations have been derived on the basis of one detector element. However, if n detector elements are used then from equation (8):

$$V_s = \frac{B}{nb} \frac{A}{T_f} \text{ radians-sec}^{-1} \tag{17}$$

and

$$T_D = \frac{n \theta^2}{S_r} \text{ seconds} \tag{18}$$

Substituting equation (18) into (16) gives:

$$NEFD = \frac{4F \sqrt{T_D S_r (n^{-1}) \Delta f}}{\pi D_o \tau_o K D^*} \tag{19}$$

37

A general equation which can be used to calculate the performance of a search system with n detectors. It is interesting to note that the equation is independent of detector size, scan velocity, etc. used in the analysis.

Source Irradiance

The irradiance or the received energy at the aperture of the infrared system from the re-entering Apollo spacecraft can be calculated as follows:

The radiation from the source, the Apollo Command Module, is considered to consist only of the thermal body radiation, although there is reason to believe that the total radiation level would be in excess of this; reference page 10.

The vehicle is approaching the infrared receiver at an aspect angle whereby the blunt face of the command module is in view and the temperature distribution across the blunt face is considered to be uniform.

The mean average surface temperature level versus time for the blunt face, windward and leeward forebody of the command module are plotted in Figure 24. Also plotted in the same figure is altitude and velocity versus time. This data was obtained from the AVCO Corporation, reference 18.

From these curves and from the previous analysis, page 20 it is not unreasonable to calculate a radiance value based on a 1000°K target which represents a conservative figure.

There are several good reasons for considering a minimum temperature condition, one is the desire to acquire the spacecraft shortly after re-entry (re-entry is considered to start at 400,000 feet), another is to be able to acquire the vehicle at any aspect angle and still another reason is the desire to maintain tracking during any skip trajectory where the heating rate is reduced.

The emissivity of the charing ablative coat on the spacecraft has been measured several times and a figure for emissivity (ϵ) of .75 is accepted.

The following definitions are set forth in the derivation of the equations, where

A_c = area of projected blunt face of the command module – cm^2

D_c = diameter of command module – 390 cm
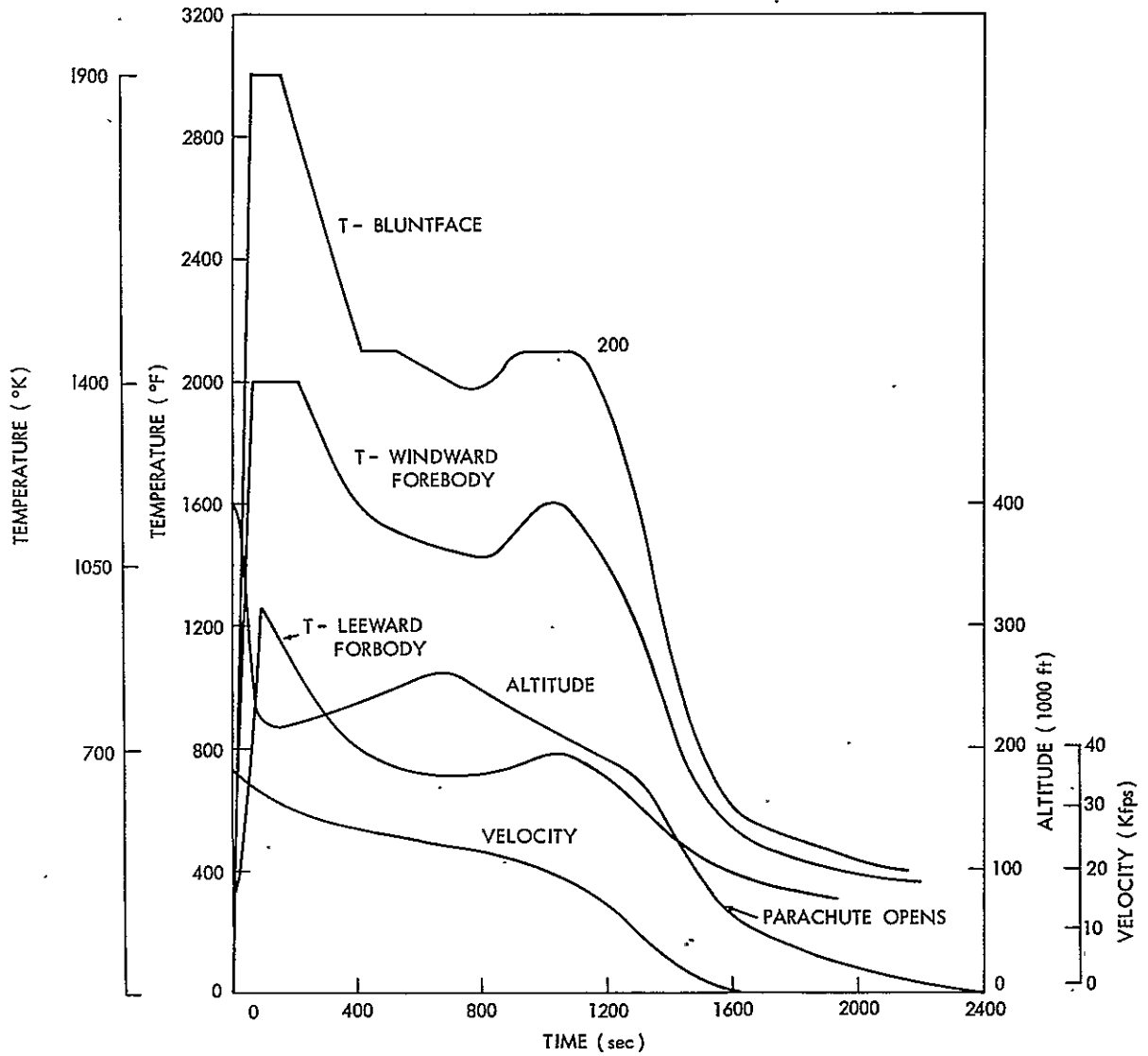
Figure 24—Surface temperature average. Typical overshoot trajectory (minimum
heating conditions). Apollo — L/D 0.5. (Courtesy AVCO Corporation).

T = temperature of command module – 1000°K

ϵ = emissivity of charing ablative material – 0.75

σ = Stefan–Boltzmann's constant – 5.673 × 10^{-12} watt cm^{-2} °K^{-4}

τ_A = transmission of the atmosphere % (dimensionless)

R = range from receiver to spacecraft – kilometers

W = radiant emittance – watt –cm^{-2}

J = radiant intensity – watt – steradian^{-1}

H = radiant power at receiver aperture – watt – cm^{-2}

ρ = percent of total radiant power at receiver waveband response
% (dimensionless)

Using the mathematical statement of the Stefan–Boltzmann law, the radiant emittance can be calculated.

$$W = \sigma \epsilon T^4 \text{ watt} - cm^{-2} \tag{1}$$

considering a Lambertian radiating surface then

$$J = \frac{WA_c}{\pi} \tag{2}$$

substituting equation (1) into equation (2) gives:

$$J = \frac{\sigma \epsilon T^4 \pi D_c^2}{4\pi}$$

$$= \frac{\sigma \epsilon T^4 D_c^2}{4} \text{ watts} - steradian^{-1} \tag{3}$$

This is the total amount of radiation emanating from the source. For a temperature of 1000°K, it is interesting to note that the peak radiant intensity falls at

approximately 3 microns. For a hotter target the peak intensity would fall at a shorter wavelength; however, the intensity at 3 microns would not be reduced. Conversely for a cooler target say 750°K, the peak radiant intensity would fall at approximately 4 microns. This relationship is shown by the series of black-body radiation curves of Figure 25.

The irradiance at the receiver aperture may be calculated taking into account the range and atmospheric transmission.

$$H = \frac{J \tau_A}{R^2} \text{ watt} - \text{cm}^{-2}$$ (4)

substituting equation (3) into equation (4) gives:

$$H = \frac{\sigma \epsilon T^4 D_c^2 \tau_A}{4 R^2} \text{ watt} - \text{cm}^{-2}$$ (5)

This then is the total amount of radiant power being received at the optical collecting aperture of the infrared system.

To calculate the irradiance over the wavelength response of the infrared system, the percentage of the energy falling at the interested wavelength band is considered.

The simplest method is to consult the tables or to use a radiation calculator such as the General Electric radiation calculator. Equation (5) is then modified by the derived percentage of radiation falling over the interested waveband.

$$H_{\lambda_1 - \lambda_2} = \frac{\sigma \epsilon T^4 D_c^2 \tau_{A (\lambda_1 - \lambda_2)}}{4R^2} P_{\lambda_1 - \lambda_2}$$ (6)

Nevertheless, for an exact mathematical treatment the equations for calculating the radiant power for a waveband of interest are presented. Using Planck's law for the spectral emittance of a blackbody at a temperature T° Kelvin and modified by the emissivity function ϵ_λ:

$$W = \epsilon_\lambda \frac{C_1 \lambda^{-5}}{e^{c_2/\lambda T} - 1} \text{ watts} - \text{cm}^{-2} - \text{micron}^{-1}$$ (7)

41
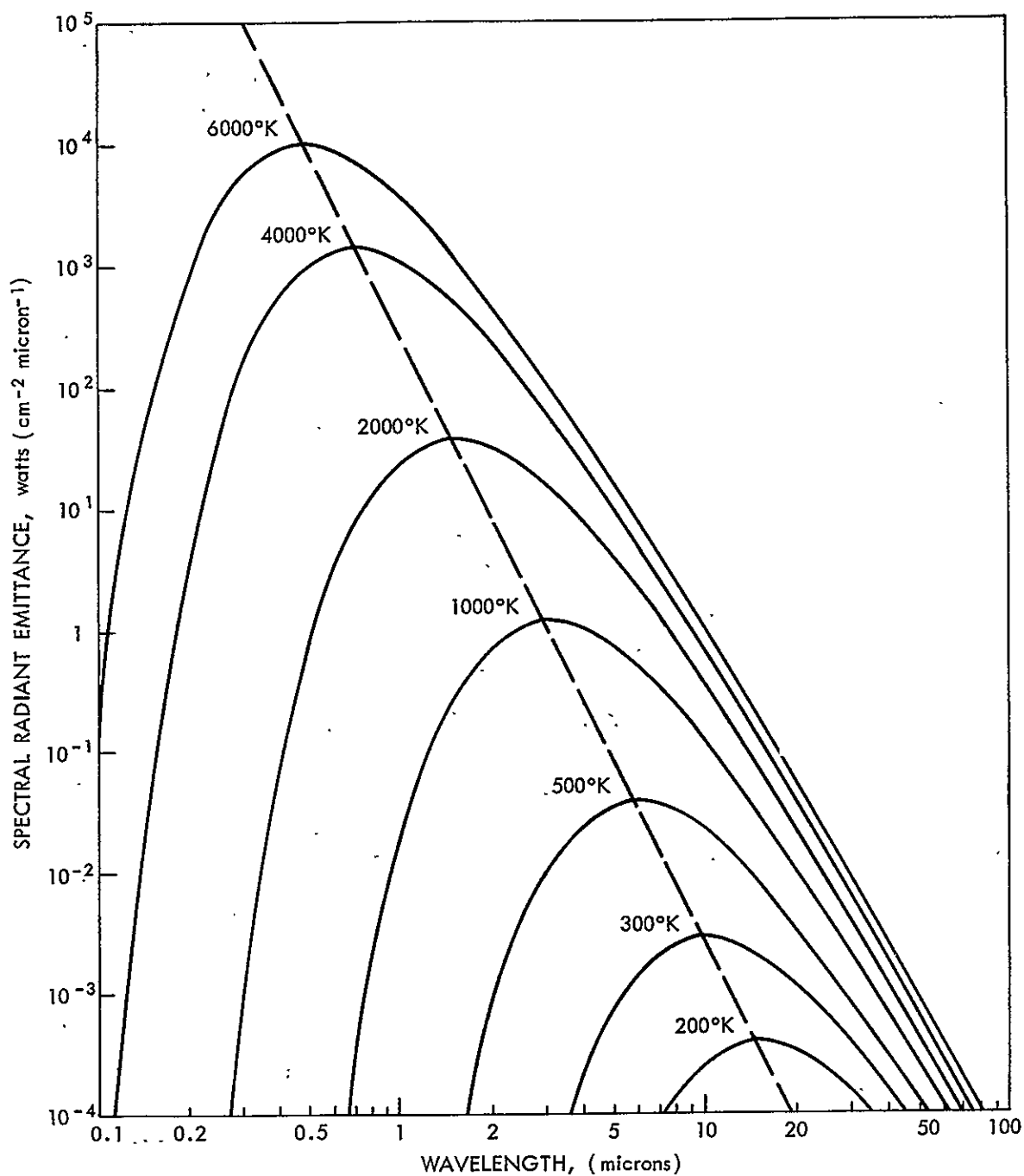
Figure 25—Spectral radiant emittance of a blackbody as a function of wavelength at various temperatures. The maximum spectral radiant emittance at a given temperature falls on the dashed curve

where

$$C_1 = 3.74 \times 10^4 \text{ watts}\,\mu^4 \text{ cm}^{-2}$$

$$C_2 = 1.43880 \times 10^4 \,\mu\,°K$$

Over the waveband of interest

$$W_{\lambda_1-\lambda_2} = \epsilon_\lambda \int_{\lambda_1}^{\lambda_2} \frac{C_1\lambda^{-5}}{e^{C_2/\lambda T} - 1}\, d\lambda \tag{8}$$

The expression for receiver irradiance ($H_{\lambda_1} - \lambda_2$) can now be presented by substituting equation (2) and (8) into equation (4)

$$H_{\lambda_1-\lambda_2} = \frac{A_c}{\pi R^2} \int_{\lambda_1}^{\lambda_2} \frac{C_1\lambda^{-5}}{e^{C_2/\lambda T} - 1}\, \epsilon_\lambda \tau_{A\lambda}\, d\lambda \tag{9}$$

Substituting appropriate values into the equation for the irradiance (H), the radiant power received by an infrared set from the re-entering Apollo spacecraft may be calculated. The simplified form of equation (6) is used.

$$H_{\lambda_1-\lambda_2} = \frac{\sigma \epsilon T^4 D_c^2 \tau_{A(\lambda_1-\lambda_2)}}{4R^2}\, P_{\lambda_1-\lambda_2}$$

The waveband considered is the 2 - 2.5 micron band. $\tau_{A(\lambda_1-\lambda_2)}$, the atmospheric transmission, for this band was calculated to be approximately 100% at 40,000 feet and with a horizontal look angle; however, a more conservative figure is used here of 70%.

R, the slant range, is taken as 500 nautical miles = 926.5 kilometers.

$P_{\lambda_1-\lambda_2}$, the percent of total radiated energy in the 2 - 2.5 micron band, at 1000°K is approximately 10%. Therefore:

$$H_{2-3\mu} = \frac{(5.67)(.75)(1 \times 10^3)^4 \times 10^{-12} (390)^2 (.7)}{(4)(926.5 \times 10^5)^2}\, 0.1 \text{ watts} - \text{cm}^{-2}$$

43

$$H_{2-3\mu} = \frac{(5.67)(.75)(15.2 \times 10^4)(7 \times 10^{-2})}{(4)(85.8 \times 10^{14})} \; 0.1 \; \text{watts} - \text{cm}^{-2}$$

$$H_{2-3\mu} = \frac{4.52 \times 10^4}{3.43 \times 10^{16}} \; 0.1 \; \text{watts} - \text{cm}^{-2}$$

$$H_{2-3\mu} = 1.32 \times 10^{-12} \; \text{watts} - \text{cm}^{-2}$$

It is interesting to compare this value for the 2 - 2.5 micron band to that of the 3 - 5 micron band, assuming the same atmospheric transmission.

For a target at a temperature of 1000°K there is 37% of the total radiated energy in the 3 - 5 micron band. Therefore:

$$H_{3-5\mu} = (13.2 \times 10^{-12})(.37) \; \text{watts} - \text{cm}^{-2}$$

$$H_{3-5\mu} = 4.9 \times 10^{-12} \; \text{watts} - \text{cm}^{-2}$$

To determine if this amount of radiant power at the aperture of the infrared receiver is sufficient for detection, the noise equivalent flux density (NEFD) is calculated from equation 19, page 37. Thus:

$$NEFD = \frac{4F \sqrt{T_D S_r (n^{-1}) \Delta f}}{\pi D_o \tau_o K D^*}$$

An infrared system is considered which is responsive over the 3 - 5 micron band. Ten InSb detectors are considered, each with a one milliradian × 3 milliradian instantaneous field of view (FOV). A D^* value of 5×10^{10} is not uncommon for these detectors. An 8 inch collecting aperture is considered. The total FOV is the hemisphere (2π steradians). The time allowed (frame time T_f) to scan this FOV is four seconds. The above parameters in tabular form are:

Number of detectors (n) = 10 InSb

$D^* = 5 \times 10^5$ cm - cps$^{1/2}$ - watt^{-1}

Inst. FOV/detector (θ) = 1×10^{-3} radian (elev.) and

3×10^{-3} radian (Az.)

Aperture diameter (D_0) = 8 inch - 20.5 cm

Frame time (T_f) = 4 seconds

f/ratio (F) = 0.8

Optical Efficiency (T_0) = 0.5

Signal Conversion Efficiency (K)

The following calculations can now be made to solve for the parameters of dwell time (T_d), search rate (S_r), and electronic bandwidth (Δf).

From equation (7), page 41:

$$S_r = \frac{AB}{T_f} \text{ where AB for a hemisphere} = 2\pi \text{ steradians}$$

$$S_r = \frac{2\pi}{4} = \frac{\pi}{2} \text{ steradians - sec}^{-1}$$

From equation (18), and considering the detectors to have a 1 mr x 3 mr inst. FOV.

$$T_d = \frac{n\theta^2}{Sr} = \frac{2(10)(3 \times 10^{-6})}{\pi}$$

$$T_d = \frac{60 \times 10^{-6}}{\pi} \text{ seconds}$$

InSb detectors have response times less than 1×10^{-6} seconds so there is no problem here of too short a dwell time. Δf, the electrical bandwidth can be calculated from the following expression, reference 19.

$$f = \frac{1}{3t_r}$$

where t_r is the rise time of the detector pulse output. In this case the rise time is considered equal to the dwell time T_d on the detector. Therefore:

45

$$f = \frac{1}{3\,T_d} = \frac{\pi}{3(60 \times 10^{-6})} \text{ seconds.}$$

$$= \frac{\pi \times 10^6}{180}$$

$$= 17.5 \times 10^3 \text{ cps.}$$

Substituting the parameters into the equation for NEFD:

$$\text{NEFD} = \frac{4(.8)\sqrt{\frac{60 \times 10^{-6}}{\pi}}\,(\pi/2)\,(1/10)\,17.5 \times 10^3}{\pi(20.5)(.5)(.6)(5 \times 10^{10})} \text{ watts} - \text{cm}^{-2}.$$

$$\text{NEFD} = 7.58 \times 10^{-13} \text{ watt} - \text{cm}^{-2}$$

Comparing this value with the received power H_λ gives a signal to noise ratio of:

$$\frac{S}{N} = \frac{H_\lambda}{\text{NEFD}} = \frac{4.9 \times 10^{-12}}{7.58 \times 10^{-13}}$$

$$S/N \approx 6.5$$

This is for a target of 1000°K at 500 nautical mile range!

As in any scanning search equipment, this ratio of peak signal to rms noise can be expressed as a function of probability of detection, false alarm rate and noise bandwidth.

The mathematical treatment of this relationship is quite involved and is beyond the scope of this report. The reader is referred to the work by Jamieson et al., Peterson et al., Middleton, Marcum, Rice and others. Reference 20, 21, 22, 23, and 24, respectively. Nevertheless, one can by a few simple calculations and the use of detection probability curves, Figure 26, determine the probability of detection for false alarm time and bandwidth versus signal to noise ratio.

Let

T_{fa} = the false alarm time (mean time between false alarms)

f = equivalent noise bandwidth = 17.5×10^3 cps
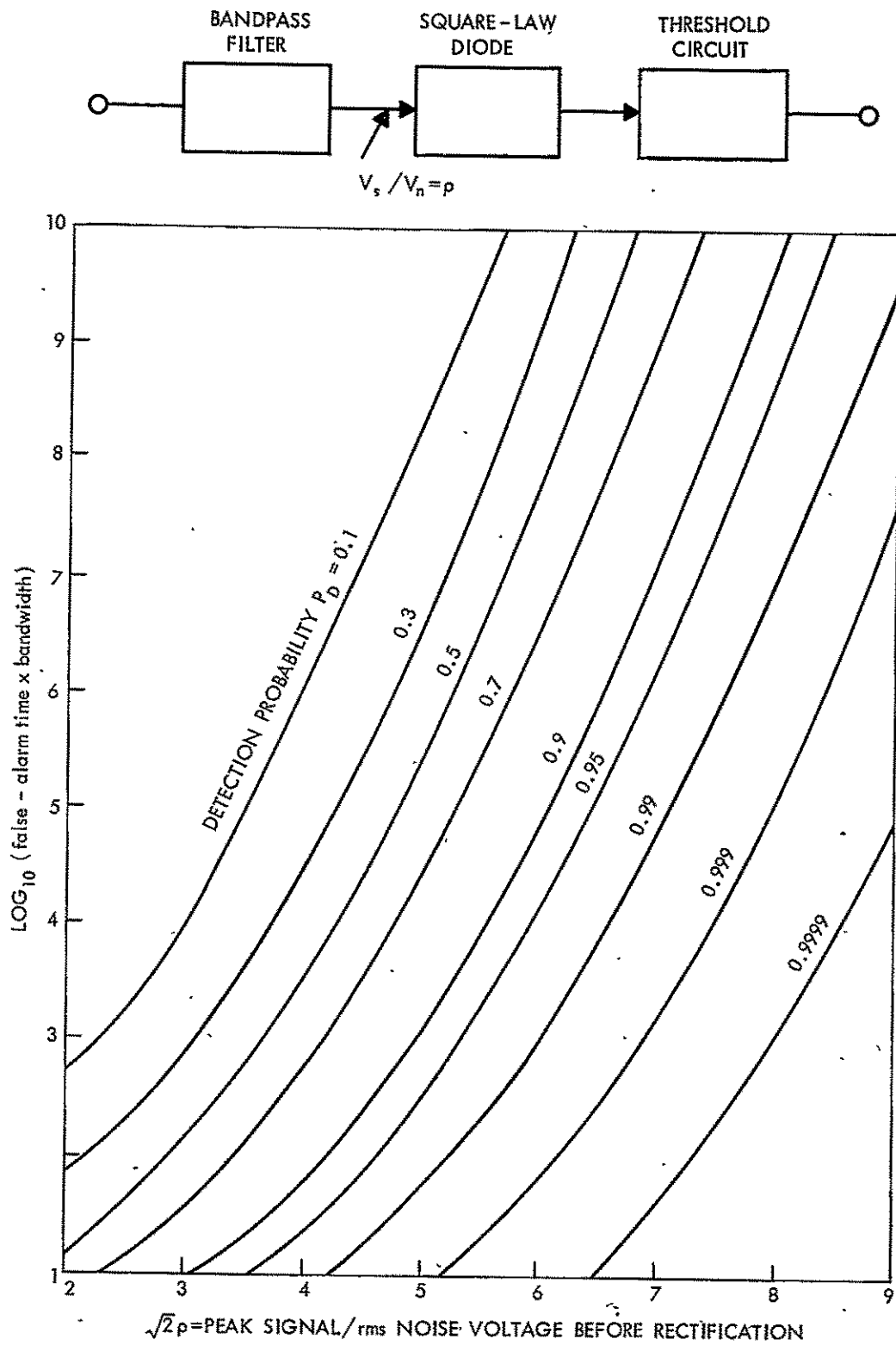
Figure 26—Signal-to-noise ratios required for specified false-alarm rates and detection probabilities. (By permission from McGraw-Hill Book Company, Inc., New York)[20]

T_f = frame time (time to scan 2π steradians) = 4 sec.

N_d = number of detector channels = 10

P_r = signal to noise ratio = 6.5

n_f = number of false alarms allowed for each scan of the hemisphere = 0.01

Therefore:

$$T_{fa} = \frac{Tf}{n_f} = \frac{4}{0.01} = 4 \times 10^2$$

then

$$T_{fa}\Delta f\ n_d = (4 \times 10^2)(17.5 \times 10^3)(10)$$

$$= 7 \times 10^7 \text{ samples/false alarm}$$

$$\log_{10} T_{fa}\ \Delta f\ n_d = 7.8451 \text{ (parameter for ordinate axis of Figure 26)}$$

The parameter for the abscissa axis of Figure 26, the peak signal to rms noise voltage is $\sqrt{2}\,P_r$.

thus

$$\sqrt{2}\,P_r = \sqrt{2}\ 6.5$$

$$= 9.2$$

entering Figure 26 at 7.8451 on the ordinate axis and 9.2 on the abscissa axis gives a detection probability of 0.999.

Accuracy Requirements

One of the major functions of the infrared system is to track the re-entering spacecraft. Tracking as used in this sense involves angle tracking only. Since it is not possible to predict the re-entry trajectory of a lifting body, the angle tracking information will be used to determine the approximate landing point of the spacecraft. Although the tracking information accuracy is broad, relatively speaking, it nevertheless is small as far as defining the landing point area.

The prediction of this impact area is quite important if a quick recovery of the astronauts and equipment is to be assured. Complicating the prediction of this area by other means is the fact that the trajectory can be completely in radio blackout. Also, if damage occurred to the spacecraft antenna during reentry, no information would be available to the ground for the location of the spacecraft.

The infrared system, nevertheless, will be able to determine the landing point to between 50 and 100 nautical miles for only one system tracking. If two infrared systems track the spacecraft at the same time, the error in determining the landing point is reduced by a factor of 10.

Calculations in support of this tracking capability have been made by Dr. Vonbun and Dr. Kalil (reference 16 and 25) respectively. These calculations assume an error of the tracker of $\pm 5 \times 10^{-3}$ radians and an error in the location of the tracker of ± 2 kilometers in both longitude and latitude. A zero error is assumed for the true vertical.

With allowable tracker errors on the order of ± 5 mr, no problem is foreseen in the mechanization of the system to achieve this accuracy if the instantaneous field of view is kept small — one to two milliradians which corresponds to 206 seconds of arc and 412 seconds of arc respectively. It is a natural consequence of the infrared system design that this field of view is obtained from the standpoint of lessening the effect of sky background and of increasing the system sensitivity. See page 36.

The positional errors placed on the location of the tracker, ± 2 km (± 1.08 nautical miles), require precise navigational equipment.

There are two approaches open to meet this requirement. First, an all inertial system tied in with the infrared system could be used. Inertial systems with better than the required accuracy have been built and are presently in use. Factors which weigh heavily on the complexity of an inertial system are things such as the duration of the flight before positional readout is required, accuracy of ground alignment referenced to a common coordinate system and available updating inputs during the flight such as stellar reference and doppler navigation.

The second approach to achieve the required accuracies is to utilize aircraft onboard navigational equipment and other available navigational aids in conjunction with a simplified inertial system that would provide local vertical information only.

Presently available navigational aids in the Western Pacific are Loran A and Loran C. Loran A at best will give a CEP of one nautical mile. Loran C capability is 1500 feet (0.25 nautical mile). Reference 26.

The coverage of the Loran A and Loran C stations, however, is not complete over the Apollo re-entry area. Approval has been granted for the construction of additional OMEGA stations which when completed would give complete world-wide coverage at accuracies comparable to Loran C. Positional heading information can be obtained from an automatic readout gyro flux gate compass which will provide a four milliradian accuracy capability.

With a quasi-inertial system, that is one which utilizes available navigational equipment coupled to a local vertical inertial gyro, it is believed that the required positional accuracies can be met.

The choice of either approach, inertial or quasi-inertial, would of course have to weigh several factors. A few of the obvious considerations are cost, accuracy, and reliability.

CONCEPTUAL CONFIGURATION

Many scanning and optical configurations are possible that could search the hemisphere, each with their own advantages and disadvantages. Two configurations worthy of further consideration are presented herein.

In arriving at these configurations, certain ground rules were set forth considering the mission requirements. First, the desire to quickly acquire the spacecraft and to maintain track even during a skip period requires a detector responsive to the cooler temperatures of the spacecraft under these conditions. Second, the requirement that the infrared system perform its mission at maximum range under daylight conditions dictates that the system be responsive at wavelengths where background radiation is at a minimum and that each detector have a small instantaneous field of view. Third, the requirement to scan the hemisphere in a short period of time requires many detectors which can have a slow response time or it requires few detectors each having a fast response time.

Indium antimonide (InSb) was chosen as the detector because of its fast response and high detectivity at the wavelength region of the spacecraft thermal body radiation and because over this region the background radiation is at a minimum.

The desire to quickly acquire the spacecraft would seem to indicate that the most desirable wavelength band would be the 8 - 13 micron window (the blackbody radiation from a 25°C object peaks at 10 microns). Being responsive at this wavelength in effect would permit "cold body" acquisition of the Apollo spacecraft even prior to re-entry. Unfortunately, the atmospheric radiation also is stronger at these wavelengths (see page 25), and detectors sensitive at these wavelengths require liquid helium cooling.

As mentioned before, page 8, there is a predominate dip in the sky background radiation which occurs conveniently across the 3 to 5 micron band (Figure 7). The temperatures which correspond to the peak blackbody radiation falling at these wavelengths are 675°C and 300°C respectively. The time history versus heat rate input and surface heating, for a nominal re-entry trajectory, shows that a surface temperature of 860°C will be reached in less than 10 seconds after re-entry (Reference 27). At this time, the spacecraft will be at 350,000 feet altitude. Detectors responsive over the 3 to 5 micron band require liquid nitrogen cooling but this is not considered a drawback because complex scanning systems utilizing liquid nitrogen detector cooling are commonly in operational use by the military services all over the world. These detectors have fast time constants <1 microsecond and only a few are required to scan the hemisphere in the allowed time.

Systems containing many detector elements can be fabricated by utilizing film deposition techniques. Films commonly employed such as PbS are responsive in the 2 to 2.5 micron region. Although the PbS detector systems have a lower noise equivalent power than the InSb systems commonly employed over the 3 to 5 micron region, they are subject to a higher environmental background radiation, variation and false target inputs. (See page 23). PbS detectors have slow response times and therefore many detectors would be required to search out the hemisphere in the frame time allowed. Associated with the utilization of many detector elements is the electronic complexity of the signal amplification, commutation and data handling. It is estimated that more than 100 PbS detectors would be required, each with its own preamplifier. Work however has been done to reduce the complexity of "many-element" systems by using molecular electronics (reference 28). A further disadvantage of these systems is that wide field of view, short focal length optics are required. The two conceptual systems presented in Figures 27 and 28 operate over the 3 to 5 micron band utilizing ten InSb detectors, each detector having a 1 mr elevation by a 3 mr azimuth instantaneous field of view. The ten elements are arranged in a linear array parallel to the horizontal plane of the scanner.

The more apparent advantage of the configuration in Figure 27 is the low profile of the turret such that there is little disturbance to the air flow external of the aircraft skin. Although there are four reflective surfaces that would attenuate an incoming ray, these surfaces can be made 95% reflective and the total efficiency of the optical system would be on the order of 81.5%. The disadvantage of the optical configuration perhaps is the requirement for a large primary mirror on the order of 24 inches in diameter; however, large portions of this mirror can be masked off to reduce scattered light effects. Note that there is no obscuration of the incoming rays by the secondary mirror. The projected image of the detector array field of view would rotate from horizontal at the horizon to vertical at zenith as the system scanned from horizon to horizon. This would not permit overlap coverage at near zenith angles which is considered a desirable feature.

Another advantage of this system is that access could be gained to the detector-electronic area for servicing inside the aircraft. Also no scan dead time is lost as the mirror rotates and imaging is achieved for 100% of a mirror rotation cycle.

The advantage of the configuration in Figure 28 is the compactness of the unit; however, the turret would project further into the slip stream outside the aircraft skin. Also, there is very little rotation of the image plane projected back into the hemisphere as the system scans through zenith. Therefore, overlap coverage would be obtained with this system. Refractive focusing optical elements are considered in conjunction with the scanning mirror (polished both sides) giving an estimated optical efficiency of 60%. If the refractive elements
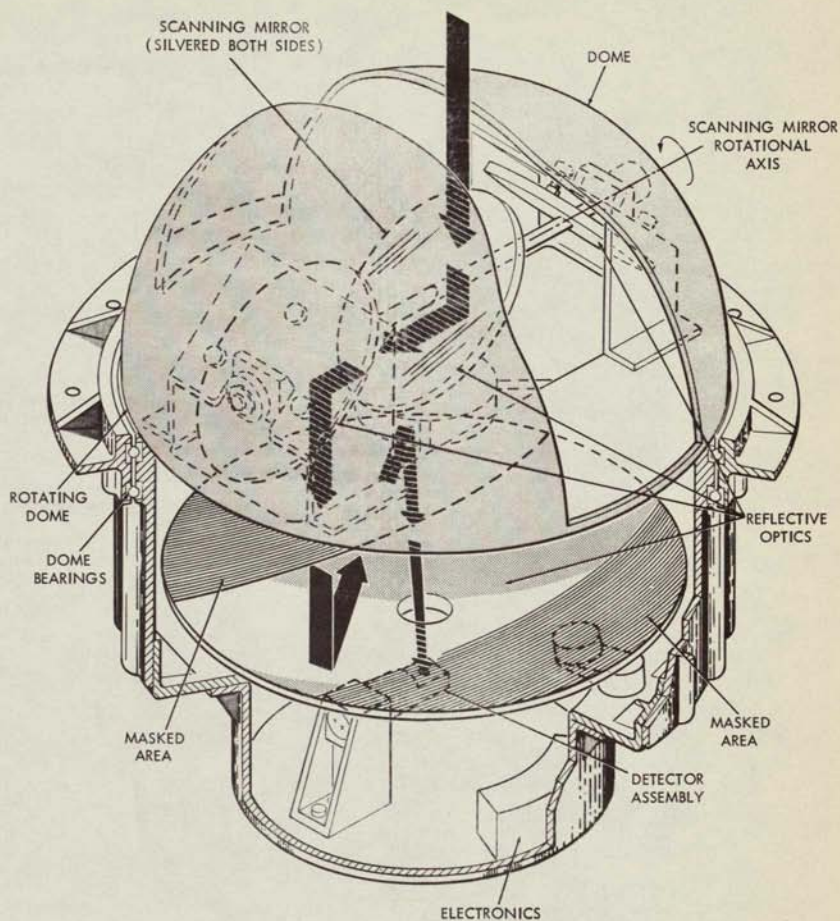
Figure 27–GSFC Infrared Hemispherical Scanner, Conceptual Design

ROTATING DOME

DETECTOR HOUSING

REFRACTIVE OPTICAL ELEMENTS

SCANNING MIRROR (SILVERED BOTH SIDES)

MIRROR ROTATIONAL AXIS

DOME BEARINGS

ELECTRONICS
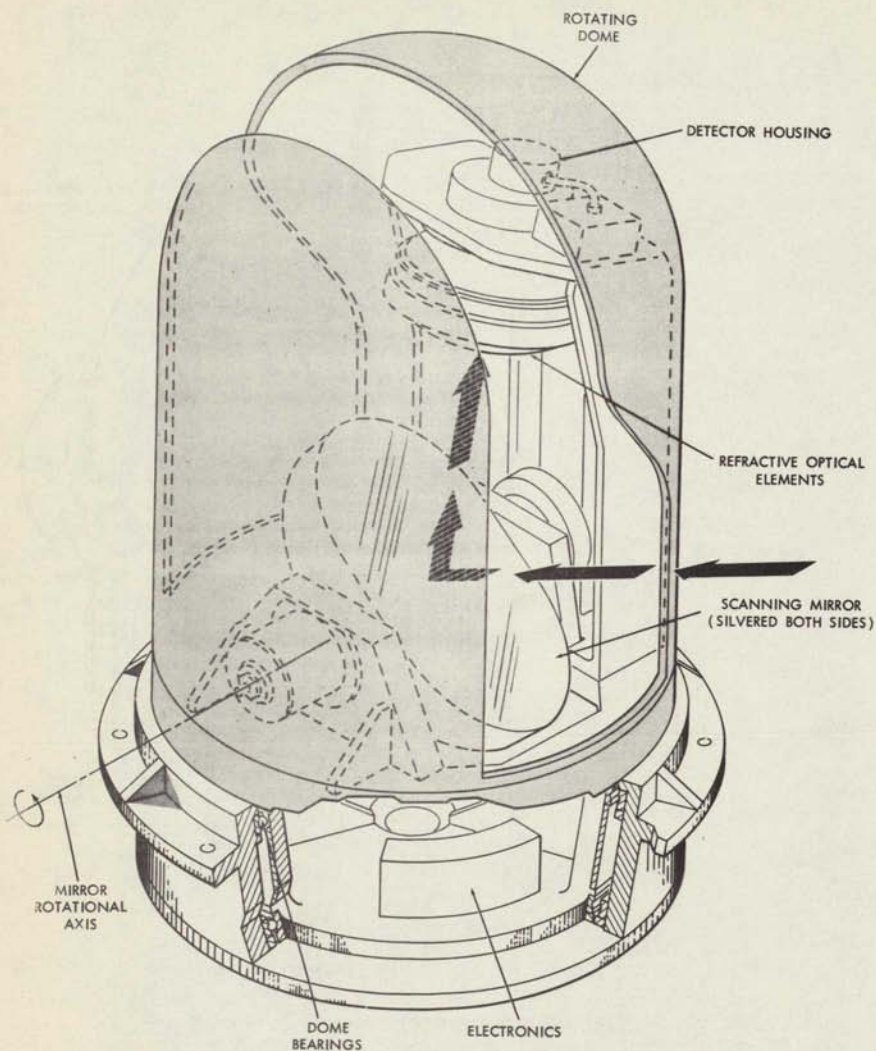
Figure 28—Infrared Hemispherical Scanner utilizing the refractive optical elements from the Aerojet W48 Scanner. (Courtesy Aerojet – General Corporation Astrionics Division)

were replaced with cassegrainian optics, a total of three reflective surfaces would then attenuate the signal and the optical efficiency would be increased to 85.5%.

Further disadvantages of the system are the inability for services access internal to the aircraft and the scan dead time which amounts to 25% of each mirror rotation.

In both systems the opening in the turret dome is narrower at the top than on the sides. This is because when viewing the spacecraft at high zenith angles (closer range) the intensity is greater and the aperture opening can be reduced to lessen the required dynamic range of the detector and signal processing electronics.

To provide an environmental seal for the dome and to maintain the aerodynamic shape of the turret, a window encloses the turret opening. This window can be made up of large flat pieces of infrared transmitting material thereby circumventing the problems of curved dome surfaces and associated optical effects.

The above comments on both systems are superficial and of course as with any complicated electro-optical-mechanical system a more detailed analysis would have to be performed before a decision could be made as to what system represented the best compromise. The author is also aware that there are other scanning configurations which could weigh heavily on those presented herein.

INTENTIONALLY

LEFT

BLANK

APPLICABLE STATE OF THE ART

General

Many infrared systems have been built and have successfully met design objectives. These systems range from the Aerial and Spacecraft search and reconnaissance type to the electronic component checker found on manufacturing production lines.

Familiar Infrared Systems

Some of the more familiar devices are the highly successful Sidewinder missile which by virtue of its infrared seeker, the missile is guided to the target; the sniperscope developed during World War II for nighttime viewing of enemy troop operations; the circuit tester used to determine "hot" circuit components as a means of bettering component or system reliability; the Tiros-Nimbus satellite radiometers used to obtain cloud temperatures and pictures over the dark side of the earth.

Applied Technology

Great advances have been made in the field of applied infrared technology and there are a number of wide field of view search systems, some with track-while-scan capability, that demonstrate the design feasibility of a hemispherical search, lock-on and track system at the sensitivity and search rate discussed in this report.

It is difficult for one not directly associated with the field of infrared technology to appreciate the scope of the advances that have been made and to be knowledgeable of the many varied systems that have been successfully built. This general lack of knowledge of the state of the art in infrared technology is with good reason understandable. Much of the data, techniques and systems which demonstrate the state of the art are classified for military reasons.

Two systems are presented, Figures 29 and 30, which have a wide field of view coverage, small instantaneous fields of view, fast response and high detectivities. Suffice it to say that there are other systems and there are more advanced operational versions of these systems which are classified. The reader is referred to the following documents for further information: Research and Development of Infrared Track-While-Scan Technique, AD337-583, Secret; AN/ALR-23 Infrared Countermeasure Receiver Set, Secret, AVCO Electronics
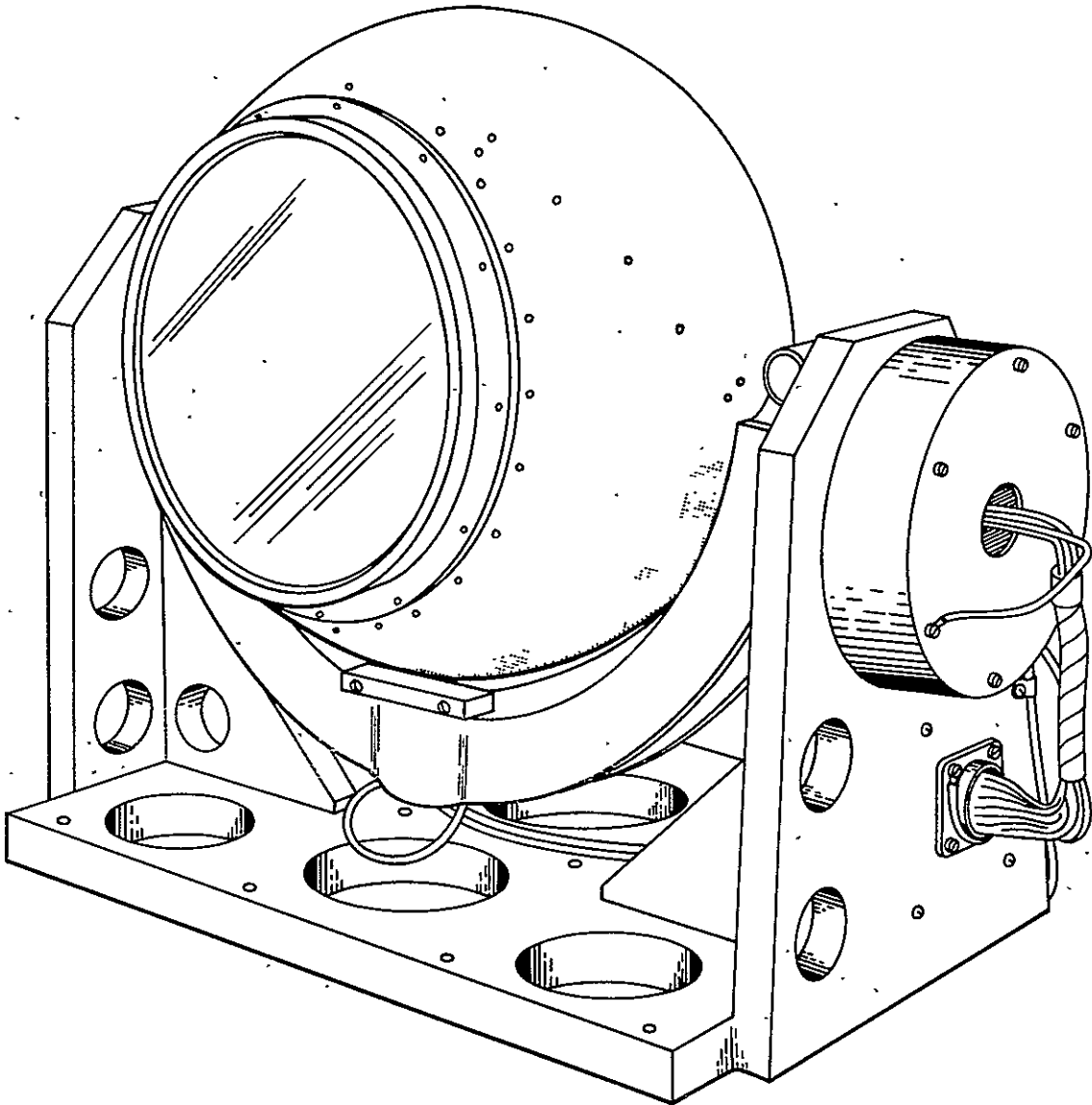
Figure 29–Aerojet Model W48 infrared search system
(Courtesy Aerojet – General Corporation Astrionics Division)
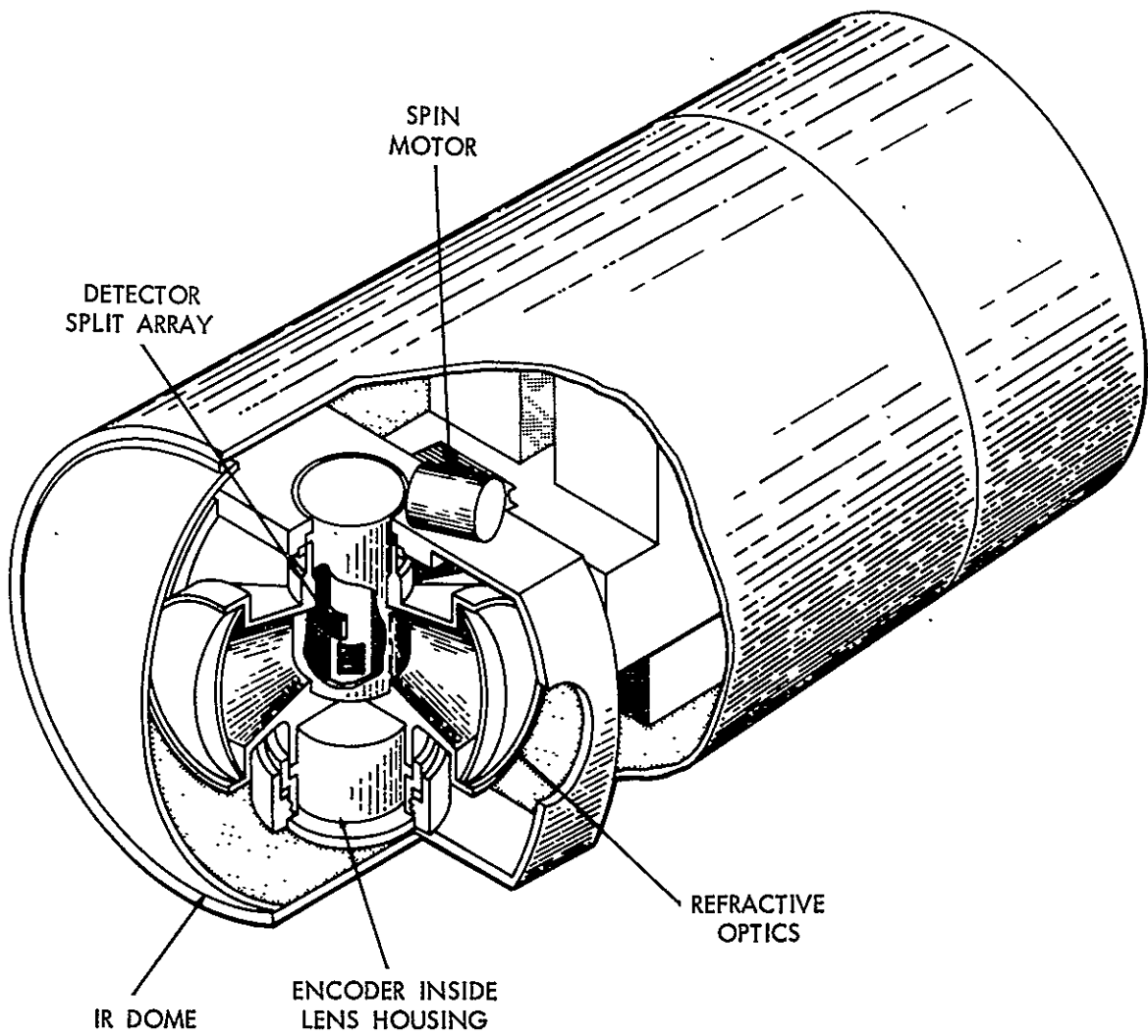
Figure 30—AVCO drum scanner. (Courtesy AVCO Electronics and Ordnance Division)

SPIN MOTOR

DETECTOR SPLIT ARRAY

REFRACTIVE OPTICS

IR DOME

ENCODER INSIDE LENS HOUSING
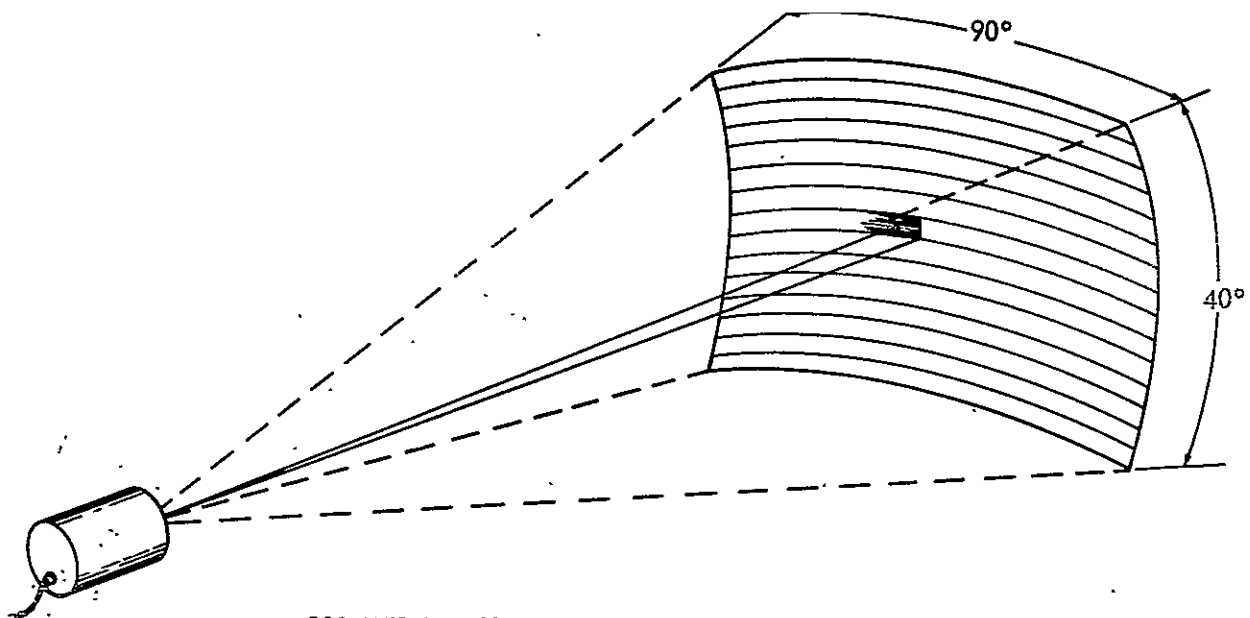
90° WIDE X 40° HIGH TOTAL SEARCH FIELD IS
COVERED 3 TIMES PER SECOND

Figure 31–AVCO drum scanner (Search/Track System) scan field.

Division, Cincinnati, Ohio; Development and Testing of the Airborne Infrared
Early Warning System (AIREW), NAVWEPS Report 7887, NOTS TP2877, Secret;
Infrared Discrimination Investigation, AD 345-671, Secret.

Figure 31 shows the field of view obtainable with the AVCO Drum Scanner.

It does not take much imagination to picture the drum scanner, for example,
mounted on a turntable such that the 90° coverage is now in the vertical direc-
tion and the turntable rotating in azimuth providing 360° coverage, thereby cov-
ering the hemisphere. With this configuration as shown in Figure 32, the total
hemisphere would be scanned in approximately three seconds with overlap cover-
age at high elevation angles.

The state of the art that is demonstrated by these systems and others at the
system, subsystem and component level would permit one to effectively utilize
this technology for the development of an infrared hemispherical scanner capable
of meeting the design requirements of search, track, and lock-on at the wave-
lengths and sensitivity levels required.

HEMISPHERE IS
COVERED IN $\approx$ 3 sec.

Figure 32—Drum scanner mounting for hemispherical coverage

INTENTIONALLY

LEFT

BLANK

RECOMMENDATIONS

I would recommend that further work be carried on in the area of infrared optical tracking of spacecraft. I feel that there is a definite place for a system which is immune to any communication blackout problems, one which is 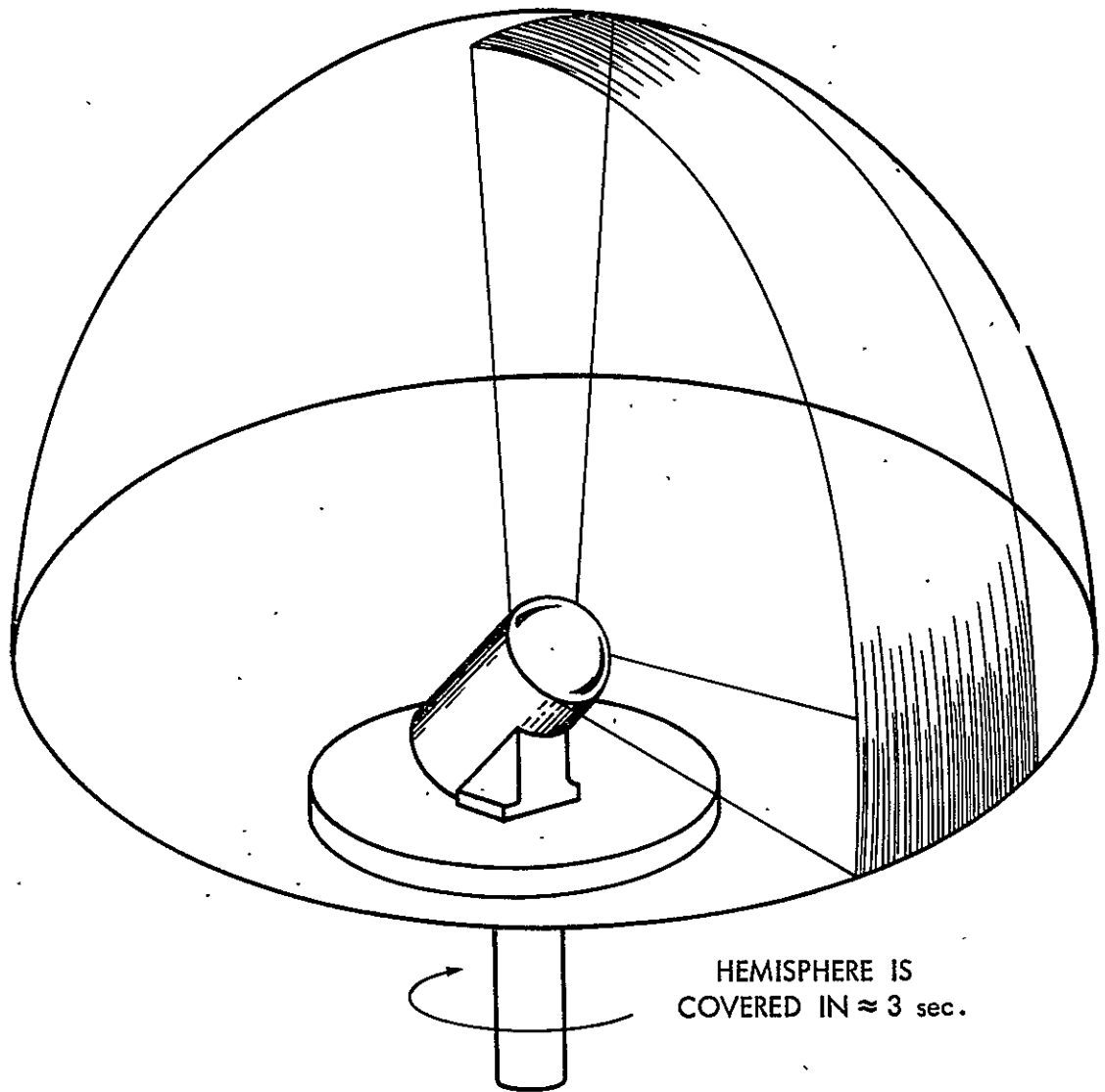completely passive, one which requires no large ship or real estate and associated large antenna investment, one which is highly mobile -- that for any unforeseen event can quickly span continents and oceans to be on site during a spacecraft re-entry, one which operates for all practical purposes above the weather on high flying jet aircraft, and one which for 500 nautical miles in any direction can acquire and track the spacecraft and from the tracking data derived predict the impact point of the spacecraft within a small area thereby aiding the quick and safe recovery of the astronauts and the spacecraft.

The system I speak about is not something that will come out of the technological advances made over the next 50 years, but is in fact a near reality. I say near, not because of technological advances that have to be made, but because systems exist today with the acquisition, range and tracking capability to perform the mission. What has to be done to in fact make a system a reality is to utilize the state-of-the-art of existing systems and to mechanize these components into a system configured to perform the desired functions.

Here, for the first time in re-entry phenomenon, do we have a sufficiently large vehicle (Apollo Command Module) traveling at super orbital velocities which will permit, during daylight, acquisition and tracking by infrared means at extended ranges.

It would seem that with the opportunity that exists, that is, of having re-entry events of such large magnitude occurring during Gemini and Apollo re-entries that every effort should be made to take advantage of these events for scientific purposes of verifying the theoretical and laboratory experimental work. What better proving ground could be obtained for gathering scientific information and determining the operational capability of prototype infrared acquisition systems.

I therefore propose that as a first step that a prototype system be built for the purpose of acquiring and tracking spacecraft from the self-generated thermal body radiation (infrared). Further I propose that this system be tested against Gemini and Apollo re-entries (several are planned before the actual Lunar Mission). Further I propose that the information and experience derived from these tests be used for further improvement and for consideration of developing additional systems for spacecraft re-entry either for Apollo backup usage or for use against spacecraft on return and re-entry into the earth's atmosphere from near planet missions. These re-entries would be at much higher velocities, 50-60,000

feet/sec versus 36,000 feet/sec. for a Lunar return. Therefore, all the problems of communication blackout, cross range and down range deviation and uncertainty of impact point would be magnified accordingly. Also less reliance would have to be placed upon the spacecraft communication equipment properly functioning because of the decrease in reliability after an extended near planet mission.

REFERENCES

1. Craig, Roger A. and Davey, William C., Thermal Radiation from Ablation Products Injected into a Hypersonic Shock Layer, NASA TN D-1978, Syst. 1963.

2. Page, William A. and Arnold, James O., Shock-Layer Radiation of Blunt Bodies at Re-entry Velocities. NASA TR R-193, April 1964.

3. Contract between Goddard Space Flight Center and Westinghouse Aerospace Division. Contract NAS5-9703: Infrared Sensor for Apollo Re-entry Acquisition, 1964.

4. Little, B. H. Jr., Aerodynamic Heating for Lunar Re-entry Vehicles, Vol. XI, Advances in the Astronautical Sciences, American Astronautical Society, 1963, pp. 767-797.

5. Lees, L., Recovery Dynamics - Heat Transfer at Hypersonic Speeds in a Planetary Atmosphere, Chapter XII, Space Technology, John Wiley & Sons, Inc., New York, 1959.

6. Page, William A., Shock-Layer Radiation of Blunt Bodies Traveling at Lunar Return Entry Velocities; IAS Paper No. 63-41, Institute of the Aerospace Sciences, January 1963.

7. Kivel B., Radiation from Hot Air and Its Effect on Stagnation - Point Heating; Journal of the Aerospace Sciences, February 1961, pp. 96 - 102.

8. Meyerott, R. E. and Sokoloff, J., Absorption Coefficients of Air; Geophysical Research Papers No. 68, ARDC, Bedford, Mass., AD252003.

9. Kruse, McGlauchlin, McQuistan; Elements of Infrared Technology, Chapter 5, John Wiley & Sons, Inc., 1962.

10. Altshuler, T. L., Infrared Transmission and Background Radiation by Clear Atmospheres; General Electric Technical Information Series, Report No. 61SD199, December 1, 1961, AD401923.

11. Murcray, D. G.; Murcray, F. H. and Williams, W. J., Variation of the Infrared Solar Spectrum between 2800 and 5100 cm with Altitude; Journal of the Optical Society of America, Vol. 54, No. 1, January 1964, pp. 23-27.

12. Bennett, H. E., Bennett Jean M. and Nagel, Max R., Distribution of Infrared Radiance over a Clear Sky; Journal of the Optical Society of America, Vol. 50, No. 2, February 1960.

13. Bell, E. E., Eisner, L., Young, J., and Oetjen, R. A., Journal of the Optical Society of America, Vol. 50, p. 1313, 1960.

14. Walker, Russell G., and D'Agati, Anthony; Infrared Stellar Irradiance, Applied Optics, Vol. 3, No. 11, November 1964.

15. Hall, Freeman F., Jr., Results of an Infrared Stellar Mapping Program, Memoires Soc. R. Sc. Leige, Cinquieme serie, tome IX, Extrait. p. 432, 1964.

16. Vonbun, F. O., Apollo Re-entry Infrared Support, Goddard Space Flight Center, X513-65-4, December 1964.

17. Jones, R. Clark: Phenomenological Description of the Response and Detecting Ability of Radiation Detectors, Proc. IRE, 47:1495 (1959).

18. Private Correspondence – Cal Bopp, AVCO Corp., Cincinnati, Ohio, 1964.

19. Moskowitz, S. and Racker, J., Pulse Techniques, Prentice Hall, Inc., 1951, Chapter 3.

20. Jamieson et al., Infrared Physics and Engineering, McGraw-Hill Book Co., Inc., 1963.

21. Peterson, W. W., Birdsall, T. G., and Fox, W. C.; The Theory of Signal Detectability, IRE Trans. on Inform. Theory, PGIT-4:171, Sept. 1954.

22. Middleton, D., and Von Meter, D.; Detection and Extraction of Signals in Noise from the Point of View of Statistical Decision Theory, Journal SIAM, 3 (4); December 1955; 4 (2), June 1956.

23. Marcum, J. I.; A Statistical Theory of Target Detection by Pulsed Radar, RAND Research Mem. Math. Appendix RM-753, July 1, 1948.

24. Rice, S. O.; Mathematical Analysis of Random Noise in Nelson Wax (ed)., "Noise and Stochastic Processes," Dover Publications, Inc., New York 1954.

25. Kalil, F., "Infrared Acquisition and Tracking System – Preliminary Mission System Specifications," Systems Analysis Office – Technical Brief, Goddard Space Flight Center, December 9, 1964.

26. Conference Results. Subject – Navigational Capabilities of JC-135 Equipment Over the Projected Apollo Re-Entry Areas. Memorandum dated Dec. 3, 1964.

27. Heat Rate Data for an Overshoot and Undershoot Re-entry Trajectory — Obtained from Brian Erb, Chief, Thermo Structures Branch; NASA, MSC - Houston, Texas, 1964.

28. Contract between Westinghouse Aerospace Division and Air Force — Contract AF33(616) 8449, Molecular Search-Track Infrared System.

29. Lehnert, R. and Rosenbaum, B, "Plasma Effects on Apollo Re-entry Communication," NASA TN D-2732, March 1965.

APPENDIX A

GSFC SPECIFICATION

INFRARED ACQUISITION AND TRACKING SYSTEM

GODDARD SPACE FLIGHT CENTER

GREENBELT, MARYLAND

INTENTIONALLY

LEFT

BLANK

TABLE OF CONTENTS

1.0 SCOPE

1.0 SCOPE

When the Apollo Command Module enters the earth's atmosphere from its lunar mission, it must dissipate a considerable amount of kinetic energy. Most of this energy is transformed into heat by compression in the stagnation region. Temperatures in the heat cap become sufficient to cause dissociation and ionization of the surrounding air causing it to become highly-conductive resulting in marked attenuation or blackout of communication signals.

This specification describes the requirements for an infrared (IR) acquisition and tracking system (IRATS). IRATS will angle-track the Apollo Command Module (spacecraft) by detecting the IR energy which is radiated as the spacecraft is heated upon re-entry into the earth's atmosphere.

Angular position information which the IRATS generates will be used for:

(a) Pointing and slaving the aircraft's unified S-band communication antenna.

(b) Trajectory calculations in real time.

(c) Providing data for post-flight analysis.

If communications between the A/RIA and the spacecraft are established prior to the initial phases of re-entry, the IRATS can be initially pointed by the angle-tracking signals from the communications antennas.

If communication signals are absent, the IR acquisition and tracking system can be made to search either a hemishperical field or a lesser field to acquire the reentering spacecraft. Once acquisition and tracking have occurred, the communications antenna can be slaved to the IR system such that communications can be quickly restored during periods of lesser attenuation of the communication signals.

Energy which the system detects will be visually presented to an operator. Once the spacecraft has been detected and discriminated from any false or background objects, an angle-tracking mode of operation will be initiated. In the angle-tracking mode, the direction to the spacecraft will be continuously determined and displayed.

Angular data (in geographical coordinates which IRATS generates) plus time, aircraft position (latitude and longitude), and identification will interface with the A/RIA communication system.

This data will be sampled and transmitted to a re-entry·ship and/or ground station. The IRATS will include an inertial reference and internally operated test equipment.

2.0 APPLICABLE DOCUMENTS

2.0 APPLICABLE DOCUMENTS

The following documents, of the exact issue shown, form a part of this specification to the extent specified herein. The contractor shall specify the applicability of all documents whose relevance is not fully defined herein. In the event of conflict between documents referenced here and other detail content of sections to follow, the detail content of sections to follow shall be considered a superseding requirement.

2.1 Specifications

MIL-E-5272C	Environmental Testing, Aeronautical and Associated Equipment, General Specification for
MIL-E-6051	Electric-Electronic System Compatibility and Interference Control Requirements
MIL-I-6181	Interference Control Requirements, Aircraft Equipment
Attachment G	Performance and Design Requirements for the Apollo/Range Instrumented Aircraft (A/RIA) System. General Specification.

2.2   Standards

MIL-STD-7A	Types of Engineering Drawings, Definition and Requirements
MIL-STD-15-1A	Graphic Symbols for Electrical and Electronic Diagrams
MIL-STD-810	Environmental Test Methods for Aerospace and Ground Equipment

3.0 REQUIREMENTS

INTENTIONALLY

LEFT

BLANK

3.0 REQUIREMENTS

3.1 Description of the Source

For the purposes of design calculations, the radiation emitted by the spacecraft shall be that presented in the Appendix.

3.2 Description of the System

3.2.1 Operation

The system shall operate automatically to search a selected field for reentering spacecraft. During search, an optical collection aperture will be made to scan a solid angle which may consist of the entire hemisphere. Signals detected shall be visually presented to an operator in azimuth and elevation referenced to the local vertical and true north. Identification and angle-tracking acquisition will be performed by the operator based on observations of the visual presentation. Automatic techniques to discriminate against undesirable targets prior to presentation shall be incorporated.

When the operator has identified the target on the display, he will position a lock-on cursor to enclose the target. Once the cursor has bracketed the target, the system can be placed into an automatic lock-on mode. In the automatic lock-on mode, the lock-on field shall be searched until lock-on occurs.

After the system locks on the spacecraft, data which indicates the angles of the LOS (line-of-sight) to the spacecraft shall be generated. Tracking shall exist until the received IR energy falls below the tracking mode threshold.

A capability shall be provided to enable the operator to return the equipment to one of the following modes in the event of loss of track:

(a) lock-on search

(b) sector search

(c) 2π search.

A preset capability shall also be provided to allow the system to return to any preset selected mode in the event of loss of track.

A capability shall be provided to position the center of either a selected search sector or the lock-on field anywhere within the search field. This capability shall be effected either automatically to the position indicated by the communication antenna pointing signals or manually.

The system shall be operable under daylight conditions. It is desirable that operation be permissible at angles as close to the LOS to the sun or moon as possible to reduce losses in coverage, while not causing permanent damage. The equipment shall exhibit full sensitivity to within three degrees of either side of the LOS to the sun or moon if scans or tracks across the sun or moon occur.

Although the system design shall be based on clear sky data, discrimination circuits to allow the system to operate in the presence of false targets shall be provided.

A simple tracking-rate storage device shall be provided to maintain smooth pointing during momentary loss of tracking signals. The rate and direction

of pointing signals shall closely approximate the

last-known rate and direction before loss of track.

It shall be possible to select use of this device or

to bypass it at the operator's discretion.

3.2.2 Configuration

The equipment shall consist of an IR Dome Assembly,

a Scan Unit, a Control Console, and an Inertial Nav-

igation System (INS).

3.2.2.1 IR Dome Assembly

The IR Dome Assembly shall be either fixed or

turret type; it shall not be a structural component

of the airframe. Dimensions of the assembly shall

not exceed that of a cylinder 30 inches in diameter,

and it shall not project higher than 20 inches above

the outer airframe skin. Its weight shall be kept

to a minimum to lessen the load factor on the air-

frame.

A modified JC-135A aircraft will be available for

installation of the IR Dome Assembly in the top of

the heated cargo compartment. The assembly

shall not compromise the integrity of the pressure
hull. Any protrusions beyond the surface of the
aircraft must be of such size and shape that any
fairing used shall not obstruct the FOV (field-of-
view) of the IRATS. It shall also be so located
that obscuration by the aircraft tail or other ap-
pendages shall be minimized. The choice of lo-
cation shall also consider any radiation effects
from the jet engines and/or exhaust.

3.2.2.2   Scan Unit

The scan unit shall include, but not be limited to,
an optical collection system, drive mechanisms,
and associated electrical and electronic devices.
The mechanisms shall provide for positioning the
optical collection system and for scanning it in
azimuth and elevation. The unit shall be located
in the IR dome. All moving or movable parts shall
be completely enclosed, but easily accessible for
maintenance from within the aircraft for ground
maintenance purposes. The weight of the Scan Unit
shall be kept to a minimum.

3.2.2.3 Control Console

The Control Console shall include the electronics necessary to process the detected data, to display the results, and to interface the tracking signals with the A/RIA, and the controls to operate the system. It shall also include required power conversion equipment. Provision shall be made to accommodate one man in a position from which he may comfortably operate the entire equipment from the console.

3.2.2.4 Intertial Navigation System (INS)

The Inertial Navigation System shall consist of an inertial platform, its associated platform electronics, a digital computer with input/output registers, a real-time clock synchronized to the master aircraft timing system, and ground-based inertial platform alignment equipment.

3.3 Performance

3.3.1 Type of System

The system shall be a passive angle-tracking system of either the track-while-scan or the search-track type.

3.3.2 Modes of Operation

The system shall have the capability to operate in the following modes:

(a) Search, in which scans of the entire field can be completely automatically performed.

(b) Sector scan, in which a smaller sector of the search field can be automatically scanned.

(c) Lock-on, in which the scan shall be automatic, and the system will acquire any object within the lock-on field which exceeds the minimum sensitivity of the system.

(d) Track, in which the aperture of the system or the LOS of a TWS mode is pointed by means of internally generated signals or is slaved to signals derived from the communications and telemetry antennas in the aircraft.

(e) Manual, in which the aperture of the optical collection system is pointed under control of the operator.

(f) Test, in which test signals are available for use in system performance evaluation, and initial platform erection and alignment. In any mode, the operator shall have the option of selecting true or relative display. Angles shall be referenced as defined in paragraph 3.3.11.

3.3.3 Search Field

A search field of 2π steradians, as defined in paragraph 3.3.5, shall be provided for all weight and air speed combinations of the aircraft in level flight (wings horizontal) at the nominal mission altitudes. The aircraft will nominally cruise at 450 knots true

air speed at an altitude between 35,000 and 45,000 feet during the mission. At these altitudes the aircraft will fly with a positive angle of attack.

3.3.4 Search Rate

The minimum search rate shall be $\pi/2$ steradians per second, based on a search of the entire hemisphere. During the search, the rate may be varied to provide redundant coverage in probable reentry areas, provided all other system performance characteristics are met.

3.3.5 Tracking Volume

The minimum tracking volume shall be a portion of a hemisphere. It shall be bounded on the bottom by the local horizontal plane and on the top by the 500,000-foot altitude surface. The maximum radius of the hemispherical portion shall be 540 nautical miles measured from the center of the aircraft.

3.3.6 Tracking Rates

Instantaneous angular tracking rates shall be 20

degrees per second, maximum, for each axis, in

any mode of operation.

3.3.7 Tracking Error

The root-mean-square angular tracking error shall not

exceed $\pm$ 5 milliradians for each axis at the time of

measurement. This error shall include all contribu-

tions of components in the system; it shall include,

but not be limited to, pointing angle error, plat-

form errors, tracking servo errors, etc. Tracking

error is defined as the difference between the actual

LOS and the indicated LOS.

3.3.8 Slewing Rates

Instantaneous slewing rates will be 20 degrees per

second, minimum, for each axis.

3.3.9 Angular Accelerations

The minimum accelerations shall permit attainment

of the maximum tracking rates from standstill in 0.2

seconds of time.

3.3.10   Detection Probability

The system design shall demonstrate a probability

of detection of at least .99 (assuming clear sky

conditions) in a maximum five seconds of time after

the spacecraft has entered the tracking volume.   De-

tection shall be defined as the recognition either by

multiple looks or of a signal exceeding a set signal-

to-noise-ratio, or both.   The multiple or singular

presence of the spacecraft signal shall in the five

seconds allowed provide the required .99 probability.

3.3.11   Acquisition Time

The time for the system to acquire the spacecraft

and begin generating angle data shall not exceed

five seconds after detection of the spacecraft.   De-

tection is defined in Paragraph 3.3.10.   Acquisi-

tion time as herein defined shall include the time

required to position the lock-on cursor about the

detected spacecraft signal, to activate the lock-on

track mode, and to position the scan unit in the re-

quired scan mode.   At the end of this time, the

IRATS shall have detected the spacecraft,

discriminated against false targets, acquired and

locked onto the spacecraft, and shall be generating

angle-track data.

3.3.12. Data Output Signals

Data output signals shall be compatible with the re-

quirements of the A/RIA. In any mode of operation,

access shall be provided to all signals. The system

shall provide the following data output signals:

(a)   Tracking Mode -- a signal which shall indicate

whether or not angle-tracking is in effect.

(b)   Target Presence -- a signal which shall indi-

cate when the target is placed in the tracking

loop.

(c)   Azimuth -- a signal which shall be representa-

tive of the azimuthal angle of the LOS to the

spacecraft relative to the aircraft's heading

or relative to true north. Relative azimuth

angles shall be measured with respect to the

aircraft's heading, zero being directly ahead

and values increasing positively clockwise

looking down on the aircraft.

100

(d)   Elevation--a signal which shall be representative of the elevation angle of the LOS to the spacecraft relative to the aircraft's yaw plane. Elevation angles shall be measured with respect to the yaw plane and values increasing positively upwards.

(e)   Present position information, in the form of longitude, latitude, and altitude.

(f)   Azimuth heading of aircraft.

(g)   True ground velocity of aircraft.

3.3.13   Data Rates

Data output signals shall be read out at a rate of at least ten per second.

3.3.14   False Alarm Rate

The system shall demonstrate a false alarm rate of less than one per minute. A false alarm shall be defined as the instance when an internal noise pulse exceeds the system signal detection threshold.

101

3.3.15 False Target Discrimination

The IRATS shall be capable of discriminating
between the Command Module and false targets
with a 99.0 percent probability of success when-
ever the line-of-sight to the spacecraft is not
blocked by clouds or other objects. False targets
include, but are not limited to:

(a) The sun

(b) Clouds which are illuminated by the sun

(c) Other luminous objects or bodies

(d) The Apollo Service Module which will be
     reentering the atmosphere behind the "real
     target."

An operator, assisted by the visual display, shall
be considered as part of the discrimination loop for
reasons of reliability, maintainability, and simplic-
ity. However, the task of discrimination should not
be left solely to the operator. Other discriminating
techniques should be employed, particularly in the
associated circuitry.

3.3.16   INS Performance Requirements

During the expected flight duration of 10 hours, the inertial system must maintain present position information to ± 3 nautical miles. The system shall provide and maintain a stable earth-centered coordinate system oriented to North, East, and Down.

3.3.16.1   INS Pre-Flight Requirements

The INS shall be capable of initial platform leveling and alignment prior to aircraft takeoff. In addition, gyro drift trimming will be measured following leveling and alignment, and the appropriate gyro drift trim constants will be calculated by the pre-flight computer program. The system shall be capable of initial read-ins of longitude, latitude, altitude, realtime, and platform constants prior to transfer to the flight mode.

3.3.16.2   Flight Mode Requirements

When the INS has been placed into the flight mode, the system shall provide:

(a) Present position information in the form of longitude, latitude, and altitude.

(b) Torquing signals to the platform gimbals to maintain the local vertical.

(c) Azimuth and elevation of the IR direction line with respect to the local horizontal and true North.

(d) Azimuth heading of the aircraft and true ground velocity.

3.3.16.3 Input and Output Information During Flight Mode

The INS shall accept angular data of the IR direction line. This set of angular data shall undergo an axis transformation and be available as direction angles referenced to the local horizontal and true north. IR angular direction information shall be read into the system at least ten times per second and available for readout two times per second.

The altimeter aboard the JC-135A shall serve as an input to the INS altitude loop computation to serve as a smoothing function for this computation.

3.4 Controls and Displays

3.4.1 Location

All operational controls, displays, and associated electronics shall be installed in the console.

3.4.2 Controls

Controls shall be provided to perform at least the following functions:

(a) Select the state of operation (on, off, or standby).

(b) Select the mode of operation as referenced in 3.3.2.

(c) Manually position the scan mechanisms and optics to point anywhere within the search field.

(d) Lock the scan mechanisms and optics in stow position.

(e) Shutter the aperture in the stowed condition.

(f) Operate the equipment test signals.

(g) Initiate the preflight and flight mode computer programs.

(h) Operate the display equipment.

(i) Position a lock-on field from anywhere on the display to bracket a detected object.

(j) Adjust the gain of signal processing electronics.

(k) Engage or disengage the tracking-rate storage device.

(l) Select the mode of operation to which the system returns after loss of signal.

3.4.3 Displays

Displays shall be provided for at least the following:

(a) To indicate the position of detected objects on a visual presentation.

(b) To indicate the angular position of the center of the lock-on field in degrees and tenths of degrees, accurate to ± 0.2.

(c) To indicate tracking status.

(d) To indicate the angular positions of the tracking aperture during the manual mode of operation.

(e) To indicate when an object in the lock-on field has exceeded the acquisition threshold.

.;(f). To indicate status of inertial system, i.e.,

platform leveling and alignment, drift time, and

flight mode.

(g) To display longitude, latitude, altitude, head-

ing, and ground speed to the pilot. In ad-

dition, these outputs shall be available for an

x-y plotter display at the navigator's console.

3.5 Electrical and Electronic Requirements

3.5.1 Power Supplies

Power will be supplied from a standard JC-135A

power source (28V, 400 cps). Designs requiring

an excess of 3.0 kilowatts shall be justified.

3.5.2 Electromagnetic Interference

The limits of specifications MIL-I-6181 and

MIL-E-6051 apply.

3.6 Reliability

The design of the system shall recognize the environ-

mental conditions imposed by the intended application

under uncontrolled climate conditions and dynamic

motions. All reasonable precautions shall be observed

to assure satisfactory mechanical, electrical, and optical

performance. The equipment shall be designed for ease

of maintenance and troubleshooting while on the ground

and up to the maximum altitudes.

3.6.1   Mean-Time-Between-Failure (MTBF)

> The system shall exhibit a MTBF of not less than
>
> 80 hours. The MTBF shall be determined by
>
> simulated operational conditions (see acceptance
>
> tests) for a period of 400 hours, with each failure
>
> being repaired and the equipment returned to op-
>
> eration. The MTBF is the quotient resulting from
>
> the division of the total operating time by the number
>
> of failures which occur.

3.6.2   Mean-Time-To-Repair (MTTR)

> The design goal for MTTR shall be less than one hour.
>
> Data accumulated during MTBF determination shall
>
> be used to determine MTTR.

3.7   Environment

The IRATS shall operate as specified under all environmental conditions which might be encountered during a mission. These include the following:

(a)   Take-off, landing, and flight operations for all aircraft speeds. The nominal cruising air speed of the aircraft shall be considered to be approximately 450 knots.

(b)   All altitudes between sea level and 45,000 feet. The nominal operating altitude shall be considered to be 35,000 feet.

(c)   All points on the earth between latitudes of 40° south and 40° north.

3.8   Documentation

3.8.1   Preliminary Design Plan

Six sets of a preliminary design plan shall be submitted for approval to the GSFC technical representative. The preliminary design plan shall include, but not be limited to, the following:

(a)   Design specification requirements of the IRATS

subsystems

(b)   Outline drawings of equipment assemblies.

(c)   Installation recommendations

(d)   Cable interconnection diagrams

(e)   Size, weight, and power consumption require-

ments

(f)   System performance characteristics

(g)   Aircraft modification recommendations

(h)   A list of recommended critical spare parts.

3.8.2   Project Reports

Project Reports shall be submitted in accordance

with Specification NASA/GSFC/TID-S-100. Types

I, II, and III therein are applicable.

3.8.3   Design Reports

Six sets of all design reports shall be submitted to

the GSFC technical representative. These design

reports shall include, but not be limited to, the

following:

(a) All final calculations performed in connection with the design

(b) Necessary preliminary sketches, drawings, and data.

3.8.4 Drawings

Three nonreproducible folded copies of the following drawings shall be submitted to the GSFC technical representative within ten calendar days after approval signature:

(a) Family tree assembly

(b) Subassembly

(c) Component

(d) Schematic

(e) Interconnection

(f) Purchased-part drawings.

In addition, one clear full-size reproducible copy of all final manufacturing drawings will be submitted to the GSFC technical representative with delivery of the system

Drawings will become the property of GSFC.

3.8.5 Test Procedures

Three sets of test procedures shall be submitted to the GSFC technical representative 30 calendar days prior to the respective scheduled tests.

3.8.6 Test Reports

Three sets of test reports shall be submitted to the GSFC technical representative within seven calendar days after completion of each test. The report format shall include, but not be limited to, the following:

(a)   Identification data

(b)   Test equipment and dates of calibration

(c)   Test data, presented in graphic form where applicable

(d)   A list of failed items, if any

(e)   An evaluation of the test results

(f)   Recommendations, if necessary.

3.8.7 Instruction Manuals

Three sets of an instruction manual shall be submitted by the contractor to the GSFC technical representative at the time of delivery of the system. The manuals shall contain information required for installation, understanding the theory of operation, operation, removal, and maintenance of the system. Included shall be photographs which clearly indicate the location of component assemblies. Instruction manuals shall be of such quality as that normally found in commercial instruction manuals.

3.9 Responsibilities

3.9.1 Contractor

The contractor's responsibilities shall include, but not be limited to , the following:

(a)   Development and fabrication of the entire system.

(b)   Performing design studies and calculations to indicate the best approach to development of the system. These shall include, but not

be limited to: Specific recommendations concerning the use of the computer available from the inertial system to integrate the various data processing requirements implemented on one central computer; specific recommendations concerning the desirability of mounting the IR scanner directly on the azimuth block of the platform to mechanically perform coordinate transformation; specific recommendations for compatibility between the master timing system on the aircraft and the INS; and specific recommendations for location of the INS.

(c)   Preparation of drawings and diagrams which illustrate the system design.

(d)   Preparation of technical manuals, drawings, diagrams, test reports, and project reports.

(e)   Preparation of test procedures to qualify system design.

(f)   Testing the system design under simulated operational conditions.

(g)   Incorporating safety features such as inter-
locks and circuit breakers, mechanical shields
necessary to minimize probability of injury to
personnel and/or equipment.

(h)   Delivering an operational system which meets
the requirements set forth herein.

(i)   Obtaining necessary documents of studies,
tests, observations, etc., available from both
Government and private sources that will
provide a familiarity with the expected en-
vironment, atmospheric, and target charac-
teristics.

(j)   Procurement or construction of units to supply
special purpose powers not available from the
standard supply in the aircraft.

(k)   Meeting the interface requirements of the
A/RIA.

(l)   Providing the simulated target for flight tests.

3.9.2 Government

Government responsibilities shall not relieve the contractor either from responsibility for satisfactory performance of work or from meeting the requirements of this specification. The Government will be responsible for the following:

(a) Coordination of all activities of the work, including visits by the contractor's representatives to other Government facilities and to facilities of contractors involved in development of the A/RIA and of Project Apollo.

(b) Approval or disapproval of all final drawings and schematic diagrams before fabrication or purchase of items involved. Seven calendar days, after receipt of drawings or diagrams, will be allotted for review.

(c) Approval or disapproval of all test procedures and test results within seven calendar days of receipt.

(d) Acceptance of a delivered system.

116

(e)   Arrangement of a contractor's visits to other

        related facilities upon submission of a re-

        quest.

(f)   Approval or disapproval of the type of visual

        presentation selected.

(g)   Modification of the aircraft for installation

        of the IRATS equipment.

(h)   Defining the interface between IRATS and the

        A/RIA.

(i)   Providing the aircraft for flight tests.

(j)   Designate a point of delivery.

3.10 Special Requirements

3.10.1   Test Sources

A stable test source shall be provided to determine

the sensitivity of the system during operation. It

shall be designed for installation aboard the air-

craft, internal or external, to the IR Dome Assembly

such that the energy is collected by the optics. Test

collimators, sources, alignment, and focusing de-

vices shall be provided and of such design that each

shall be operable by normal skilled operators.

3.10.2 Optical Shielding

Shielding shall be provided to mask fixed sources of the intense energy to prevent damage to the system.

3.11 Spare Parts

Critical spare parts shall be available prior to start of flight tests. A recommended list of spare parts shall be submitted to GSFC with delivery of the system.

4.0   INSPECTION, TEST, AND ACCEPTANCE

INTENTIONALLY

LEFT

BLANK

4.0   INSPECTION, TEST, AND ACCEPTANCE

4.1   Equipment .

Preliminary inspection will be performed at the contractor's plant by the contracting officer's technical representative. Factory testing will be performed by the contractor according to an approved copy of test procedures. Tests will be witnessed by the contracting officer's technical representative(s). Applicable methods of MIL-STD-810 apply. The contractor shall disprove to the satisfaction of the NASA/GSFC technical representatives the applicability of any methods of MIL-STD-810 not included in his test procedures.

Flight tests will be performed by the contractor according to an approved copy of test procedures. Locations for the flight tests will be designated by GSFC. An aircraft and a simulated target will be used to perform the tests. All tests will be witnessed by the contracting officer's technical representative(s).

Final acceptance will be performed by the contracting officer's technical representative(s) at GSFC

121

4.2 Other

All other items will be accepted by the contracting officer's technical representative at destination.

5.0   PREPARATION FOR DELIVERY

INTENTIONALLY

LEFT

BLANK

5.0   PREPARATION FOR DELIVERY

5.1   Preservation, Packing, and Packaging

The equipment and associated parts, unless otherwise specified by the contracting officer, shall be secured and handled so as to ensure safe domestic transportation of the equipment and acceptance by common or other carrier at the lowest rate to the point of delivery. Equipment shall be able to withstand storage, rehandling, and reshipment without the necessity of repacking.

5.2   Packing Slips

The contractor shall be required to include a packing slip with each shipment to the Government. This packing slip shall include the following information:

(a)   Contract number

(b)   Equipment nomenclature

(c)   Manufacturer's part number or serial number.

5.3   Shipping Identification

The contractor shall place in a readily accessible spot, on the exterior of all shipping containers, the follow-information:

(a)   Equipment nomenclature

(b)   Model number or serial number

(c)   Contract number.

5.4   Critical Spare Parts

Critical spare parts shall be wrapped or boxed as a unit and identified by name, symbol number and part number. All units shall be packed and shipped in one container where practicable.

APPENDIX

APPENDIX

For purposes of this specification, the Apollo Command Module may be assumed to have the following characteristics for the various reentry trajectories to be expected:

The projected area of the spacecraft is approximately 12.2 square meters. Its surface temperature is approximately $1000^{\circ}K$ to $2000^{\circ}K$ at the heat shield (leading surface). These temperatures vary with range and altitude and are subject to some change with time when more detailed analyses become available. The target shall be considered to be a gray body, Lambertian radiator with an emissivity of 0.75.
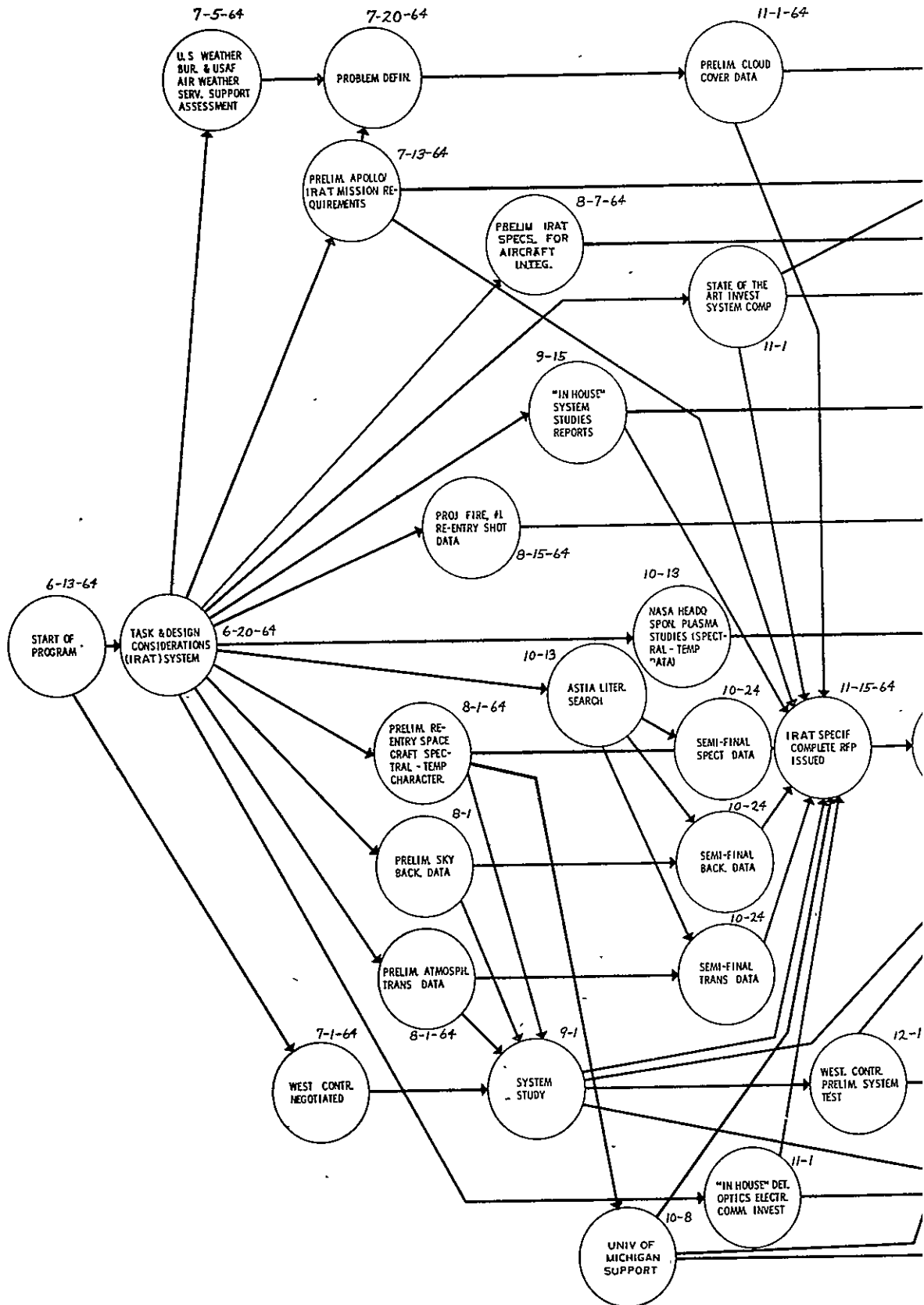
APPENDIX B

.

131

INTENTIONALLY

LEFT

BLANK

6-1-65 — MORE COMPREHEN CLOUD COVER DATA

3-1-65 — AVCO TWS SYSTEM TEST

6-15-65 — SEMI-FINAL MISSION REQUIREMENTS

8-15-65 — SEMI-FINAL SPECS FOR AIRCRAFT INTEG.

ASSES OF BIDDER CAP-ABILITIES

-1-65

5-15-65 — CONSID OF PROM AREAS TO BE DEV

4-1-65 — PROJ FIRE #2 RE-ENTRY SHOT

2-1 — RAT PROP. RECEIVED

IRAT PROP EVALUATION

4-15-65 — CONTRACT AWARD

7-15-65 — IRAT STUDY PHASE & PRELIM DESIGN

3-15-65

6-15-65 — FINAL BACKGROUND DATA

6-15-65 — FINAL ATMOS TRANS DATA

7-1-65 — SYSTEM FIELD EVALUATION

3-1-65 — PRELIM. RESULTS "IN HOUSE" INVEST.

4-15-65 — CONT OF INHOUSE INVEST CONTRACT MONITORING

CONT CLOUD
COVER ANALYSIS
[PRED - ACTUAL
COND VERIF.]

11-1-66

FINAL
MISSION
REQUIR

5-1-67

FINAL
SPECS FOR
AIRCRAFT
INTEG

CONTIN
AWARENESS
OF AIRCRAFT
INTERFACE
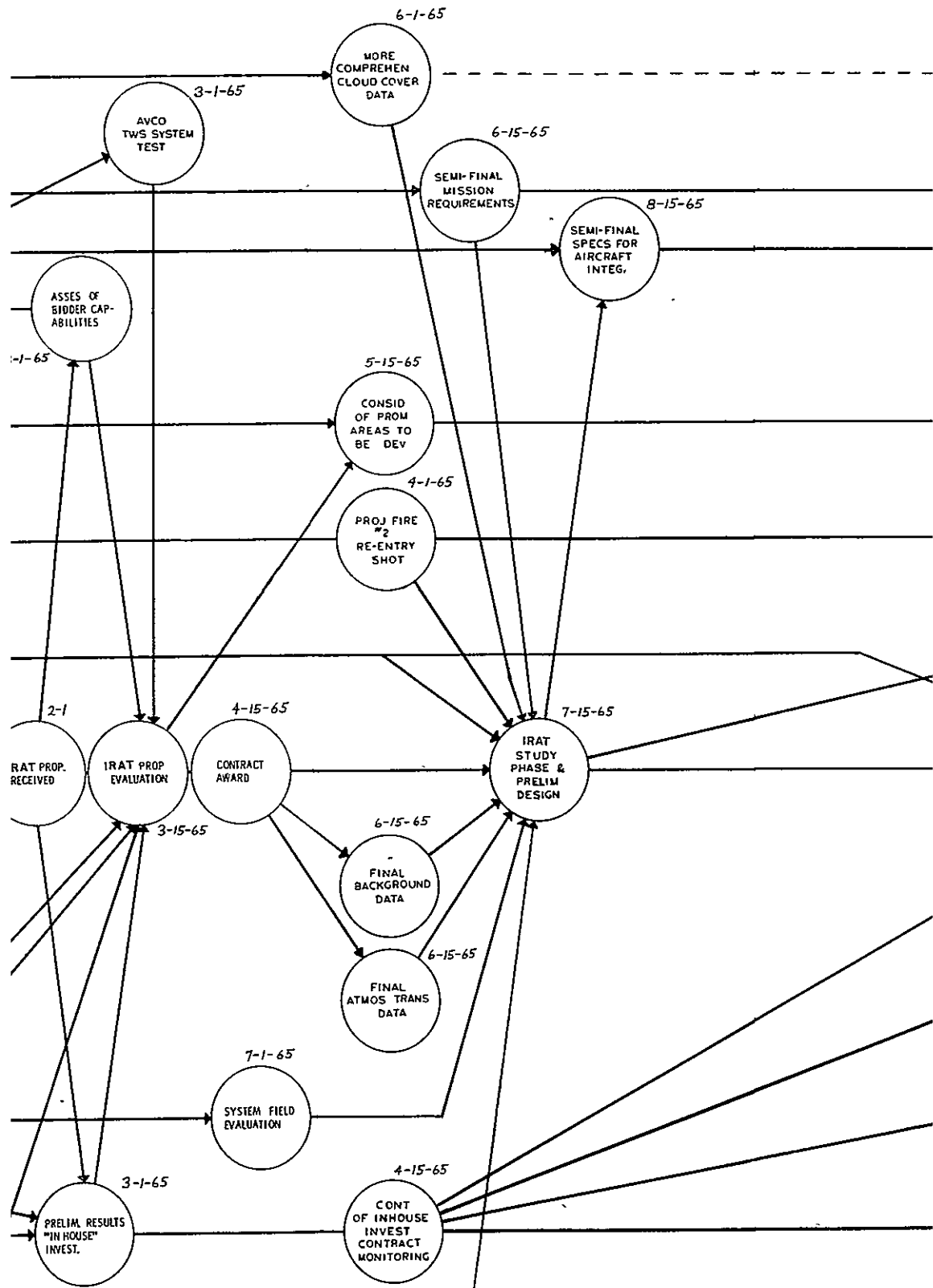
3-15-66

PREL
RESULTS OF
DEV AREAS

CONTIN
SUPPORT OF
NEW DEV
AREAS

1ST Qtr. 67

APOLLO
FULL SCALE
BOOSTED
RE-ENTRY

CONTIN
INPUT FROM
APOLLO TESTS

3-15-66

CRITICAL
SPARE
PARTS
ORDERED

CONTIN
OF TESTING
PROGRAM

FLYABLE
PROTOTYPE

FLIGHT
TEST

FLIGHT
OPER UNITS
& SPARES
SPEC & ORD

INTEG &
TESTING OF
OPERATIONAL
UNITS

9-15-66   *9-15-66*   *4-1-67*   *2-1-67*

OPTICS
STRUCT
MOUNTS

CONT INVEST
SUPPORT OF
SYSTEMS CONTR.

9-15

ELECT
ATA HAND
DISCRIM
TECH

CONT INVEST
SUPPORT OF
SYSTEMS CONTR.

9-15

CHANISMS
& SERVOS

CONT INVEST
SUPPORT OF
SYSTEMS CONTR.

9-15

I R
ETECTORS

CONT INVEST
SUPPORT OF
SYSTEMS CONTR.

CONTIN
U OF MICH
SUPPORT

133

APPENDIX C

135

THE EFFECT OF CLOUDS ABOVE 35,000 FEET ON INFRARED
SPACECRAFT TRACKING OVER THE WESTERN PACIFIC OCEAN

by

Kenneth M. Nagler, Head
Spaceflight Meteorology Group
National Weather Satellite Center
U. S. Weather Bureau
Washington, D. C. 20235

November 20, 1964

THE EFFECT OF CLOUDS ABOVE 35,000 FEET ON INFRARED SPACECRAFT TRACKING OVER THE WESTERN PACIFIC OCEAN

INTRODUCTION

In evaluating the possible use of an airborne Infrared Re-Entry
Acquisition Seeker (IRAS) at an altitude of about 35,000 feet, it
is necessary to know something about the clouds which exist above
that level in the region in which the spacecraft re-entry is planned.
For the Apollo mission, the re-entry according to present plans
(Vonbun, 1964) would most likely occur between the equator and
35N and between 140E and 170W for a landing in the proposed
northern hemisphere landing area just east of the Hawaiian Islands.
For the proposed southern hemisphere landing area east of American
Samoa, the probable limits of the re-entry area would be from the
equator to 35S and between 130E and 180 degrees. The re-entry
probability would, of course, be much higher for certain small
portions of these areas.

An attempt has been made to assess the effect of clouds above
35,000 feet in this region. In practically no area of the world
is there sufficient information on which an accurate evaluation
of the effect of clouds above such a level could be based. In the
region of concern there is very little information for such an
evaluation. Nevertheless, with considerable subjectivity it is
possible to come to some general conclusions of the probable
effect of clouds above 35,000 feet on an operation using the IRAS
to track a re-entering Apollo spacecraft.

Figures 1 through 4 show relative zones of cloud cover above
35,000 feet for the months of February, May, August, and
November. The significance of the zones and the sources of
information are discussed below.

DISCUSSION OF FIGURES 1 - 4

The boundaries of the zones and the significance of the zones
must be considered as very rough, resulting from limited and
questionable data and subjective judgment.

In Zone A, the best for operation of the IRAS, there is a low
frequency of high clouds, such that 90 percent of the time, or
more, clouds should not interfere substantially for high view

angles (within about 45 degrees of the zenith). As the viewing angle approaches the horizon, naturally, the chances for successful tracking are diminished, but even for low viewing angles the chances are fairly good in this zone.

In Zone B, there should be sufficiently clear skies above 35,000 feet for high-angle viewing between about 50 and 90 percent of the time, with a lesser chance for lower viewing angles. Extratropical disturbances will cause intermittent cloudiness on the poleward portions of this zone, while closer to the equator, various tropical weather disturbances will contribute to the high cloudiness.

In Zone C, good viewing conditions for even high angles would occur less than half of the time, and chances for success at low angles would be very small.

As to the nature of the clouds likely to occur above 35,000 feet, cirrus (ice-crystal) clouds would be by far the dominant type, but at times there would be some towering cumulus or altocumulus composed of water droplets.

The cirrus clouds in the area are of a number of varieties, ranging from widely scattered wispy patches of cirrus uncinus (H-1 in the international code) to thick cirrostratus overcast (H-7 in the international code). In the equatorial convergence area and in the various disturbances which are intermittent much of the cirrus is of the spissatus variety, originating from the upper portions of cumulonimbus clouds but moving away from and persisting much longer than the parent clouds. These cirrus can vary greatly in their thickness, uniformity and areal extent.

In the higher latitudes in the area of concern, particularly in the winter season some of the cirrus--again varying considerably-- is that associated with the jet stream (the high speed core of the upper westerly winds). Particularly in the tropics the cumuliform clouds extend well above 35,000 feet. In disturbed areas such clouds would be very common, with a number of individual storms or lines or areas of storms within sight of a high flying aircraft.

SOURCES OF INFORMATION

1. Aircraft observations. The most direct of the information sources is the summary of cloud observations above 35,000 feet

in the area of concern, prepared by the National Weather Records
Center, Asheville, North Carolina, specifically for this study.
Based on high-level aircraft weather observations in the period
1959 through 1963, frequencies of layer clouds above 35,000 feet
were compiled in three categories: One to five-tenths of the sky
covered, more than five-tenths of the sky covered, and layer
clouds reported, but amount not stated. The frequency of cumulus
clouds reported above 35,000 feet was also compiled, although the
fraction of the sky covered was not considered since such informa-
tion was not generally available in the reports. The observations
were summed for each 5-degree "square" of latitude and longitude.

These data have several shortcomings. The most significant is
that observations are available for only a small portion of the area
of concern, namely along the air routes between Honolulu and Japan,
Honolulu and the Philippines, and between Honolulu and New Zealand
and eastern Australia. No reports were available for most of the area.

Also, there are not enough observations to give valid, long-range
statistics. Finally, there may be biases in aircraft observations --
biases whose effects are hard to judge. Pilots making routine in-
flight weather observations may sometimes ignore clouds well above
them or may not report thin cirrus clouds, thus leading to an under-
estimate of the frequency of high-level clouds.

On the other hand, the failure to report thin cirrus clouds may, in
fact, yield statistics more applicable to the IRAS evaluation. The
thin clouds not reported might well be sufficiently transparent in the
infrared to permit spacecraft tracking--at least for high viewing angles.

2. . Infrared observations from TIROS IV. Several meteorological
satellites have yielded infrared radiation measurements which can be
used to approximate the temperature of the radiating cloud "surface"
and hence the altitude of the cloud tops, as discussed, for example,
by Bandeen, Halev and Strange (1964). The information already
processed is generally in the form of averages for various time
periods and averages over fairly large areas. Either form of
averaging makes the results difficult to interpret, since the average
value may be representative of a cloud-top height generally present
over the area and period involved; or it may be an intermediate value
between higher and lower cloud heights which were present in the area
or time period over which the average was made.

One set of daily infrared radiation values averaged for relatively.
small areas (2-1/2 degrees of latitude on a side) were available

141

from TIROS IV from a study made by the Planetary Meteorology Branch, Meteorological Satellite Laboratory, National Weather Satellite Center. The frequencies of radiation values equal to or less than 0.20 ly min $^{-1}$, 0.23 ly min $^{-1}$, and 0.26 ly min $^{-1}$ were abstracted for each of these areas for February and May of 1962 and grouped (for convenience) in 5-degree squares.

The exact significance of the selected radiation values is difficult to assess in terms of cloud height, (1) because of calibration difficulties in relating the values to specific black-body temperatures, (2) because the radiation, particularly in the case of cirrus clouds, is not just from the upper surface but comes in part from within or even below the cloud, depending on its density and (3) because the level in the atmosphere associated with a specific temperature (and hence radiation value) varies with location and with time.

For most of the area under consideration (except for the higher latitudes) the height equivalents were estimated very roughly as follows:

0.20 ly min $^{-1}$	38,500 feet
0.23	34,500
0.26	30,000

The frequencies of radiation values of 0.26 ly min $^{-1}$ or less (Figures 5 and 6) were considered of greatest significance in this study even though the estimated black-body temperature represented would indicate a cloud height of about 30,000 feet rather than 35,000 feet. Comparison with other data gave the impression of a better fit of the 0.26 ly min $^{-1}$ values, probably because there is an averaging over an area and perhaps because of calibration errors in assessing the raw data.

These frequencies showed the abundance of high cloudiness in the convergence zone and the sparsity of high clouds in the subtropics. They represent only partial coverage for one February and one May, however, so may deviate substantially from valid long-period data; therefore, they were used as guidance material only.

3. Surface observations. From land stations in the area there are records of cloud observations which could be used to get statistics on high clouds of various types. Also, records of weather observations from ships could be used to get frequencies of various cloud types and amounts for various subdivisions of the area of concern.

There are several obvious shortcomings in the use of surface
weather observations to assess cloudiness above 35,000 feet,
however. For one thing, estimates of the heights of high clouds
are not normally given, and, even when available, are not very
reliable. Also, whenever there are abundant low or middle clouds,
observing of the high clouds is either impossible or unreliable.

Accordingly, in this initial survey of the distribution and effects
of clouds over 35,000 feet in height, surface observations have
been used only where available in convenient summaries and only
for areas where lower clouds are not very abundant.

Specifically, (from Rofe) cloud data for Australia were used in the
evaluation; and from U. S. Navy (1956, 1957, 1959) available analyses
of the frequency of relatively clear areas ($<$ two-tenths total sky cover)
were considered in drawing the maps of clouds above 35,000 feet, as
were analyses of the frequency of precipitation--as an indication of
areas of substantial cloudiness.

4. TIROS cloud pictures. Average cloud cover charts have been
prepared from TIROS nephanalyses by several investigators, notably
Clapp (1964). The TIROS cloud pictures and the resulting analyses
are not suited for quantitative cloud height determination, but the
patterns of cloud cover are useful in judging the locations of the
clearer or stormier areas, and hence the areas of probable minimum
and maximum frequencies of high clouds.

5. Other sources of information. There are a great many articles
in the meteorological literature which bear on the general subject of
high clouds or which give some specific information for pertinent
parts of the world. These contributed to a general impression of
what to expect in the re-entry area but did not give specific informa-
tion. Articles of a general nature include Palmer, Nicholson and
Shimaura (1956) and Stone (1957).

As an example, there are a number of studies dealing with the high
clouds associated with the jet stream, such as Schaefer (1953),
Conover (1959), Riehl (1962) and Kadlec (1964). Most such studies
have been made over North America but can be used in evaluating
cloudiness over the higher latitudes of the possible re-entry area,
where the jet stream is common and well developed in the winter
half of the year.

143

Limited but specific information on high tropical cloudiness is given by Littlejohns (1958) and Ryan (1959).

CONCLUSION

Although there are many uncertainties, it appears that chances for acquisition and tracking of the incoming spacecraft by means of the IRAS would be good for most of the area of concern. At or above an altitude of 35,000 feet in both hemispheres there is a zone where cloud cover is sufficiently good most of the time even for low viewing angles. There is also a zone--primarily in the equatorial region where high cloudiness is very common, so that the IRAS would not have a good chance of working well. Even here, however, if there is a capability of moving to a different location, say fifty miles or so distant from the optimum site for a particular re-entry, the chances are fair for at least partial coverage.

PROBLEMS AND RECOMMENDATIONS

This study has been of a preliminary nature, but there is not adequate information available to give accurately the probabilities for successful use of the IRAS over the Western Pacific area even if a more sophisticated study were attempted.

Some additional information could be developed, however, if the time and effort are warranted:

1. Further use of TIROS and possibly NIMBUS infrared radiation data could be made. For example, with some programming and considerable computer time, the frequency distribution of the radiation values for the smallest area observed by the radiometer (about 60 km on a side for a view straight down) could be obtained.

2. Aircraft weather observations not on file at National Weather Records Center, Asheville, North Carolina could probably be obtained from other sources; for example, from airlines or from other countries with frequent flights in the Western Pacific.

3. Further information could be obtained from summaries of surface weather observations, which could cast some light on the upper cloud statistics, but which would still have the shortcomings mentioned earlier.

144

4. Perhaps some arrangement could be made to obtain more detailed in-flight reports tailored to the IRAS problem, by direct contact with one or more of the airlines with routes in the area of concern.

5. The ideal (and most expensive) approach is the scheduling of special flights to add to the climatology of clouds above 35,000 feet, but, mainly, to measure the effects of cirrus on simulated operations using some prototype IRAS equipment.

REFERENCES

BANDEEN, W. R.; HALEV, M.; and STRANGE, I. A Radiation Climatology in the Visible and Infrared From the TIROS Meteorological Satellites. NASA Goddard Space Flight Center, Prepared for International Radiation Symposium, International Association of Meteorology and Atmospheric Physics (I. U. G. G.) Leningrad, August 1964.

CLAPP, P. F. Global Cloud Cover for Seasons Using TIROS Nephanalyses. Monthly Weather Review, November 1964.

CONOVER, J. H. Cloud Patterns and Related Air Motions Derived by Photography. Blue Hill Meteorological Observatory, Milton, Massachusetts. 1959.

KADLEC, P. W. A Study of Flight Conditions Associated With Jet Stream Cirrus, Atmospheric Temperature Change, and Wind Shear Turbulence. Eastern Air Lines Meteorology Department, Miami, Florida, June 1964.

LITTLEJOHNS, L. W. High Cloud Structure in Equatorial South-East Asia. Meteorological Magazine. 87:1958.

PALMER, C. E.; NICHOLSON, J. R.; and SHIMAURA, R. M. An Indirect Aerology of the Tropical Pacific. University of California Institute of Geophysics, Oahu Research Center, June 1956.

RIEHL, H. Jet Streams of the Atmosphere. Technical Paper No. 32. Department of Atmospheric Science. Colorado State University, Fort Collins, Colorado, May 1962.

ROFE, B. Geophysical and Meteorological Data of Woomera Ranges. Commonwealth of Australia, Weapons Research Establishment.

RYAN, P. 1959, Height of Cirrus Cloud Tops in Tropics. Australian Meteorological Magazine. Melbourne, No. 25 76-77.

SCHAEFER, V. J. The Use of Clouds for Locating the Jet Stream. The Aeroplane, October 30, 1953.

STONE, R. G. A Compendium on Cirrus and Cirrus Forecasting. Air Weather Service Technical Report 105-130, March 1957.

U. S. NAVY.   Marine Climatic Atlas of the World, Volumes II, III
and V.   North Pacific Ocean NAVAER 50-1C-529, 1956; Indian Ocean
NAVAER 50-1C-530;1957; and South Pacific Ocean NAVAER 50-1C-
532; 1959.

VONBUN, F. O.   Re-Entry Tracking for Apollo.   NASA Goddard
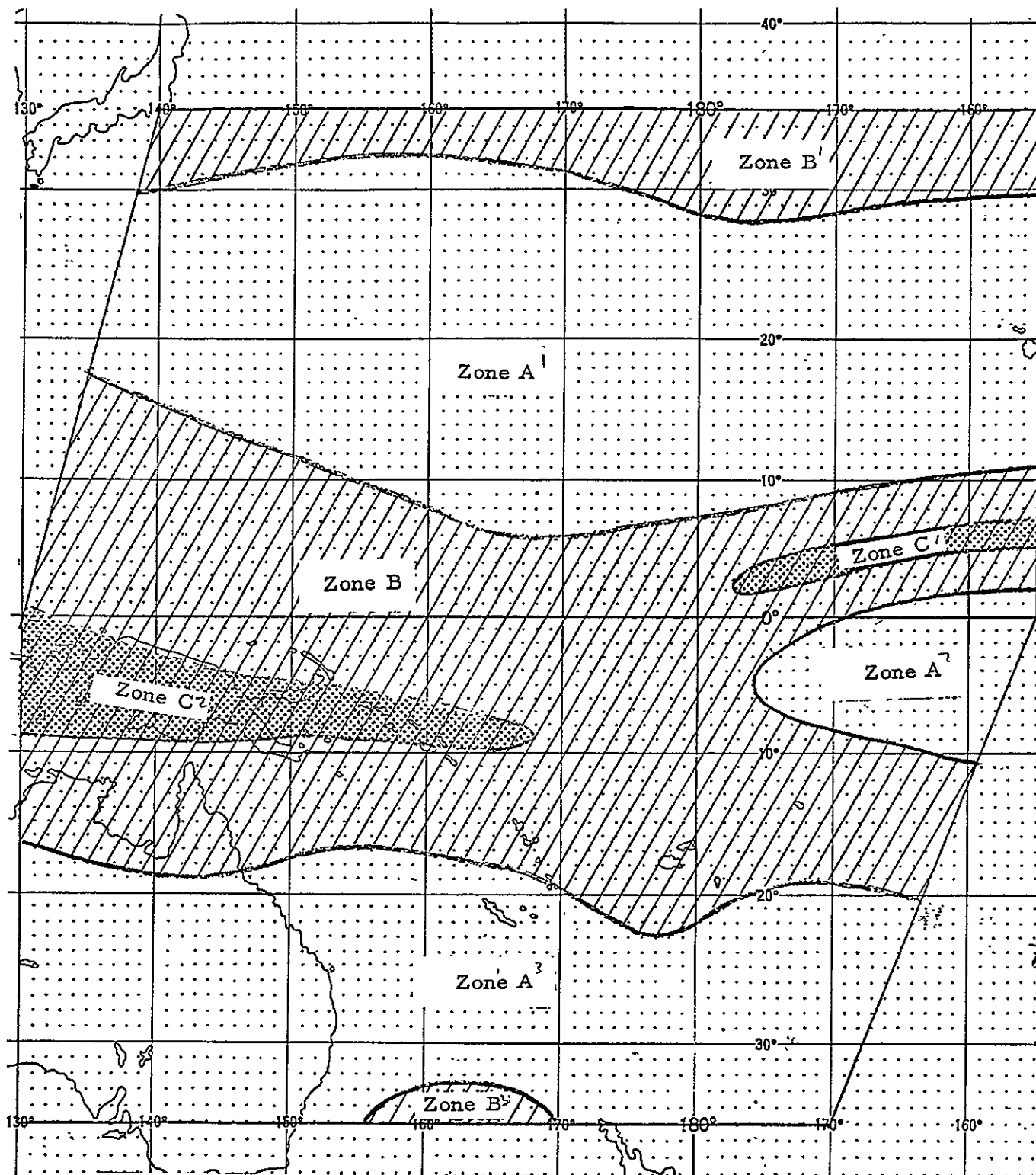Space Flight Center.   March 6, 1964.

Figure 1. Zones indicating the relative chances of success of an IRAS mission at 35,000 feet, FEBRUARY. See text for explanation.
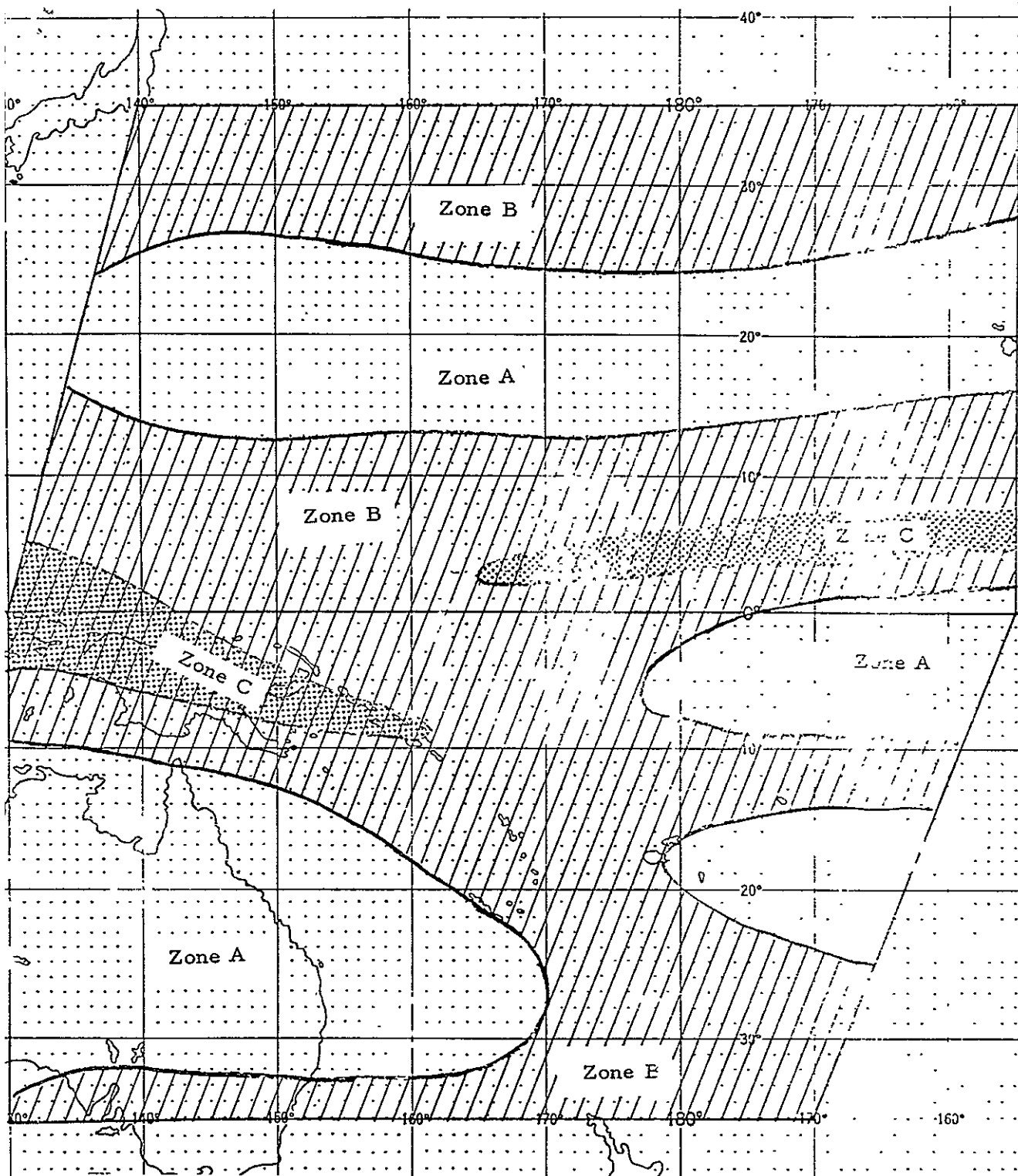
148

Figure 2. Zones indicating the relative chances of success of an IRAS mission at 35,000 feet, MAY. See text for explanation.

149

Figure 3. Zones indicating the relative chances of success of an IRAS mission at 35,000 feet, AUGUST. See text for explanation.
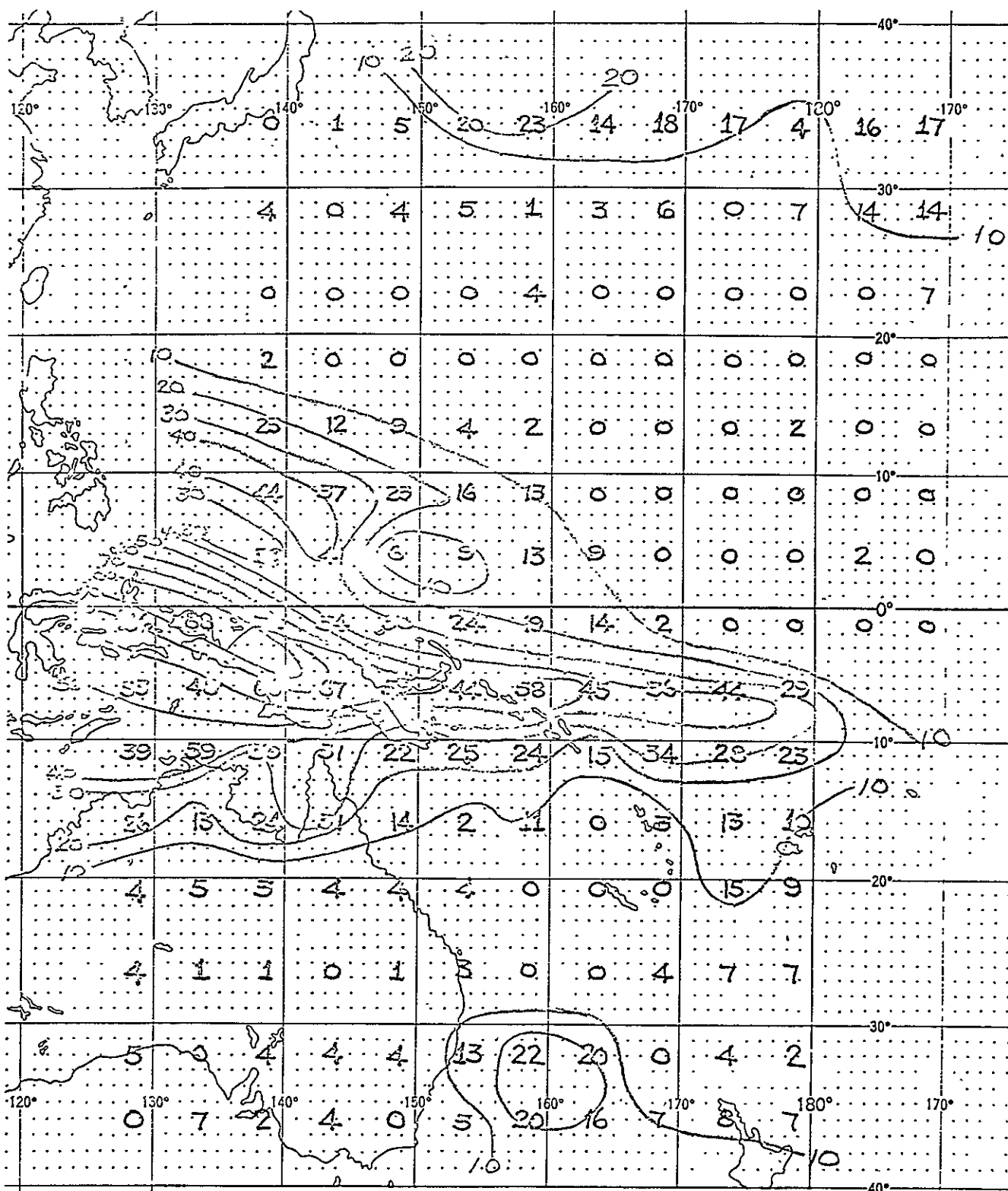
150

Figure 4. Zones indicating the relative chances of
success of an IRAS mission at 35,000 feet, NOVEMBER.
See text for explanation.
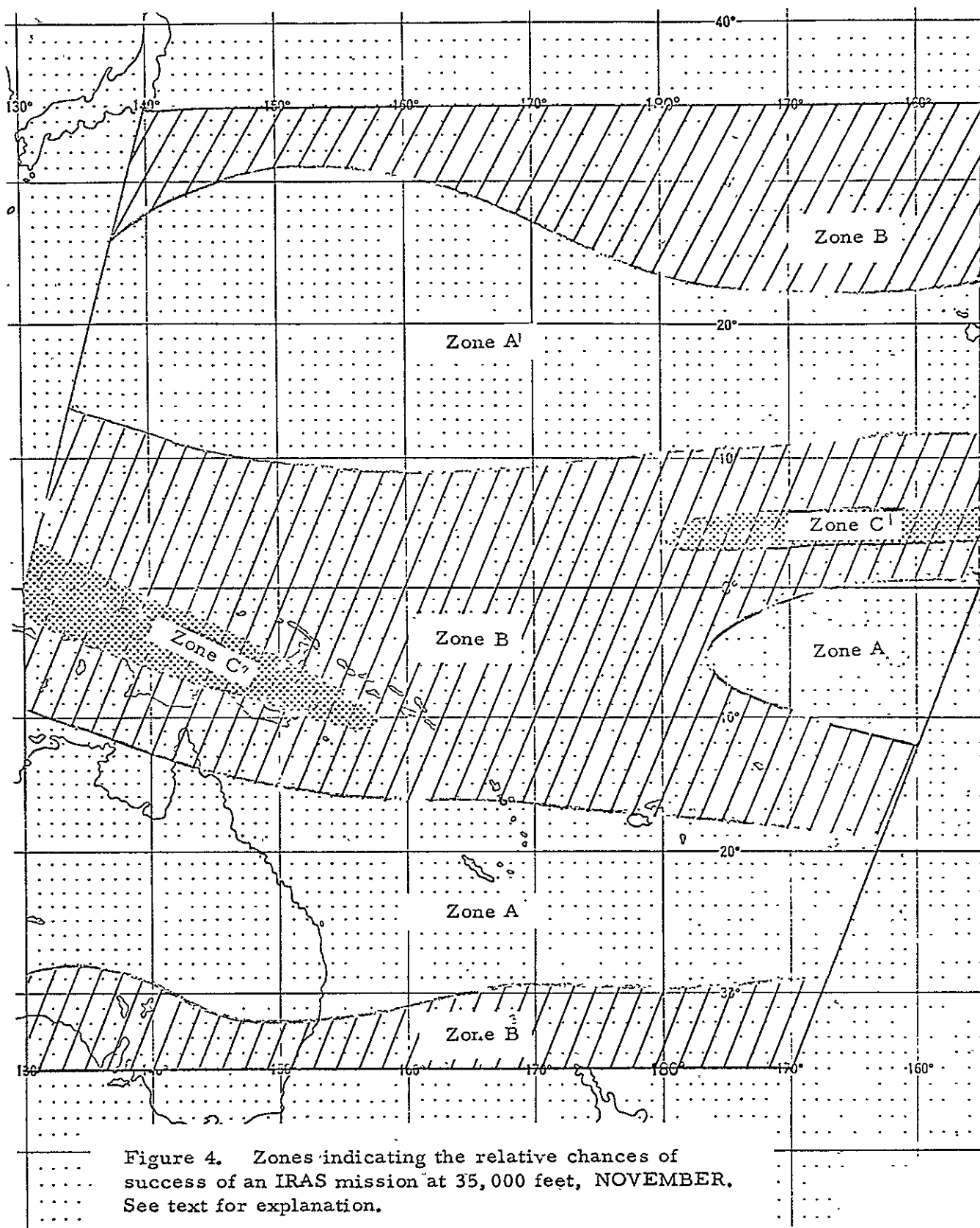
Figure 5. Frequency of infrared radiation values of
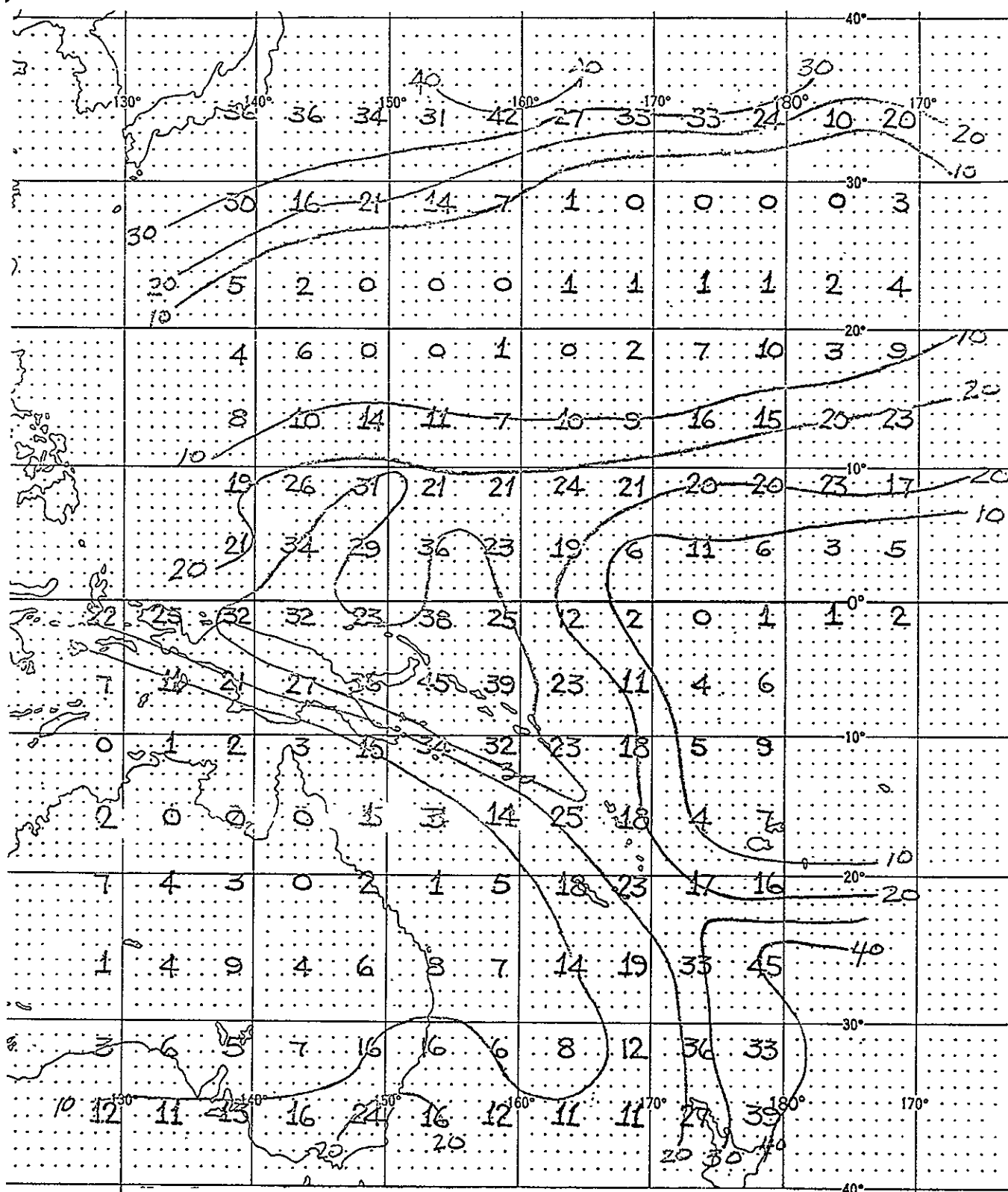0.26 ly min $^{-1}$ or less as estimated from TIROS IV,
February 1962.

Figure 6. Frequency of infrared radiation values of 0.26 ly min^{-1} or less as estimated from TIROS IV, May 1962.